



The Journal of Gemmology

2015 / Volume 34 / No. 6





Gem-A

THE GEMMOLOGICAL ASSOCIATION
OF GREAT BRITAIN



Gem-A Conference 21-22 November 2015

The **Gem-A Conference** will be held on **21-22 November 2015**, at the **Royal Institute of British Architects (RIBA)** in Marylebone, London. Incorporating the 18th Symposium of the Federation of European Education in Gemmology (FEEG), this year's Conference promises to be bigger and better than ever, with a host of exciting speakers, events and workshops scheduled over the weekend.

Visit www.gem-a.com or email events@gem-a.com to book your place.

Understanding Gems

Join us.



COLUMNS

467 What's New

Automated melee screening device | DFI Mid-UV Laser⁺ diamond screening system | DiaCam360 | GemmoSphere | News on cobalt diffusion treatment of spinel, diamond-diamond doublet, temporary diamond colour treatment and low-temperature heat treatment of Mozambique ruby | *ICGL Newsletter* | Microcrystalline silica online lectures | *What's New in the Mineral World?*

470 Practical Gemmology

A matched pair of opals, with a catch

472 Gem Notes

Chrysocolla chalcedony from Spain | Rhodochrosite from Brazil | Tourmaline mining in the DRC | Colour-zoned Cr- and V-bearing tourmaline from Kenya | Heart of Pearls tagging system | Modern doublets | Fracture-filled synthetic emerald, with synthetic quartz inclusions | Glass imitations of Cu-bearing Mozambique tourmaline | Quartz imitation of star sapphire | Chromium-diffused corundum | Lead-glass-filled yellow sapphires



ARTICLES

Feature Articles

490 Green-Luminescing Hyalite Opal from Zacatecas, Mexico

By Emmanuel Fritsch, Peter K. M. Megaw, Tyler L. Spano, Boris Chauviré, Benjamin Rondeau, Michael Gray, Thomas Hainschwang and Nathan Renfro

510 Raman Spectroscopy of Ancient Beads from Devín Castle near Bratislava and of Four Intaglios from other Archaeological Finds in Slovakia

By Magdaléna Kadlečíková, Juraj Breza, Lubomír Vančo, Miloš Gregor and Igor Bazovský

Gemmological Briefs

518 The First Undisclosed Colourless CVD Synthetic Diamond Discovered in a Parcel of Natural Melee-Sized Diamonds

By Thomas Hainschwang and Franck Notari

524 The 'Coffee-and-Cream' Effect in Chatoyant Cabochons

By Harold Killingback

532 Conferences

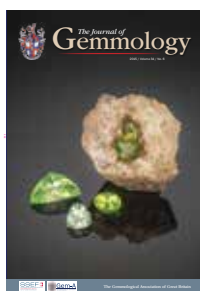
Sinkankas Opal Symposium | AGA Las Vegas | Mallorca GemQuest | Scottish Gemmological Association | Swiss Gemmological Society

540 Gem-A Notices

547 Learning Opportunities

551 New Media

555 Literature of Interest



Cover Photo:

The colour appearance of this rough and cut hyalite opal from Zacatecas, Mexico, is due to its green daylight-induced fluorescence. The cut gems weigh 1.34–5.67 ct and were faceted by Michael Gray; the specimen and 5.67 ct stone are courtesy of Kristalle, Laguna Beach, California, USA. Photo by Orasa Weldon.

The Journal is published by Gem-A in collaboration with SSEF and with the support of AGL and GIT.





Editor-in-Chief

Brendan M. Laurs
brendan.laurs@gem-a.com

Production Editor

Mary A. Burland
mary.burland@gem-a.com

Marketing Consultant

Ya'akov Almor
bizdev@gem-a.com

Executive Editor

James H. Riley

Editor Emeritus

Roger R. Harding

Assistant Editor

Michael J. O'Donoghue

Associate Editors

Edward Boehm, *RareSource, Chattanooga, Tennessee, USA*; Alan T. Collins, *King's College London*; John L. Emmett, *Crystal Chemistry, Brush Prairie, Washington, USA*; Emmanuel Fritsch, *University of Nantes, France*; Rui Galopim de Carvalho, *Portugal Gemas, Lisbon, Portugal*; Lee A. Groat, *University of British Columbia, Vancouver, Canada*; Thomas Hainschwang, *GGTL Laboratories, Balzers, Liechtenstein*; Henry A. Hänni, *GemExpert, Basel, Switzerland*; Jeff W. Harris, *University of Glasgow*; Alan D. Hart, *The Natural History Museum, London*; Ulrich Henn, *German Gemmological Association, Idar-Oberstein*; Jaroslav Hyršl, *Prague, Czech Republic*; Brian Jackson, *National Museums Scotland, Edinburgh*; Stefanos Karamelas, *Gübelin Gem Lab Ltd., Lucerne, Switzerland*; Lore Kiefert, *Gübelin Gem Lab Ltd., Lucerne, Switzerland*; Hiroshi Kitawaki, *Central Gem Laboratory, Tokyo, Japan*; Michael S. Krzemnicki, *Swiss Gemmological Institute SSEF, Basel*; Shane F. McClure, *Gemmological Institute of America, Carlsbad, California*; Jack M. Ogden, *Striptwist Ltd., London*; Federico Pezzotta, *Natural History Museum of Milan, Italy*; Jeffrey E. Post, *Smithsonian Institution, Washington DC, USA*; Andrew H. Rankin, *Kingston University, Surrey*; George R. Rossman, *California Institute of Technology, Pasadena, USA*; Karl Schmetzer, *Petershausen, Germany*; Dietmar Schwarz, *AIGS Lab Co. Ltd., Bangkok, Thailand*; Menahem Sevdemish, *GemeWizard Ltd., Ramat Gan, Israel*; Guanghai Shi, *China University of Geosciences, Beijing*; James E. Shigley, *Gemmological Institute of America, Carlsbad, California*; Christopher P. Smith, *American Gemological Laboratories Inc., New York*; Evelyne Stern, *London*; Elisabeth Strack, *Gemmologisches Institut, Hamburg, Germany*; Tay Thyé Sun, *Far East Gemological Laboratory, Singapore*; Pornsawat Wathanakul, *Gem and Jewelry Institute of Thailand, Bangkok*; Chris M. Welbourn, *Reading, Berkshire*; Joanna Whalley, *Victoria and Albert Museum, London*; Bert Willems, *Leica Microsystems, Wetzlar, Germany*; Bear Williams, *Stone Group Laboratories LLC, Jefferson City, Missouri, USA*; J.C. (Hanco) Zwaan, *National Museum of Natural History 'Naturalis', Leiden, The Netherlands*.

Content Submission

The Editor-in-Chief is glad to consider original articles, news items, conference/excursion reports, announcements and calendar entries on subjects of gemmological interest for publication in *The Journal of Gemmology*. A guide to the preparation of manuscripts is given at www.gem-a.com/publications/journal-of-gemmology.aspx, or contact the Production Editor.

Subscriptions

Gem-A members receive *The Journal* as part of their membership package, full details of which are given at www.gem-a.com/membership.aspx. Laboratories, libraries, museums and similar institutions may become Direct Subscribers to *The Journal* (see www.gem-a.com/publications/subscribe.aspx).

Advertising

Enquiries about advertising in *The Journal* should be directed to the Marketing Consultant. For more information, see www.gem-a.com/publications/journal-of-gemmology/advertising-in-the-journal.aspx.

Copyright and Reprint Permission

Abstracting with credit to the source, photocopying isolated articles for noncommercial classroom use, and photocopying by libraries for private use of patrons, are permitted. Requests to use images published in *The Journal* should be directed to the Editor-in-Chief. Give the complete reference citation and the page number for the image(s) in question, and please state how and where the image would be used.

The Journal of Gemmology is published quarterly by Gem-A, The Gemmological Association of Great Britain. Any opinions expressed in *The Journal* are understood to be the views of the contributors and not necessarily of the publisher.

Printed by DG3 (Europe) Ltd.

© 2015 The Gemmological Association of Great Britain

ISSN: 1355-4565



21 Ely Place
London EC1N 6TD
UK

t: +44 (0)20 7404 3334
f: +44 (0)20 7404 8843
e: information@gem-a.com
w: www.gem-a.com

Registered Charity No. 1109555
Registered office: Palladium House,
1-4 Argyll Street, London W1F 7LD

President

Harry Levy

Vice Presidents

David J. Callaghan, Alan T. Collins,
Noel W. Deeks, E. Alan Jobbins,
Michael J. O'Donoghue,
Andrew H. Rankin

Honorary Fellows

Gaetano Cavalieri, Terrence S.
Coldham, Emmanuel Fritsch

Honorary Diamond Member

Martin Rapaport

Honorary Life Members

Anthony J. Allnutt, Hermann Bank,
Mary A. Burland, Terence M.J.
Davidson, Peter R. Dwyer-Hickey,
Gwyn M. Green, Roger R. Harding,
John S. Harris, J. Alan W. Hodgkinson,
John I. Koivula, Jack M. Ogden,
C.M. (Mimi) Ou Yang, Evelyne Stern,
Ian Thomson, Vivian P. Watson,
Colin H. Winter

Chief Executive Officer

James H. Riley

Council

Mary A. Burland, Jessica M. Cadzow-
Collins, Paul F. Greer, Alan D. Hart,
Nigel B. Israel, Jonathan Lambert,
Richard M. Slater, Miranda E.J. Wells

Branch Chairmen

Midlands – Georgina E. Kettle
North East – Mark W. Houghton
South East – Veronica Wetten
South West – Richard M. Slater

Understanding Gems™

What's New

INSTRUMENTS AND TECHNIQUES

Automated Melee Screening (AMS) Device

After several years in development, in early 2015 The De Beers Group of Companies' International Institute of Diamond Grading and Research released their diamond melee screening device to the broad diamond trade. The AMS device automatically tests colourless to near-colourless parcels. The samples are fed from a hopper to a fibre-optic probe that is linked to two spectrometers. The instrument accommodates up to 500 carats of 0.01–0.20 ct round brilliants at a time, and can process 360 samples per hour. The AMS will refer for further testing all synthetics and simulants, and typically ~98% of natural diamonds will 'pass' and require no further examination (type II stones are referred for further testing). It has a 42 × 26 × 23 cm footprint and comes with a compact computer that is used to control the instrument. The cost is US\$55,000 plus a three-year software licence, support and warranty contract paid in annual instalments of \$10,000. For more information, visit www.iidgr.com/en/services/verification-instruments or email contact@iidgr.com.



Rachelle Grabowski (info@rcopriter.com)

DFI Mid-UV Laser⁺ Diamond Screening System

In March 2015, GGTL Laboratories announced the commercialisation of their Diamond Fluorescence Imaging (DFI) Mid-UV Laser⁺ diamond screening system. This instrumentation, which is available to diamond and jewellery manufacturers and dealers, uses a combination of fluorescence microscopy with photoluminescence and Raman

spectroscopy. The system employs up to six different UV excitations plus a 405 nm (violet) laser, and contains optical components of the highest quality. It permits the screening of up to 3,000 near-colourless diamonds per hour when used by a well-trained technician. (To guarantee best results, the system is non-automated, and the operator will be able to efficiently screen melee parcels after a brief training period.)

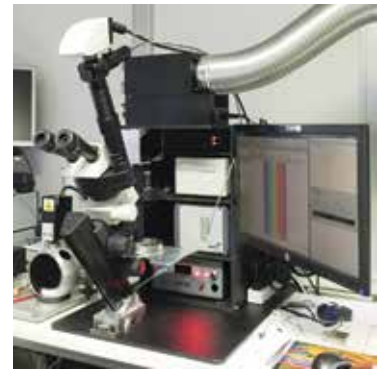
Loose as well as mounted diamonds of any size and shape can be tested, and the results are typically final: natural, synthetic or imitation. Generally there is no need to send questionable stones to a laboratory for further analysis.

Besides the screening of (near-)colourless diamonds, the DFI system can be used for many other gemmological applications, such as the testing of corundum and spinel for synthetics, simulants and treatments. (Users highly experienced in fancy-colour diamond identification can also use it for screening such gems, but this task is far more difficult.) The instrument has a low operational cost of US\$1,000 per year (not including electricity) when used eight hours per day.

Interested parties can visit the Geneva or Balzers laboratory for a demonstration. For more information, visit www.ggtl-lab.org/science/newsletter (click on GGTL Newsletter No. 4) or email info@ggtl-lab.org.

*Dr Thomas Hainschwang FGA and Franck Notari
(thomas.hainschwang@ggtl-lab.org)*

*GGTL Laboratories
Balzers, Liechtenstein and Geneva, Switzerland*



DiaCam360 for Onsite Diamond Photography

Released by Shirtal Diamonds in February 2015 during the International Diamond Week in Ramat Gan, Israel, the DiaCam360 enables portable



professional-quality diamond photography using electronic scanning so diamonds can remain on premises. The device can create high-quality photos and 360° interactive videos of diamonds of various shapes weighing up to 20 ct. The scans are

customizable, and can accommodate a written description as well as a company logo. DiaCam360 files may be embedded into retailer websites, Rapnet, or other selling platforms.

The DiaCam360 does not require additional camera equipment or special photography skills. The device package includes cloud storage for up to 300 scans, quarterly cleaning/calibration and software updates. Visit www.diacam360.com.

Rachelle Grabowski (info@copywriter.com)

GemmoSphere UV-Vis-NIR Spectrometer

In late May 2015, at the JCK jewellery show in Las Vegas, Nevada, USA, M&A Gemological In-

struments (MAGI) debuted a prototype of the GemmoSphere. This UV-Vis-NIR spectrometer has a wavelength range of 365–1000 nm with 1 nm resolution. It produces consistent and repeatable readings due to a precisely manufactured integrating sphere/sample chamber. It is specifically designed to fit an accessory for liquid nitrogen immersion of the sample, which is an important capability for diamond analysis. Following MAGI's philosophy of providing the gemmologist with instruments that are simple and straightforward to use, the GemmoSphere comes with software that provides a user interface consistent with both the GemmoRaman532 and GemmoFTIR spectrometers. Orders for the GemmoSphere will be taken starting in August 2015 (approximately €6000) from MAGI's website (www.gemmoraman.com/GemmoSphere.aspx) and from company representatives.

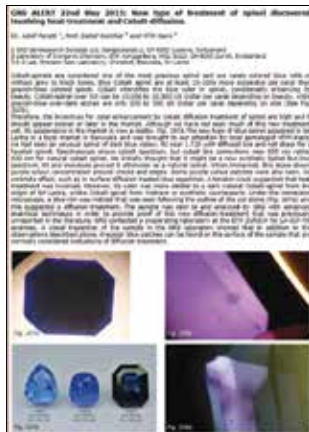


*Alberto Scarani and Mikko Åström (info@gemmoraman.com)
M&A Gemological Instruments
Rome, Italy and Järvenpää, Finland*

NEWS AND PUBLICATIONS

Cobalt Diffusion Treatment of Spinel

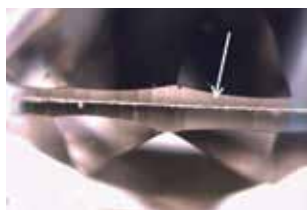
In May 2015, GRS GemResearch Swisslab issued an alert informing the trade about a new colour enhancement of spinel using cobalt diffusion treatment. The report describes a 5.95 ct very dark blue stone that was obtained from a local market in Beruwala, Sri Lanka. Visit www.gemresearch.ch/news/2015-05-22_Diffusion_Treatment/index.htm.



In June 2015, the Gemological Institute of America (GIA) posted a more detailed report on this treatment that describes the properties of 18 samples obtained from a company in Bangkok, Thailand, that reportedly developed the treatment. The samples weighed 0.35–4.99 ct and showed medium to dark blue coloration. The report can be downloaded at www.gia.edu/gia-news-research/cobalt-diffusion-natural-spinel-report.

Diamond-Diamond Doublet Detected in Antwerp

In September 2014, HRD Antwerp issued an online report (www.hrd.be/en/news/a-different-type-of-deception-diamond-diamond-doublet) on a diamond-diamond doublet. As with other doublets, this composite was comprised of two stones cemented together at the girdle. What made this doublet unusual, however, was that both pieces were diamond. Microscopic analysis of the 0.89 ct sample showed unusually strong internal reflections as well as a join line in the middle of the faceted girdle.



The binding material was evidenced by a different RI than the stones, as well as gas bubbles. IR spectroscopy confirmed that both sections of the composite were type IaAB diamond, although tests did not reveal whether they were natural, treated or synthetic.

It is likely that more such diamond-diamond doublets will enter the market; fortunately, their strong internal reflections and join lines make these doublets easy for experienced diamond graders to detect.

Rachelle Grabowski (info@rcopywriter.com)

GIA Laboratory Alert for Diamond Colour Treatment

In May 2015, the GIA Laboratory indicated that approximately 500 colourless to near-colourless diamonds that were submitted mainly to their Israel laboratory appeared to have been subjected to a new treatment that temporarily masks the body colour of the stone (see www.gia.edu/gemlab/laboratory-alert-may-2015). This may improve the apparent colour by up to three grades. The stones ranged from 0.44 to 5.19 ct and were mostly colour-graded E–H. GIA has posted the report numbers for these diamonds on the website above, and has requested that anyone who has such stones resubmit them for review.

ICGL Newsletter

The International Consortium of Gem-Testing Laboratories has released the Summer 2015 issue of their newsletter (No. 2/2015), available at <http://icglabs.org>. It focuses on tourmaline from Afghanistan, with rarely seen photos of the mines as well as images of exceptional specimens and inclusion features seen in faceted stones.



Low-Temperature Heat Treatment of Mozambique Ruby

In April 2015, the GIA Laboratory posted a report describing the treatment process and identifica-



tion of red-to-pink corundum that has undergone low-temperature treatment. Experiments were performed on Mozambique ruby in collaboration with heat treaters in Sri Lanka and Thailand (where the temperatures reached approximately 550–750 °C). Access the report at www.gia.edu/gia-news-research-low-temperature-heat-treatment-mozambique-ruby.

Microcrystalline Silica Online Lectures

Noted volcanologist Dr Marco Campos-Venuti has developed a comprehensive series of free video lectures on the genesis of microcrystalline silica. The lectures are available at www.agatesandjaspers.com/VIDEO.html, which provides links to the videos on YouTube. Each narrated and illustrated lecture is approximately 15–30 minutes long and covers a unique subtopic related to jasper, agate, or silica. Dr Campos-Venuti starting posting the videos in April 2015, and new lectures are released weekly. Topics include oceanic, volcanic and chemical jaspers, 'thunder eggs', chalcedony, banded agate, lace agate and natural glasses. The entire lecture series comprises 25 videos.

Rachelle Grabowski (info@rcopywriter.com)

What's New in the Mineral World?

For years, *Mineralogical Record* has issued free online reports titled *What's New in the Mineral World?* that document new mineral finds as well as old specimens that become available on the market. Although oriented toward mineral collectors, some items of interest to gemmologists that appeared in 2014 include tourmaline from Brazil, Tanzania and Nepal; gem-quality wurtzite and colour-change axinite-(Mg) from Merelani, Tanzania; demantoid from Iran; benitoite from California; and daylight-luminescent hyalite opal from Mexico (as reported in this issue of *The Journal*). In recent years, the reports have been posted in the months of March–April, July–August, and November–December. Visit www.mineralogicalrecord.com/whatsnew.asp.

What's New provides announcements of new instruments/technology, publications, online resources and more. Inclusion in What's New does not imply recommendation or endorsement by Gem-A. Entries are prepared by Brendan Laurs unless otherwise noted.

A Matched Pair of Opals, with a Catch

Alan Hodgkinson

Fine black opals that display the entire spectrum of vivid play-of-colour are seldom encountered. To find such a pair of black opals that match well in shape, colour and pattern is even rarer. The fairly well-matched pair shown in Figure 1 is even more unusual, as one sample is natural and the other is synthetic! Can you tell the difference by looking at the photograph? Admittedly, making this distinction from a photo is more demanding than seeing the samples in the hand. Look first—the answer is revealed below.

The natural stone's identity is well established: it comes from the Lightning Ridge area of New South Wales, Australia, and was probably mined in the late 1920s. Such material found near the surface tends to be stable and not craze, since it has had a long period to acclimatize to the near-surface environment.

The synthetic opal was cut from a parcel of rough that was generously donated to this author for teaching purposes by New York opal dealer Gerry Manning. The specimens covered a range of opal varieties, including milky white material with little play-of-colour, lively 'crystal' opal and semi-black specimens. At the top end of appearance, there emerged after cabochon-cutting a number of attractive black opals—all of which were synthetic. They



Figure 1: These two gems show vivid play-of-colour and are fairly well-matched according to their shape, colour and pattern. The 3.00 ct stone on the left is a natural black opal from Lightning Ridge, Australia, while the 2.14 ct sample on the right is a synthetic opal. Photo by A. Hodgkinson.

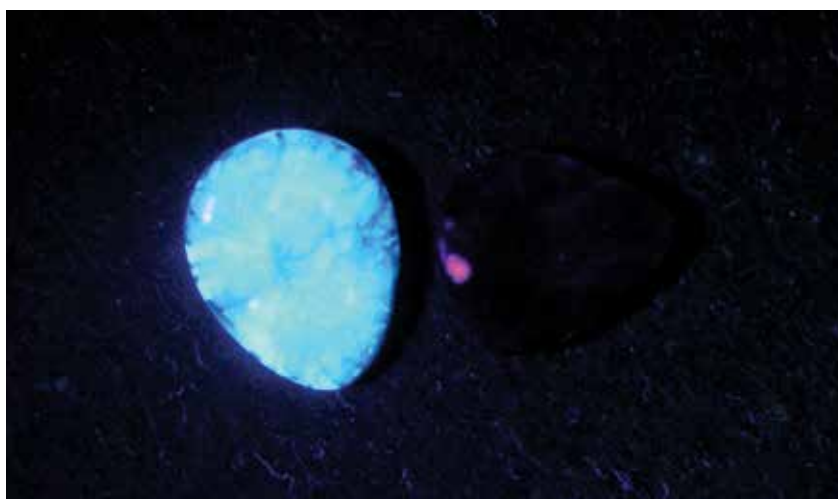


Figure 2: The samples in Figure 1 are shown exposed to 365 nm long-wave UV radiation from an LED lamp. The natural opal fluoresces bright pale blue, while the synthetic is inert (the violet area is a reflection from the lamp on the edge of the cabochon). Photo by A. Hodgkinson.

were produced by Kyocera Co. of Japan, which had bought the patent from the original commercial opal synthesizer: a Frenchman named Pierre Gilson. 'Gilson-created Opal'

initially appeared in 1974, two years after his patent was issued, and 10 years after the original breakthrough by Australians P. J. Darragh, A. J. Gaskin and J. V. Sanders (Nassau, 1980).

There appeared to be no telltale ‘chicken wire’ pattern in the synthetic opal cabochons when viewed superficially with a 10× loupe. However, further examination between crossed polarizers revealed a small area of this pattern in one of the samples. Nevertheless, gemmologists should be careful with using the ‘chicken wire’ pattern to identify synthetic opal, since in this author’s experience a similar structural appearance may be seen in some opals from Virgin Valley, Nevada.

Long-wave UV radiation provides a useful indication of natural opal (i.e. a strong pale blue fluorescence is often seen), but the less-experienced gemmologist may believe this applies only to white or ‘crystal’ opal. In fact, the natural black opal in Figure 1—seen on the left—showed strong fluorescence (Figure 2). The luminescence shown in the photo was induced by a 365 nm LED lamp. When a traditional long-wave UV lamp was used, the fluorescence was greenish blue and not as strong. While it is known that some synthetic opal does fluoresce a strong bluish white to long-wave UV radiation (e.g. Gunawardene and Mertens, 1984), what clinched the natural identity of this stone was its phosphorescence. After the UV lamp was switched off, the opal continued to emit a dim whit-



Figure 3: Some reportedly ‘synthetic’ opals (actually simulants) contain so much plastic stabilizer that they burn when exposed to flame. These simulants are distinct from those that are entirely plastic. Photo by A. Hodgkinson.

ish blue glow for 10 seconds (initially at perhaps 20% of the brightness of the fluorescence). It is interesting to note that the fluorescence pattern mirrored some subtle structural anomalies seen in the play-of-colour of the opal. Short-wave UV radiation at 253 nm also induced similar fluorescence and phosphorescence.

For many years, Manning was plagued by companies selling so-called ‘Japanese’ synthetic opals—under the ‘Gilson’ name—that contained up to 50+% of a plastic filler. (Such material does fluoresce to long-wave UV radiation, but there is no phosphorescence.) So exasperated was Manning

that he delighted in setting fire to the blatant counterfeit material with a cigarette lighter (e.g. Figure 3). Rather than a synthetic, this plastic-rich material is described more accurately as an opal *simulant*. Gilson’s material is correctly described as *synthetic*, although some have questioned the use of this terminology for his later production.

Just as for natural opal, the Gilson synthetic shown on the right in Figure 1 would not ignite if combustion tested. However, there is a strong possibility that any opal specimen, whether natural or synthetic, would craze or even crack if so burned. Obviously, observing the fluorescence/phosphorescence of opal is a much better alternative than burning it, which is perhaps the ultimate example of destructive testing.

References

- Gunawardene M. and Mertens R., 1984. Gilson created fire opal imitation with play of colours. *Journal of Gemmology*, **19**(1), 43–53, <http://dx.doi.org/10.15506/jog.1984.19.1.43>.
- Nassau K., 1980. *Gems Made by Man*. Chilton Book Co., Radnor, Pennsylvania, USA.

Alan Hodgkinson FGA DGA is a gemmology instructor and lecturer from Ayrshire, Scotland. E-mail: alan-hodgkinson@talktalk.net

Renew your Membership to continue using your FGA or DGA status and to gain access to *The Journal of Gemmology*, *Gems&Jewellery* and *GemTalk*, and to receive discounts on events and on Gem-A Instruments purchases

Contact membership@gem-a.com today to renew

Gem Notes

COLOURED STONES

Chrysocolla Chalcedony from Spain

Chrysocolla chalcedony is an attractive green-to-blue material that is commonly marketed as 'gem silica'. At the 2015 gem shows in Tucson, Arizona, USA, Gems in Gems (Seville, Spain) had some chrysocolla chalcedony from a new locality: Rio Tinto in the Seville area of Spain. Sold as 'Sea Stone', the material was gathered in May 2014 from the surface of an old copper mine. Approximately 40 kg of rough material were recovered from a silicified zone of the deposit, which also contained chalcedony pseudomorphs after barite, calcite and other minerals.

Nearly 20 cabochons containing chrysocolla chalcedony have been polished so far, in sizes from 17 × 25 mm to 22 × 38 mm. The material ranges from green (Figure 1) to greenish blue (Figure 2), and forms irregular masses within various amounts of matrix. Particularly common are chrysocolla chalcedony infillings in milky white vein quartz. The diaphaneity of the chrysocolla chalcedony ranges from translucent to semi-transparent. According to Gems in Gems, the material has not been treated in any way.



Figure 1: Spain is the source of this chrysocolla chalcedony (~3.2 cm wide), which formed in association with milky white vein quartz. Courtesy of Gems in Gems.

Recently a new locality in the same area was discovered that contains even thicker veins of chrysocolla chalcedony, so the outlook for future production of high-quality material is quite encouraging.

Acknowledgement: Gems in Gems is thanked for donating to Gem-A the cabochon shown in Figure 2 (left).

Brendan M. Laurs FGA

Figure 2: Cabochons of the Spanish chrysocolla chalcedony (here, containing predominantly greenish blue masses) have been cut with varying amounts of matrix. Photos by B. M. Laurs (left, 3.1 cm tall) and courtesy of Gems in Gems (right, image width 5 cm).



Rhodochrosite from Brazil

Rhodochrosite usually occurs as translucent to opaque, fine-grained aggregates, often showing a banded pattern of white and pink due to the presence of impurities. Less common are transparent gem-quality pink-to-red crystals, known particularly from the Sweet Home mine in Colorado, USA, and also from the Kalahari Desert region in South Africa and from Guangxi, China (e.g. Webster, 1994; Moore et al., 1998; Lees, 2009).

During the 2015 Tucson gem shows, gem dealer Mark Kaufman (Kaufman Enterprises, San Diego, California, USA) had some rough and cut transparent rhodochrosite from another locality: Brazil. He obtained 12 damaged crystals that were reportedly mined several years ago from a pegmatite in Minas Gerais State. Kaufman faceted 15 stones ranging from 0.4 ct to nearly 8 ct, and loaned one cut specimen and one crystal (Figure 3) to this author for examination.

The crystal weighed 16.99 g, and the cushion-shaped faceted stone measured 16.60 × 9.56 × 5.92 mm and weighed 7.78 ct. The crystal showed a somewhat thick tabular habit, with large prismatic and rhombohedral faces. Several shallow cleavage fractures were present just under the crystal's surface, oriented in three directions parallel to the rhombohedral faces (Figure 4, left). The surface itself appeared slightly etched with a matt lustre, but the inner part of the crystal appeared to be completely transparent and very clean.



Figure 3: This crystal and faceted stone of rhodochrosite from Brazil weigh 16.99 g and 7.78 ct, respectively. Photo by Dirk van der Marel.

The faceted stone showed a saturated red-pink colour and high transparency. The stone displayed strong doubling of the facet junctions, consistent with the large double refraction of carbonate minerals such as rhodochrosite. RI readings confirmed this, with one shadow line at a minimum value of 1.603 and a higher value that was above the limit of the refractometer (i.e. greater than ~1.79). The birefringence of rhodochrosite is 0.22 (e.g. Webster, 1994), which means that the higher RI was probably around 1.823. The lower RI of 1.603 stayed constant when the stone was rotated 360° on the hemicylinder. As rhodochrosite is uniaxial negative, this indicates that the table was cut exactly 90° to the c-axis, parallel to a prismatic crystal face.

Moderate dichroism was observed, in pinkish red (red in the crystal) and light pinkish orange.

Figure 4: Near the surface, the rhodochrosite crystal showed perfect cleavage (left, image width 0.9 mm). Needle-like inclusions were present in the otherwise exceptionally clean, faceted rhodochrosite (right, image width 0.5 mm). Photomicrographs by J. C. Zwaan.

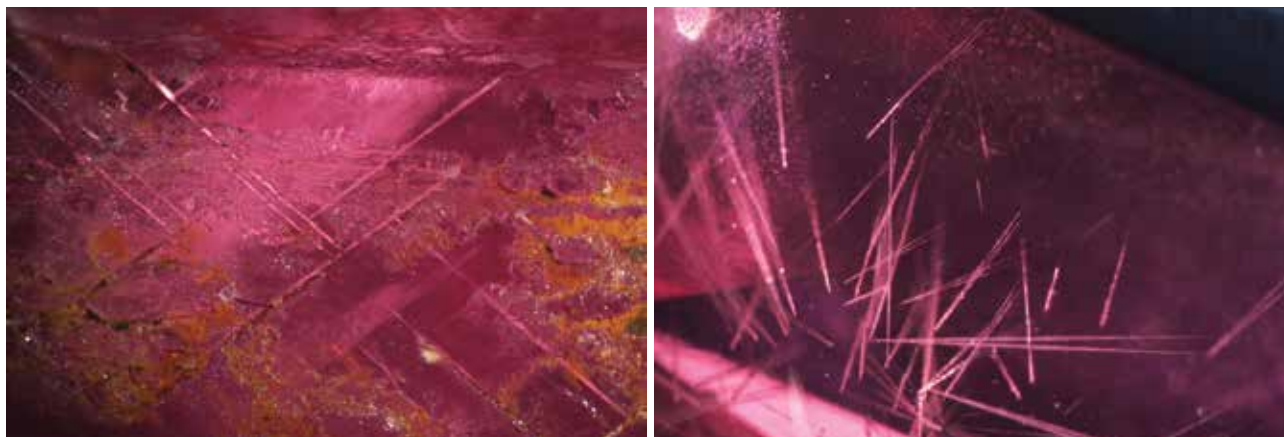
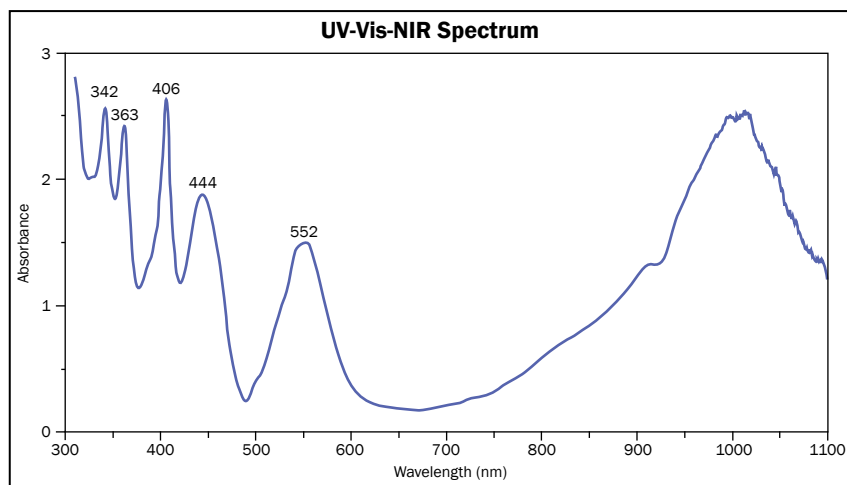


Figure 5: This UV-Vis-NIR spectrum of the Brazilian rhodochrosite crystal, taken parallel to the c-axis, shows absorption peaks on the left side that are due to the presence of Mn^{2+} , and a broad band centred around 1000 nm that is related to Fe^{2+} .



The samples were inert to long-wave UV radiation, but fluoresced a weak red to short-wave UV. A prism-type spectroscope showed a dark band at ~410 nm and weaker bands at ~450 and 550 nm. These properties, and a hydrostatic SG of 3.72, are fairly consistent with those expected for rhodochrosite (with the RI and SG values being the highest known for this mineral; cf. Webster [1994], who reported RIs of 1.600–1.820 and an SG range of 3.45–3.70).

The faceted stone contained needle-like inclusions on one side (Figure 4, right), but was otherwise clean. Raman analysis of these inclusions at the surface of the stone was not conclusive; the weak spectra suggested the presence of barite and mica. The needles were not seen in the crystal fragment, which instead contained small two-phase inclusions. Raman analysis of the stone itself revealed an almost perfect (99%) match with rhodochrosite from the Sweet Home mine in the RRUFF database.

Energy-dispersive X-ray fluorescence spectroscopy (EDXRF) analyses showed mainly Mn and some Fe, with traces of Ca and Mg. Taking into account the presence of CO_2 , recalculated values gave 55.6–56.0 wt.% MnO, 5.48–5.74 wt.% FeO, 0.26–0.29 wt.% CaO and ≤ 0.30 wt.% MgO. Chemical analysis further indicated that the small amount of matrix on one side of the crystal (Figure 3) consisted of K-feldspar and iron sulphide.

Ultraviolet-visible–near infrared (UV-Vis-NIR) absorption spectra (e.g. Figure 5) gave a more detailed picture of what was observed with the spectroscope, with pronounced peaks at ~340, 360 and 410 nm, accompanied by bands at ~440 and 550 nm, and a broad band around 1000

nm, creating a transmission window at around 650–700 nm that is responsible for the pink-red colour. The left part of the spectrum is similar to that of manganese(II) hydrate $[Mn(H_2O)_6]^{2+}$, with all the peaks attributed to the electron transitions related to the presence of Mn^{2+} , while the broad band at around 1000 nm is related to the presence of Fe^{2+} (cf. Jørgensen, 1954).

In light of rhodochrosite's perfect cleavage in three directions, as well as the softness of the material (3½–4 on the Mohs scale), the remarkably clean gemstone of 7.78 ct, which did not show any sign of incipient cleavage, is a true piece of craftsmanship.

Although Kaufman's supplier did not indicate the exact origin of this material within Brazil, a small amount of similar gem-quality

Figure 6: Although not studied for this report, these specimens of rough (5 cm across) and cut (11.97 ct) rhodochrosite also were produced in Brazil, from the Toca da Onça pegmatite in Minas Gerais State. Photo courtesy of Elliott/Fine Minerals International.



rhodochrosite was reportedly found at a granitic pegmatite (Xanda mine) in Minas Gerais in 2013 (www.minfind.com/mineral-203128.html), and rhodochrosite also was recovered prior to May 2014 at the Toca da Onça pegmatite (Virgem da Lapa, Jequitinhonha Valley, Minas Gerais; Figure 6). According to Daniel Trinchillo (Fine Minerals International, Edison, New Jersey, USA), the latter discovery may have produced >500 g of rough material. The Toca da Onça pegmatite has historically been mined for blue tourmaline.

*Dr J. C. (Hanco) Zwaan FGA
(hanco.zwaan@naturalis.nl)*

*National Museum of Natural History 'Naturalis'
Leiden, The Netherlands*

References

- Jørgensen C.K., 1954. Studies of absorption spectra—IV. Some new transition group bands of low intensity. *Acta Chemica Scandinavica*, **8**, 1502–1512, <http://dx.doi.org/10.3891/acta.chem.scand.08-1502>.
- Lees B., 2009. Gem News International: Gem-quality rhodochrosite from China. *Gems & Gemology*, **45**(1), 60–61.
- Moore T., Lees B.K., Weinrich K.J., Voynick S., Murphy J.A., Hurlbut J.F., Reynolds T.J., Aument-Modreski R., Misantoni D. and Silberman M.L., 1998. The Sweet Home mine, Park County, Colorado. *Mineralogical Record*, **29**(4), 7–153.
- Webster R., 1994. *Gems: Their Sources, Descriptions and Identification*, 5th edn., revised by P.G. Read. Butterworth-Heinemann, Oxford, p. 1026.

Tourmaline Mining in the Democratic Republic of the Congo

For many years, the Democratic Republic of Congo (DRC) has been a source of gem tourmaline—particularly the Virunga region in North Kivu, located north of the capital city of Goma (Laurs et al., 2004; Henn, 2010). In April 2014, gem dealer Farooq Hashmi (Intimate Gems, Glen Cove, New York, USA) visited another tourmaline-producing area in DRC: Numbi, in the South Kivu region. Located 40 km (by air) west of Goma, Numbi is reached from Goma by travelling by car for approximately three hours on mostly unpaved roads and then by motorbike for another three to four hours on a rough muddy track.

Hashmi reported that there were two main mining areas for tourmaline near Numbi; at both localities, columbite-tantalite minerals are recovered as a by-product. One area is about 30 minutes' walk from the town, and is situated in a lush valley. The alluvial deposits there were mined from beneath 1–4 m of overburden using simple hand tools (e.g. Figure 7). Small gasoline-powered pumps were used to remove water from the pits. Hashmi witnessed active mining in several pits, and also passed numerous abandoned diggings over a distance of 1–2 km. The second mining area was reached by hiking

Figure 7: This open pit near Numbi, DRC, is being excavated with hand tools to reach an alluvial layer containing gem tourmaline and columbite-tantalite minerals. Photo by Farooq Hashmi.



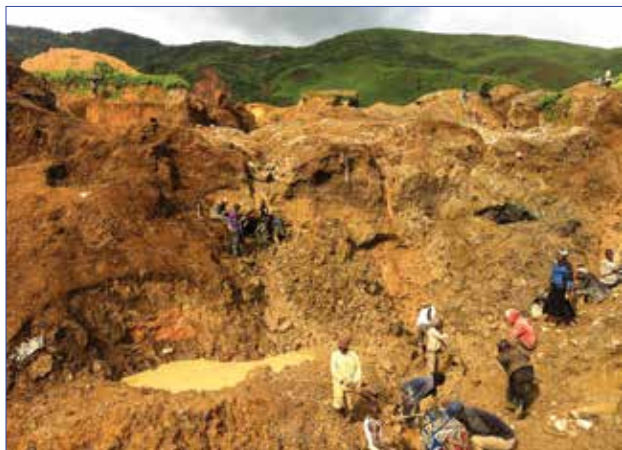


Figure 8: Tourmaline is also mined from the base of this hillside near Numbi. Photo by Farooq Hashmi.

an additional 1 km, and was located at the base of a hillside (e.g. Figure 8). Here eluvial and possibly some primary deposits were being mined, again using hand tools. Some morganite and pale yellow apatite also were recovered from unspecified deposits in the Numbi area, but the latter was generally not of gem quality.

The miners sold their production to brokers, who then distributed the material to others in Numbi town before it was taken to Goma. Hashmi saw 50–100 kg of tourmaline rough while in Numbi, but most was fractured and suitable only for cutting cabochons. He obtained ~3 kg of clean material (e.g. Figure 9), and the largest clean piece ('peach' coloured) weighed ~20 g. Most of the tourmaline was yellowish green to green (60–70%) and orangy pink to purplish pink (30–40%); blue was rarely seen, unlike from the North Kivu area mentioned above.



Figure 9: Tourmaline rough from the Numbi area is typically green or pink and shows variable amounts of rounding. Photo by Farooq Hashmi.

The Numbi mining area appears to be quite extensive, and should continue to produce small amounts of gem tourmaline for several years.

Brendan M. Laurs FGA

References

- Henn U., 2010. Turmaline aus dem Kongo. *Gemmologie: Zeitschrift der Deutschen Gemmologischen Gesellschaft*, **59**, 111–113.
- Laurs B.M., Simmons W. and Falster A., 2004. Gem News International: Gem tourmaline from Congo. *Gems & Gemology*, **40**(3), 263–265.

Colour-zoned Cr- and V-bearing Tourmaline from Kenya

Green tourmaline containing Cr and/or V, commonly known as 'chrome tourmaline' in the trade, is an attractive gem variety known mainly from East Africa. During the 2015 Tucson gem shows, gem dealer Dudley Blauwet (Dudley Blauwet Gems, Louisville, Colorado, USA) had some unusual colour-zoned chrome tourmalines that reportedly came from Makuki, Kenya. He first encountered this material in August 2014, when he obtained four gem 'pencils' (6.41 g total

weight) from an East African rough dealer. The crystals were colour-zoned perpendicular to the c-axis in shades of light and dark green. Cutting of two of these crystals yielded gems weighing 4.44 and 6.11 ct. Blauwet loaned one crystal and one of the faceted stones to these authors for examination (Figure 10).

The crystal was a well-formed trigonal prism weighing 1.68 g and measuring 21.27 × ~6.7 mm. The faceted stone weighed 6.11 ct and measured



Figure 10: These rough and cut Cr- and V-bearing tourmalines show distinct colour zoning perpendicular to the c-axis. The crystal is ~21 mm long and the cut stone weighs 6.11 ct. Photo by B. Williams.

18.04 × 6.42 × 5.85 mm; it was polished in the classic tourmaline style of a step cut with a long keel oriented parallel to the c-axis. Both samples were similar in colour and also in their colour variations, ranging from a medium-dark green to a light yellowish green with some colour banding. The gems appeared darker when viewed down the c-axis, as expected for tourmaline, but did not exhibit the typical over-dark appearance (or 'closed' c-axis) seen in many tourmalines of comparable saturation.

The faceted sample was eye-clean and exhibited some minor planar growth zoning in the microscope. The crystal exhibited several shallow cracks approximately perpendicular to the c-axis. Viewed through a Chelsea colour filter, both stones displayed shades of red and pink, with the redder reactions corresponding to areas of darker green coloration. RI values varied along the length of the faceted stone: at the darker end they were 1.617 and 1.638 (birefringence 0.021), while the lighter end gave readings of 1.610 and 1.630 (birefringence 0.020). Raman spectroscopy confirmed the stones were tourmaline, with peaks characteristic of elbaite, uvite and dravite. (Quantitative chemical analyses would be necessary to establish the actual tourmaline species present.) Qualitative EDXRF spectroscopy

showed a higher Ca content in the darker end of the cut stone. The tourmaline chromophores Ti, V, Cr, Mn and Fe were all present in minor amounts, with much more V in the darker green areas, together with somewhat higher Ti and Cr concentrations.

Dichromatism was observed when a light was shined along the c-axis (Figure 11): both samples showed a red tint when viewed down the longer light paths. This appearance has also been referred to as the *Usambara effect* (e.g. Halvorsen, 2006; Pearson and Hoover, 2014).

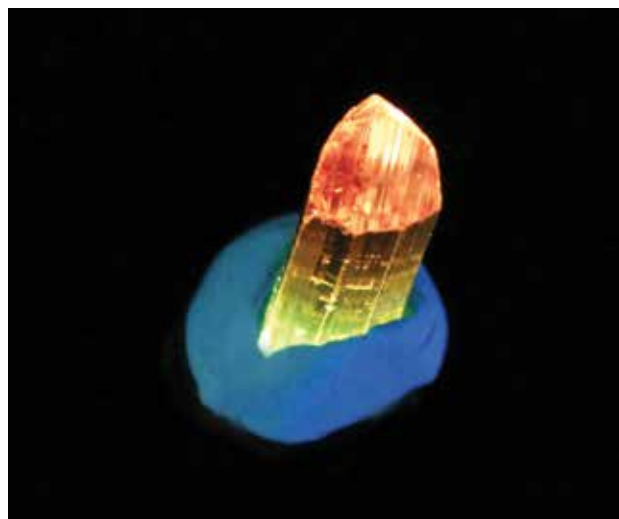
Blauwet reported obtaining some additional crystals of Makuki tourmaline from his supplier at the 2015 Tucson gem shows. Most of this later material was not colour zoned, and it was faceted into nine pieces weighing a total of 20.05 carats. It is unclear if more of this tourmaline will become available in the future.

Cara Williams FGA and Bear Williams FGA
(info@stonegrouplabs.com)
Stone Group Laboratories
Jefferson City, Missouri, USA

References

- Halvorsen A., 2006. The Usambara effect and its interaction with other colour change phenomena. *Journal of Gemmology*, **30**(1), 1–21, <http://dx.doi.org/10.15506/jog.2006.30.1.1>.
- Pearson G. and Hoover D., 2014. Dichromatism, the cause of the Usambara and the alexandrite colour-change effects. *Australian Gemmologist*, **25**(2), 62–70.

Figure 11: A red tint is seen when the tourmaline is viewed along the longer light path, down the c-axis. The crystal is ~6.7 mm in diameter. Photo by B. Williams.



PEARLS

Pearl Marking: An Innovative Non-destructive Method

During the past few years, the gem and jewellery market has increasingly demanded better product knowledge, in particular regarding product origin and traceability. Various worldwide organizations have attempted to address this need with 'best practice' codes and verification systems. The cultured pearl industry also faces issues of traceability, and since the culturing process often uses a bead for nucleation, several projects have focused on the concept of bead marking and related means of recognition (Hänni and Cartier, 2013).

In March 2014, a relatively new technique for pearl tagging called 'Heart of Pearls' (HoP) was presented to the LFG (French Gemmological Laboratory) by Jean-Pierre Le Pollès (Auffargis, France). The technique was designed with the cultured pearl industry in mind, but it may be applied to natural as well as cultured pearls, including those mounted in jewellery.

The HoP concept is very simple: application of a very small label designed not to distract the eye but nevertheless to be quite easy to find with magnification. The microscopic label (e.g. Figure 12) carries a high-resolution holographic image to ensure authenticity, and further security is provided by an embedded invisible coding. (Note: To protect the security of this technique, which is patent pending, the coding specifications are not described here, and the tags shown in this report are samples.) The tag is personalized by an alphanumeric code that is integrated within its



Figure 12: This example of the 'Heart of Pearls' marking technique shows an octagonal tag measuring 400 µm across that is glued to the surface of a *Pinctada margaritifera* cultured pearl. The tag is inscribed with 'A.BCD', which is clearly visible with a gemmological microscope. The tag is surrounded by a hardened layer of colourless transparent glue. Photomicrograph by O. Segura.

structure. In this way, the tag can include relevant data such as the cultured pearl's quality grade, geographical origin, farm name, year of harvest, type of host mollusc, ethics label, ID number, brand and security key. The data on the tag are listed on three lines using a combination of letters or numbers (Figure 13), and can be customized according to local regulations or a customer's request. The label is affixed using a proprietary UV-fluorescent glue, thus enabling the tag to be quickly located (Figure 14). The colour of the glue's fluorescence is controlled by various

Figure 13: Data on the HoP tag may be coded in three lines, as shown in this example for a cultured pearl produced in the Cook Islands in 2014. Courtesy of Jean-Pierre Le Pollès.

 A hexagonal tag with a vibrant, multi-colored background. The word 'VALID' is repeated in various colors and orientations. Overlaid on this pattern are three lines of white alphanumeric text: 'CK 14', 'XXXX', and 'PR 99'.

Key	
CK:	Cook Islands ISO 3166-1-alpha-2
14:	2014
XXXX:	ID number and/or pearl grade
PR:	Producer
99:	Security key



Figure 14: When exposed to long- or short-wave UV radiation, the glue used to affix the HoP tag in this prototype example fluoresces blue, while the surrounding cultured pearl is inert, enabling the marker to be easily located. The size of the fluorescent spot is approximately 1 mm in diameter. Photomicrograph by O. Segura.

dopants, and a different luminescence colour can be assigned according to the type of mollusc and/or country of origin. Both the fluorescence and the information on the tag can be observed with an inexpensive pocket microscope equipped with 60× magnification and a UV LED (e.g. Figure 15).

All of the usual laboratory techniques that are used to analyse pearls (X-radiography, spectroscopy, etc.) can be accomplished without the results being disturbed by the tag. If necessary, the tag and its UV-fluorescent glue can be removed using nail polish remover (acetone). Thus, the cultured or natural pearl may be returned to its initial state without any remnants of the tagging process; the final consumer may therefore return it to its pristine state without any damage if they wish to do so.



Figure 15: A pocket microscope can be used to read an HoP tag, and also to view the UV luminescence colour of the glue that is used to affix it. Photo by Jean-Pierre Le Pollès.

Olivier Segura (o.segura@bjop.fr)
Laboratoire Français de Gemmologie
Paris, France

Reference

Hänni H.A. and Cartier L.E., 2013. Tracing cultured pearls from farm to consumer: A review of potential methods and solutions. *Journal of Gemmology*, **33**(7–8), 239–245, <http://dx.doi.org/10.15506/jog.2013.33.7.239>.

SYNTHETICS AND SIMULANTS

Modern Doublets, Manufactured in Germany and India

At the November 2014 Hong Kong Jewellery and Gem Fair, one of the authors (HAH) noticed some attractive faceted stones in colours resembling popular gem materials (e.g. Figure 16). These samples were actually doublets produced by a German lapidary, Viktor Kämmerling of Idar-Oberstein. They were manufactured using

colourless gem materials cemented by an artificial resin that had been dyed to create strikingly realistic gems. Both the crown and pavilion consisted of beryl (for emerald substitutes), topaz (for imitations of spessartine, tanzanite, Paraíba tourmaline and rubellite), tourmaline (for another Paraíba tourmaline substitute) and quartz (for imitations of



Figure 16: These doublets display various colours and optical effects. Samples 1–15 weigh 1.71–8.83 ct, and consist of colourless natural gemstone crowns and pavilions that are glued together with a coloured binder to create the illusion of popular gem varieties. The other samples weigh 2.29–13.79 ct, and display iridescence (no. 18) or contain pieces of foil in the cementing layer that produce different optical effects (nos. 16 and 17). Photo by H. A. Hänni.

peridot, aquamarine, topaz, morganite, amethyst, ametrine, bicoloured tourmaline and prehnite). The gems typically weighed between 2 and 10 ct and were available in calibrated sizes.

Additional high-quality doublets were seen by the authors in February 2015 at the Inhorgenta show in Munich, Germany. A small number of these gems were on display at the booth of Gemstones Corp. (Jaipur, India), which revealed additional colours; some were even bicoloured. They were priced inexpensively and sold as quartz doublets, the majority as oval cuts weighing ~8 ct. Also on display were quartz doublets showing interesting visual effects (again, see Figure 16): red needle-like inclusions (similar to rutilated or tourmalinated quartz), flat metallic inclusions with the appearance of gold and samples showing remarkable iridescence.

The results of our investigations of 18 samples are reported in Table I, and preliminary observations of some of these doublets were given by Hänni (2014). The dye that was used to impart such a realistic colour appearance to those manufactured by Viktor Kämmerling was either dissolved in the binder or consisted of tiny pigment grains suspended in the resin (e.g. Figure 17, left). The desired saturation of the colour was achieved by adjusting the concentration of dye in the resin and the thickness of the glue layer (e.g. Figure 17, right). In the examined samples, this layer varied from about 0.1 mm ('morganite' no. 11) to less than 0.05 mm (centre portion of 'bicoloured tourmaline' no. 14). The character of the colourless parts and the thin coloured glue layer was best observed in immersion (Figure 18, left). The cement typically contained various

Figure 17: Left: The glue layer in a tanzanite-coloured topaz doublet (no. 7) contains red and blue pigment particles and some gas bubbles (left, image width ~2 mm). Right: The girdle area of the tanzanite imitation displays a coloured glue layer with a thickness of ~0.025 mm. Photomicrographs by H. A. Hänni.

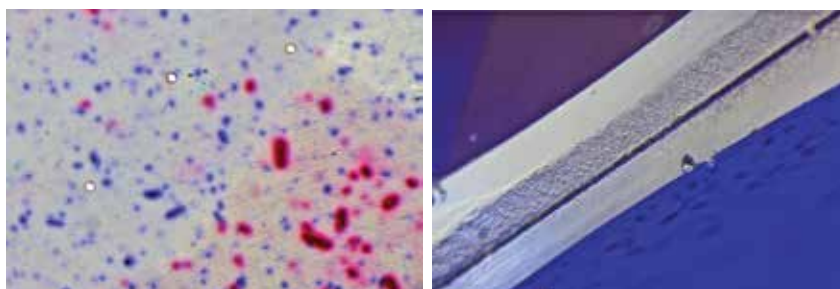


Table I: Properties of some doublets from Viktor Kämmerling and Gemstones Corp.

No.	Colour	Gem imitated	Weight (ct)	Crown/pavilion*	Internal features	
					In crown and pavilion	In glue layer
1	Green	Emerald	5.35	Beryl/beryl	Clouds, fine tubes	Small gas bubbles
2	Green	Emerald	3.86	Beryl/beryl	Partially healed basal fractures, veils	Small gas bubbles
3	Blue-green	Paraíba tourmaline	1.71	Tourmaline/tourmaline	Open fissures, fluids	Small gas bubbles
4	Blue-green	Paraíba tourmaline	3.36	Topaz/topaz	Partially healed fractures, two-phase inclusions	Very small pigment particles
5	Red	Rubellite	4.45	Topaz/topaz	None	Distinct pigment particles
6	Orange	Spessartine	4.71	Topaz/topaz	None	Some bubbles, small particles
7	Violet	Tanzanite	4.49	Topaz/topaz	Metallic inclusion	Bubbles, red and blue particles
8	Yellow-green	Peridot	8.83	Quartz/quartz	None	Extended bubble fields
9	Light blue	Aquamarine	7.54	Quartz/quartz	Very small fluid(?) blebs	Dust and some bubbles
10	Light blue	Topaz	8.64	Quartz/quartz	None	Dust and some bubbles
11	Orangey pink	Morganite	8.21	Quartz/quartz	Two-phase negative crystals	Bubbles and pigment particles
12	Violet	Amethyst	8.66	Quartz/quartz	None	Bubbles and pigment particles
13	Violet and yellow	Ametrine	8.30	Quartz/quartz	None	Bubbles and pigment particles
14	Red and green	Bicoloured tourmaline	8.37	Quartz/quartz	None	Bubbles and pigment particles
15	Milky green	Prehnite	8.48	Quartz/quartz	Irregular fine fibres	Bubbles and minor pigment particles
16	Colourless with 'golden' inclusions	Gold-in-quartz	13.79	Quartz/quartz	None	Metallic foils
17	Colourless with narrow foil strips	Rutilated or tourmalinated quartz	2.29	Quartz/quartz	None	Metallic foils
18	Various iridescent	Girasol	4.28	Quartz/quartz	None	Gelatinous appearance

* Identified by Raman spectroscopy using a B&W Tek MiniRam 785 instrument equipped with a >300 mW 785 nm laser.

amounts of gas bubbles. In some gems, the bubbles were sparse and dispersed sporadically, while in others they were more abundant and concentrated near the girdle of the sample (Figure 18, right).

Natural inclusions in the crown and pavilion components of the doublets were seen in only some samples (see Table I). For the quartz samples from Viktor Kämmerling, Fourier-transform infrared (FTIR) spectroscopy with

a PerkinElmer Paragon 1000 spectrometer showed typical bands for natural quartz in the 4000–3000 cm^{-1} range, especially the 3595 cm^{-1} band (Zecchini and Smaali, 1999). Both parts of quartz sample no. 15 contained abundant, randomly oriented, fine fibres. Observation of the stone's surface with a scanning electron microscope showed only pits corresponding to these inclusions, which were filled with debris from the tin polishing wheel.

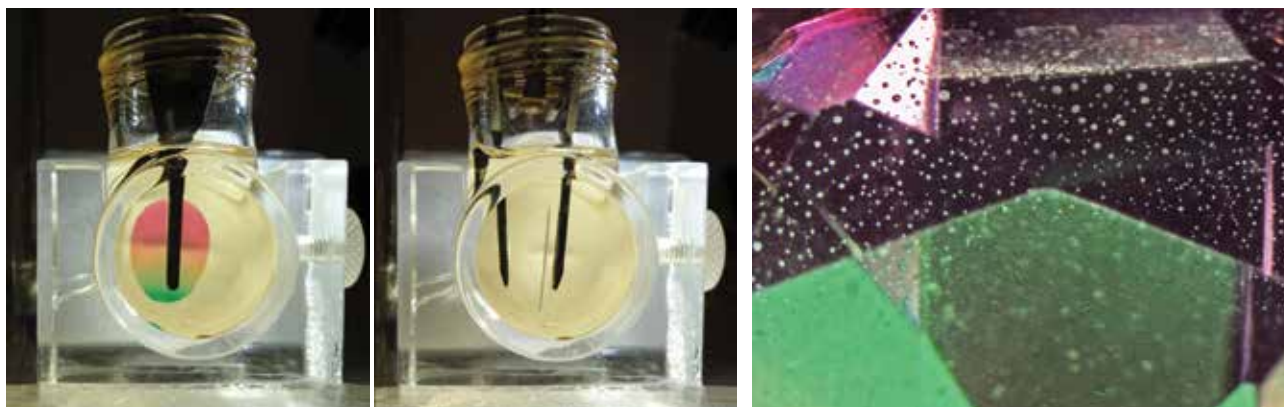
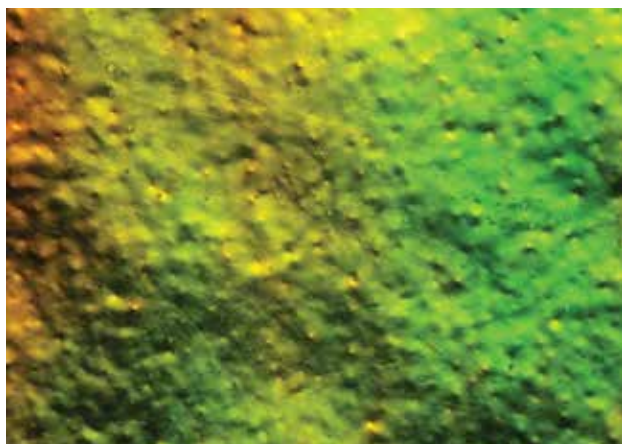


Figure 18: Left: A quartz doublet imitating bicoloured tourmaline (8.37 ct; no. 14) is shown immersed in benzyl benzoate, in views both perpendicular (left side) and parallel (right side) to the girdle plane. Right: The bicoloured tourmaline imitation contains a more concentrated area of gas bubbles near the girdle area (image width ~5 mm). Photos by H. A. Hänni.

Two of the quartz doublets from Gemstones Corp. were found to have thin metallic foils in the cement layer. One of these samples (no. 16) had ‘golden’-coloured foil, simulating gold-in-quartz. The other sample (no. 17) revealed narrow foil strips in geometric orientations. The iridescent doublet (no. 18) contained a gelatinous-appearing glue layer that was bright green, yellow or violet depending on the viewing angle when observed in reflected light (e.g. Figure 19). The constituent quartz of these doublets was identified as natural by FTIR spectroscopy, with bands at 3595, 3482 and especially 3379 cm^{-1} . A peak at $\sim 3480 \text{ cm}^{-1}$ is typically associated with rock crystal quartz (Choudhary, 2010).

It is not difficult to recognize the composite character of these doublets when they are unmounted and immersed in water or another

Figure 19: The glue layer in the iridescent quartz doublet (no. 18) displays various colours depending on the viewing angle, and contains numerous gas bubbles. Photomicrograph by U. Henn; image width ~10 mm.



medium (cf. Henn, 2002). Viewed from the side with a 10× loupe, the girdle plane displays a narrow dark colour band of less than a millimetre. The colourless topaz, beryl or tourmaline used for these doublets may contain inclusions typical for these gem materials, and their conclusive identification as doublets is established by observation of the coloured binder layer. In addition, the doublets will show a peculiar behaviour in the polariscope, with no distinct extinction, which points toward an assembled stone.

Acknowledgements: We thank Viktor Kämmerling and R. K. Jain for providing samples for this study. Daniel Mathis of Zentrum für Mikroskopie ZMB of Basel University is acknowledged for the SEM analysis of sample no. 15.

Dr Henry A. Hänni FGA (*b.a.baenni@gmail.com*)
GemExpert, Basel, Switzerland

Dr Ulrich Henn FGA
German Gemmological Association
Idar-Oberstein, Germany

References

- Choudhary G., 2010. Another interesting composite – diamonds and rock crystal. *Gems & Jewellery*, **19**(3), 20–21.
- Hänni H.A., 2014. Doublets – Long time no see. *InColor*, **27**, 26–27.
- Henn U., 2002. Zusammengesetzte Steine – eine aktuelle Betrachtung. *Gemmologie: Zeitschrift der Deutschen Gemmologischen Gesellschaft*, **51**(1), 13–28.
- Zecchini P. and Smaali M., 1999. Identification de l’origine naturelle ou artificielle des quartz. *Revue de Gemmologie*, **138/139**, 74–83.

Fracture-filled Synthetic Emerald, with Synthetic Quartz Inclusions

Recently, the Gem Testing Laboratory, Jaipur, India, received a 1.15 ct, green, oval mixed cut, measuring $8.02 \times 5.86 \times 4.06$ mm (Figure 20). Initial observation with the unaided eye suggested it was emerald. RI values were 1.580–1.587 (birefringence 0.007), the hydrostatic SG was 2.70 and it displayed typical chromium absorption with the desk-model spectroscope. All of these features are consistent with emerald. Viewed with the microscope, however, strong wavy ‘chevron’ growth features were seen throughout the stone (Figure 21); in addition, some reflective liquid ‘fingerprints’ were present, mostly in one direction. These features are indicative of a hydrothermal synthetic origin. The gem also contained surface-breaking fractures that displayed blue, green and ‘golden’ yellow colour flashes (Figure 22)—suggestive of fissures that have been filled with resin—along with a few reflective patches that resulted from incomplete fracture filling.

Microscopic examination also revealed a few colourless crystals in the synthetic emerald. On careful examination, some of these crystals were found to be associated with nail-head spicules (again, see Figure 22), while others formed isolated clusters of elongated inclusions. Closer observation of one of the spicules showed a hemispherical ‘head’ that appeared to be composed of tiny grains, some of which were granular and frosty (Figure 23, left). The isolated clusters (i.e. without a spicule) consisted of euhedral prismatic bipyramidal crystals (Figure 23, right). The morphology of these crystals,



Figure 20: This 1.15 ct oval mixed cut proved to be a fracture-filled hydrothermal synthetic emerald. It was also unusual for its synthetic quartz inclusions. Photo by G. Choudhary.

particularly the larger ones, resembled that commonly seen in quartz.

Raman analysis of the crystals, present as the ‘head’ of the spicules as well as isolated clusters, using a 532 nm laser, confirmed they were quartz. The spectra showed characteristic major peaks in the $2000\text{--}200$ cm^{-1} region at ~ 1157 , 1080, 807, 464, 353, 263 and 206 cm^{-1} . FTIR spectroscopy was further used to confirm this emerald as synthetic. The spectra displayed a sharp line at ~ 5280 cm^{-1}

Figure 22: Surface-reaching fissures in the synthetic emerald display flash-effect colours suggestive of fracture filling by a resin, along with some reflective patches of uneven filling. The presence of resin was confirmed by FTIR spectroscopy. Also note the nail-head spicule (centre-right of view), consistent with the synthetic origin. Photomicrograph by G. Choudhary; image width 3.3 mm.

Figure 21: The strong wavy ‘chevron’ growth pattern indicates that the synthetic emerald in Figure 20 was grown by a hydrothermal process. Photomicrograph by G. Choudhary; image width 4.2 mm.

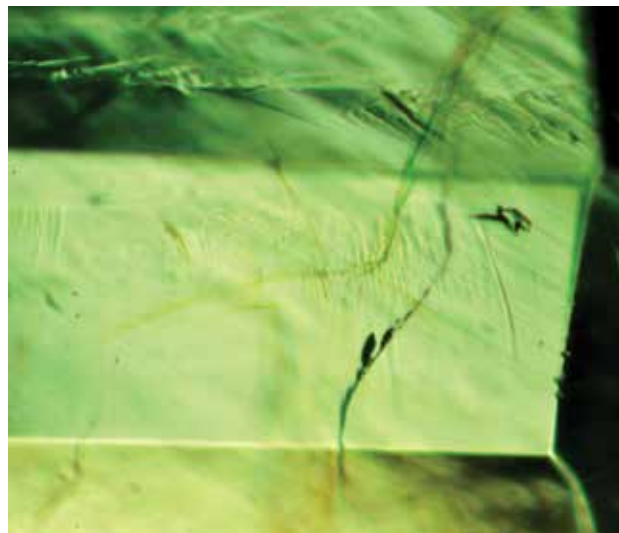
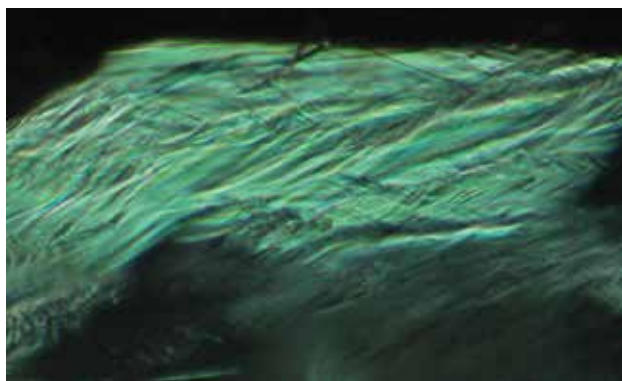
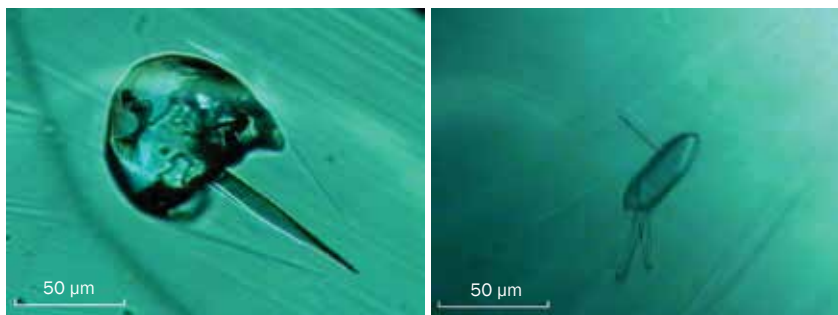


Figure 23: On the left, this spicule in the synthetic emerald consisted of a hemispherical 'head' composed of tiny grains, some of which were granular and frosty.

Raman analysis of the 'head' showed the presence of quartz. The photo on the right shows an inclusion cluster of well-formed crystals that also were identified as quartz by Raman spectroscopy. Photomicrographs by G. Choudhary.



(type II water) with side bands for type I water at around 5500–5380 cm^{-1} and 5150–5040 cm^{-1} , an absorption band ranging from 4000 to 3400 cm^{-1} and general absorption below 2100 cm^{-1} . The synthetic origin was revealed by the 2400–2200 cm^{-1} region, with bands at ~2358, 2340 and 2328 cm^{-1} . The CO_2 band at ~2358 cm^{-1} is usually present in association with a feature at 2291 cm^{-1} in natural emerald (not present in this sample) and also the bands at ~2340 and 2328 cm^{-1} are typical of synthetic emerald (Giard et al., 1998). The FTIR spectra additionally displayed features at ~3060, 3032, 2923 and 2871 cm^{-1} that are associated with resin, consistent with the flash effects mentioned above.

The 'head' of the spicules in synthetic emeralds is usually composed of grains of synthetic phenakite, beryl, chrysoberyl, gold or other mineralizers (Choudhary and Golecha, 2007).

The presence of synthetic quartz inclusions in synthetic emerald—either as the 'head' of spicules or forming isolated clusters—has not been reported previously to this author's knowledge. In addition, the fracture filling of this synthetic emerald is quite unexpected, and could have occurred when the gem was accidentally mixed into a parcel of natural stones.

Gagan Choudhary FGA (gagan@gjepcindia.com)
Gem Testing Laboratory
Jaipur, India

References

- Choudhary G. and Golecha C., 2007. A study of nail-head spicule inclusions in natural gemstones. *Gems & Gemology*, **43**(3), 228–235, <http://dx.doi.org/10.5741/gems.43.3.228>.
- Giard D., Giuliani G., Cheilletz A., Fritsch E. and Gonther E., 1998. *L'éméraude - Connaissances Actuelles et Prospectives*. Association Française de Gemmologie, Paris, France, 81–95.

Glass Imitations of Cu-bearing Mozambique Tourmaline

Alluvial deposits in the Mavuco area of north-eastern Mozambique are famous for producing copper-bearing tourmaline in a variety of colours (e.g. Laurs et al., 2008a). At the 2015 Tucson gem shows, Michael Puerta (Intimate Gems, Glen Cove, New York, USA) showed one of these authors (BML) three pebbles that he obtained in Mavuco in June 2014. Although their general appearance was quite convincing for rough alluvial tourmaline (Figure 24), Puerta felt that they did not seem 'right'.

One of the pebbles showed an attractive 'neon' blue colour that is typical of Cu-bearing tourmaline (although not commonly encountered in unheated rough from Mavuco), and another one was a purplish pink that, for Cu-bearing

Figure 24: These pebbles were sold as Cu-bearing tourmaline in Mavuco, Mozambique, but they actually consist of glass. The blue and dark yellow samples are each ~1.4 cm wide. Photo by B. M. Laurs.



tourmaline, is well-known to turn blue after heat treatment. The third sample was a dark yellow that is not typical of Mavuco tourmaline, although similar stones have been mined from the nearby Muva deposit (Laurs et al., 2008b). The first indication that all three pebbles were imitations was revealed when examining them with a loupe. Rather than uniformly smooth waterworn surfaces, they showed randomly oriented tiny chipped areas that produced glassy reflections in bright light. This was suggestive of an artificial tumbling process, commonly done to glass imitations. The rough surface of the pebbles made it impossible to look for gas bubbles or other indications of a glass in their interior. However, hydrostatic SG measurements yielded values of 2.49–2.51, which are within the range of glass and much lower than typical values for this tourmaline (3.01–3.09; Laurs et al., 2008a). Raman analysis gave indistinct patterns that are typical of glass, confirming our suspicion that these pebbles were glass imitations of tourmaline.

Imitations consisting of glass (and other materials such as fluorite and amethyst) are

known to occur in parcels of rough tourmaline from Mavuco (Laurs et al., 2008a). When Puerta purchased these samples, the dealer (whom he trusted) stated his absolute belief that they were natural tourmaline. Obviously these imitations were introduced at some point in the supply chain, and they were convincing enough to fool local dealers. The tiny reflective chips on their surface and unexpected colour of the dark yellow pebble provide useful field indications that such pebbles are imitations.

Brendan M. Laurs FGA

Eric W. Fritz FGA

Gem-A, Tucson, Arizona, USA

References

- Laurs B.M., Zwaan J.C., Breeding C.M., Simmons W.B., Beaton D., Rijdsdijk K.F., Befi R. and Falster A.U., 2008a. Copper-bearing (Paraíba-type) tourmaline from Mozambique. *Gems & Gemology*, **44**(1), 4–30, <http://dx.doi.org/10.5741/GEMS.44.1.4>.
- Laurs B.M., Zwaan J.C., Simmons W.B. and Falster A.U., 2008b. Gem News International: Tourmaline from Muva, Mozambique. *Gems & Gemology*, **44**(3), 273–275.

Quartz Imitation of Star Sapphire

In late 2013, a 7.65 ct oval blue cabochon displaying asterism (Figure 25) was submitted to American Gemological Laboratories for a report. The client believed it was a star sapphire. Initial visual observation showed that the bottom of the cabochon was flat, whereas most star sapphires have a convex bottom (to retain weight, in light of their high value), so this was our first indication that something was amiss. Also, there was no visible parting in the sample, another common feature of star sapphire. Most importantly, the base of the cabochon was coated with a grainy blue material. Observing the stone in profile view showed that it was actually colourless (Figure 26), and the basal coating was the source of its blue colour when viewed face-up.

Visible-range spectroscopy showed cobalt-related features, rather than the standard iron absorption typically seen in blue sapphire. Chemical analyses of the coating with EDXRF

spectroscopy detected high concentrations of Pb and traces of Co. Microscopic observation of the colourless dome revealed small colourless

Figure 25: This 7.65 ct imitation resembles a star sapphire, but actually consists of colourless natural star quartz with an amorphous blue coating on the base of the cabochon. Photo by Bilal Mahmood.





Figure 26: In profile view, it became apparent that the cabochon in Figure 25 is actually colourless. The blue colour viewed face-up is due to a coating on the bottom of the cabochon. Photo by Kelly Kramer.

inclusions and/or negative crystals, primary fluid inclusions and tiny, very fine, oriented needles (which caused the asterism). The cabochon was transparent to semi-transparent, and a bull's-eye optic figure was easily detected using a standard polariscope. Together with a spot RI reading of 1.54, the microscopic features and optic figure

were consistent with natural star quartz. Mid-IR spectroscopy confirmed this identification.

We concluded that this cabochon consisted of natural, colourless star quartz that had been backed with a lead-based amorphous material that was coloured blue by cobalt. A similar cabochon, consisting of enamel-backed star quartz, was reported by Krzemnicki and Hänni (2001).

The spot RI reading and bull's-eye optic figure, along with the lack of parting and the blue coating on the flat bottom of this cabochon, made this imitation detectable even without advanced testing equipment. This piece serves as a reminder that careful observation and basic gemmological testing remain effective for detecting certain limitations.

Wendi M. Mayerson (wmayerson@aglgemlab.com)
 American Gemological Laboratories
 New York, New York, USA

Reference

Krzemnicki M.S. and Hänni H.A., 2001. Gem News International: Enamel-backed quartz as a star sapphire imitation. *Gems & Gemology*, **37**(2), 155.

TREATMENTS

Chromium-diffused Corundum

Recently, two stones were submitted to the American Gemological Laboratories that provide a reminder for the potential of old treatments to reappear in the marketplace. The two purple-pink gems weighed 0.83 and 0.95 ct (Figure 27). The client had purchased them as part of a larger acquisition of various gem varieties, from a trader selling old stock that had been in his inventory for more than 20 years.

Microscopic observation of both stones revealed traits consistent with pink sapphires that had been heated (Figure 28), including zones of partially dissolved rutile inclusions, heavily altered crystals and partially healed fissures with a frosted appearance. In addition, their surfaces were heavily pitted (Figure 29). When viewed face-up with the unaided eye, they showed relatively even coloration, yet with magnification they had an atypical patchy appearance. Viewed

in immersion, they displayed the distinctive uneven coloration from one facet to another that is associated with diffusion treatment (Figure 30). These observations, coupled with relatively high concentrations of chromium (~2.5 wt.% Cr₂O₃)

Figure 27: These two purple-pink gems (0.83 and 0.95 ct) proved to be Cr-diffused natural corundum. Photo by Bilal Mahmood.





Figure 28: Various thermally altered internal features were present in the Cr-diffused sapphires, confirming their natural (not synthetic) origin. These include lines of stringers composed of fine rutile particles (left), negative crystals with associated partially healed stress fractures (centre) and partially healed fissures with a frosted appearance (right). Photomicrographs by C. P. Smith; magnified 40× (left and centre) and 62× (right).

recorded with EDXRF spectroscopy, confirmed that the two samples consisted of natural corundum that had been subjected to Cr-diffusion treatment. The EDXRF analyses also showed traces of Fe, Ti and Ga in both stones (Table II).

Refractive index readings of both stones revealed uncharacteristically high values (Table II), together with indistinct shadow edges at ~ 1.76 and 1.77 corresponding to typical corundum values. The high RIs are due to the enriched Cr content near the surface resulting from the diffusion treatment, while the typical values are produced from the underlying corundum where the Cr had not penetrated. Additional gemmological properties collected from these samples are listed in Table II.

Although the client had presumed these sapphires had been heated, he was very surprised

Figure 29: Due to the very shallow penetration of the Cr-diffused layer, only a light repolishing was performed after the treatment process, leaving remnants of a heavily pitted surface that were evident on the vast majority of the facets. Photomicrograph by C. P. Smith; magnified 38×.



to learn that they had been diffusion treated, as he was unaware that Cr-diffusion treatment even existed. It has been many years since Cr-diffused natural corundum was first reported (McClure et al., 1993), and this treatment was short-lived due to the apparent difficulty of diffusing Cr. Further attempts at Cr diffusion resulted in the inadvertent overgrowth of synthetic ruby onto a natural corundum host (Smith, 2002). Although both of these treatment processes were done on a limited basis, a small number of these gems did make their way into the gemstone market.

It has been more than two decades since the author has encountered Cr-diffused natural corundum, and the present stones stand out as a reminder that such uncommon products may be

Figure 30: The two sapphires appeared evenly coloured when viewed face-up with the unaided eye, but when immersed in baby oil the patchy uneven coloration associated with Cr-diffused corundum became readily apparent. Photomicrograph by C. P. Smith; magnified 12×.



Table II: Gemmological properties of the Cr-diffused natural corundum samples.

Weight	0.95 ct	0.83 ct
Refractive indices (table facet)	Indistinct shadow edges: 1.76 and 1.77	
	More distinct: 1.780 and 1.788	More distinct: 1.772 and 1.780
Optic character	Uniaxial negative	
UV fluorescence Long-wave Short-wave	Strong red Weak red with chalky blue-white patches	
Visible spectrum	Standard chromium absorption	
Mid-infrared spectroscopy (structurally bonded OH groups)	Weak 3309 cm ⁻¹	Weak 3309 cm ⁻¹ Nominal 3232 cm ⁻¹
EDXRF spectroscopy*	Cr: 2.39 Fe: 0.08 Ti: 0.03 Ga: 0.01	Cr: 2.59 Fe: 0.02 Ti: 0.14 Ga: 0.01

* EDXRF values are calculated as approximate wt.% oxides.

recycled back into the gem market at any time. Therefore gemmologists, appraisers and jewellers must remain aware of not only what is currently taking place in terms of treatments and synthetics, but also what has been done in the past.

Christopher P. Smith FGA (chsmith@aglgemlab.com)
American Gemological Laboratories
New York, New York, USA

References

McClure S.F., Kammerling R.C. and Fritsch E., 1993. Update on diffusion-treated corundum: Red and other colors. *Gems & Gemology*, **29**(1), 16–28, <http://dx.doi.org/10.5741/gems.29.1.16>.
Smith C.P., 2002. “Diffusion ruby” proves to be synthetic ruby overgrowth on natural corundum. *Gems & Gemology*, **38**(3), 240–248, <http://dx.doi.org/10.5741/gems.38.3.240>.

Lead-glass-filled Yellow Sapphires

Lead-glass-filled rubies and blue sapphires have been known for several years and have made a big impact on the jewellery market. Some of the treated rubies display an attractive colour and large size, and are priced inexpensively (McClure et al., 2006; Laurs, 2008). Recently, lead-glass-filled yellow sapphires have appeared in the market. This treated material is available in Chanthaburi, Thailand, and it is being sold to dealers at very low cost, by the kilogram.

In February 2015, our laboratory received a large parcel of some 600 faceted pieces (average ~5 ct each) of yellow sapphires for testing and certification. Our client understood that they were glass-filled, but wanted to be sure that the lot was not mixed with synthetic yellow sapphires containing induced flux feathers. We chose 28 pieces showing various shades of yellow and ‘golden’ yellow coloration for examination (Figure 31). Viewed with the microscope, they

exhibited greenish blue, ‘golden’ yellow and brown colour flashes along glass-filled fractures (Figure 32), which also contained gas bubbles

Figure 31: These yellow to ‘golden’ yellow lead-glass-filled sapphires (4.05–5.28 ct) were studied for this report. Photo by Aatish Panjekar.



of various sizes and shapes (Figure 33). These features are typical of lead-glass-filled corundum (e.g. McClure et al., 2006). Other inclusions consisted of fine needles, feathers (Figure 32), tabular brown crystals (Figure 33) and lamellar twinning. Unlike the blue colour concentrations in lead-glass-filled blue sapphires, there was no obvious yellow colour concentration in these samples. EDXRF spectroscopy confirmed that the filler was indeed lead glass. For academic interest, the hydrostatic SG for all 28 pieces was found to be in the range of 4.02–4.04.

Our observations confirmed that this parcel consisted entirely of natural corundum that was filled with colourless lead glass. The starting

Figure 32: Greenish blue colour flashes are commonly visible in the yellow lead-glass-filled sapphires, along with feathers. Photomicrograph by Aatish Panjekar; magnified 60×.

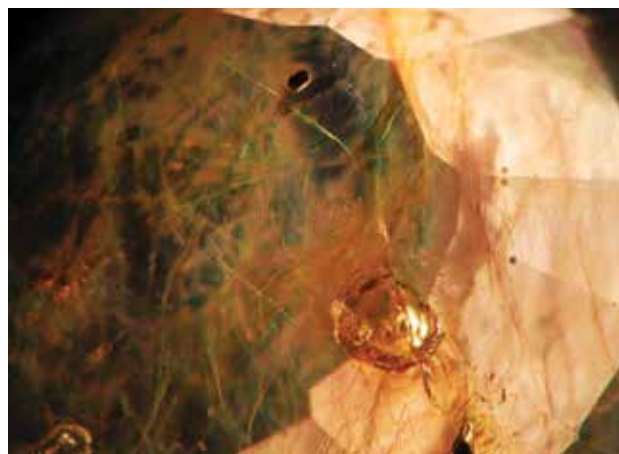
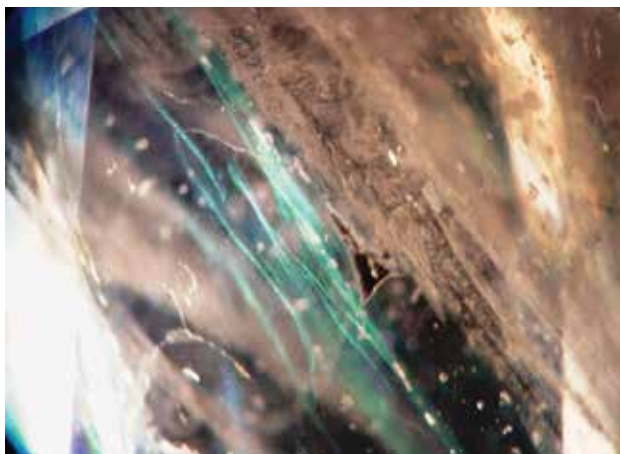


Figure 33: This lead-glass-filled yellow sapphire contains large gas bubbles, colour flashes along some filled fractures, and a tabular brown crystal (top-centre). The lead glass is colourless but reflects the coloration of the host sapphire, making it appear yellow or 'golden' yellow along some filled fractures. Photomicrograph by Aatish Panjekar; magnified 60×.

material used for the treatment probably consisted of pale yellow material of very poor transparency.

*Jayshree Panjekar FGA
(jayshreepanjekar@gmail.com)
Pangem Testing Laboratory
Pune, India*

References

- Laurs B.M., Ed., 2008. Gem News International: Tucson 2008. *Gems & Gemology*, **44**(1), 74–75.
- McClure S.F., Smith C.P., Wang W. and Hall M., 2006. Identification and durability of lead glass-filled rubies. *Gems & Gemology*, **42**(1), 22–36, <http://dx.doi.org/10.5741/gems.42.1.22>.

Attend our regular Gem Central sessions to brush up on your knowledge and network with fellow gemmologists

Visit our website or contact events@gem-a.com for more information

Green-Luminescing Hyalite Opal from Zacatecas, Mexico

*Emmanuel Fritsch, Peter K. M. Megaw, Tyler L. Spano, Boris Chauviré,
Benjamin Rondeau, Michael Gray, Thomas Hainschwang
and Nathan Renfro*

Green daylight-fluorescing hyalite opal was discovered in Mexico's Zacatecas State in 2013. It occurs as botryoidal coatings commonly up to 1 cm thick along fractures and cavities in a poorly welded rhyolitic tuff. The material possesses spectacular colour behaviour, appearing near-colourless or pale-to-moderate yellow in incandescent light and vivid greenish yellow to yellowish green in indirect sunlight. The daylight-induced green luminescence is related to the presence of trace amounts of the uranyl molecule (UO₂)²⁺. Several dozen high-quality transparent gemstones in the 1–6+ ct range have been faceted from this material so far, in addition to hundreds of smaller stones. The gems typically contain two-phase fluid inclusions and curved deposition marks, and they show bright interference colour patterns between crossed polarizers. This hyalite is not porous, and contains approximately 2.7 wt.% H₂O, which is remarkably low among gem opals. The radioactivity of the opal is within background levels, and does not pose any health concern.

The Journal of Gemmology, 34(6), 2015, pp. 490–508, <http://dx.doi.org/10.15506/JoG.2015.34.6.490>
© 2015 The Gemmological Association of Great Britain

Introduction

Gems coloured mostly by luminescence are truly rare. Therefore, when a new gem material is discovered that is undoubtedly coloured by luminescence, it attracts a great deal of attention. Such is the case with the daylight-fluorescing, vivid green transparent hyalite that was recently unearthed in Zacatecas, Mexico (Fritsch et al., 2014; see Figure 1 and the cover of this issue). The material was first brought to market in October 2013, when five weathered specimens of rough opal showing moderate green daylight luminescence were given to one of the authors (PKMM) by a well-known importer

of mineral specimens and lapidary rough from Mexico. Some of the initial specimens were sold at the February 2014 Tucson gem shows, and they attracted much attention because of their noticeable change from nearly colourless to vivid green in indirect sunlight (Moore, 2014). Reaction to the phenomenon by specimen collectors was very positive, so reconnaissance prospecting was undertaken by author PKMM to help determine the quality and quantity of material available. This initial work showed that the strongly luminescent material is sparsely distributed, but a small amount of facetable opal was recovered. Some of the faceted gems were available at the 2015 Tucson



Figure 1: This matrix specimen (2.5 cm wide) and the cut gemstones (1.34–3.93 ct) show the range of colour appearance resulting from green daylight-induced fluorescence in hyalite from a relatively new deposit in Zacatecas, Mexico. They have been photographed using daylight-equivalent strobe lights (top) and using incandescent modelling lamps within the same strobe fixtures (bottom). The gems were faceted by author MG. Photos by Orasa Weldon.

shows, and were sold as Electric Opal (trademark pending) because of their vivid green colour in daylight. The largest faceted gem weighed almost 6 ct (see cover of this issue), and hundreds of smaller stones were available in calibrated sizes down to 3 mm.

The mining site lies on the top of a steep 250-m-high mesa, so the use of heavy equipment is impractical and all digging has been manual. The difficult access, sparseness of material and reliance on manual labour will probably limit future supply to a small multiple of the production to date. This article documents in detail the geological occurrence and the luminescence phenomenon that makes this opal such an attractive gem material.

Opal Generalities and Classification of Hyalite

The gem species opal— $\text{SiO}_2 \cdot n\text{H}_2\text{O}$ —is typically associated with play-of-colour material from

Australia and more recently Ethiopia, both of which are abundant in today's market. But the term *opal* more generally refers to a range of hydrated silica materials. In the broadest sense, opal may be divided into microcrystalline and amorphous material (Graetsch, 1994; Gaillou et al., 2008a). The microcrystalline varieties comprise opal-C (rare) and opal-CT (quite common), which are basically poorly crystallized cristobalite (C) with more-or-less tridymite-like (T) stacking. Both cristobalite and tridymite are polymorphs of nominally pure SiO_2 . They represent the bulk of 'volcanic' opal, such as fire opal from Mexico (Fritsch et al., 2006) and material from Ethiopian deposits (Rondeau et al., 2010). Amorphous opals are divided into two categories (Langer and Flörke, 1974): opal-AG and opal-AN. Opal-AG is a gel-like (G) aggregate comprised of regularly ordered hydrated silica spheres, often $<1 \mu\text{m}$ in size, with open space between the spheres (e.g. Stephant et al., 2014). It is quite common, often displays play-of-colour caused by diffraction of

light from regularly stacked spheres of similar diameter, and includes material from Australia and Brazil. Opal-AN consists of hydrated silica molecules that are network-forming (N), and therefore it resembles a glass (Flörke et al., 1973). Since opal-AN does not have a regular array of spheres or any specific microstructure, it is always ‘common’ opal (i.e. does not exhibit play-of-colour). Opal-AN is also known as *hyalite*. It is relatively uncommon in volumes adequate for faceting, and thus is rarely used as a gem material. One of the few examples is botryoidal white opal from Milford, Utah, USA (Johnson and Koivula, 1997).

Green-Fluorescing Hyalite

Most hyalite strongly fluoresces green under both long-wave (LW) and short-wave (SW) UV radiation. In some cases (e.g. from the Erongo Mountains of Namibia, Madagascar and the Thomas Range in Utah, USA; www.mindat.org), hyalite may show a moderate-to-strong yellow-green coloration in daylight, as judged from photographs and unpublished reports, with the green component possibly originating from luminescence (although this has not been confirmed). Strong green fluorescence to *visible light* has not been reported from these localities, however, making the material described in this article quite unusual.

Crowningshield (1985) described one example of a transparent faceted opal with strong green daylight fluorescence that allegedly originated from Mexico. Its properties, general appearance and microtexture closely match those of the present material. Since there was no evidence of older workings in the currently known mining area, that stone may have come from the surface at the current area or from another incidental find, possibly in a similar geological context elsewhere in Mexico.

Other Daylight-Fluorescing Materials

Luminescence probably contributes to the coloration of several gem varieties, but its influence on visual appearance is hard to quantify (Fritsch and Rossman, 1988; Fritsch and Waychunas, 1993). Nevertheless, there are a few

well-documented examples with luminescence induced by visible light, and probably the most famous category comprises certain yellow diamonds, such as a stone owned by Pedro II, the last emperor of Brazil (Moses, 1997; Fritsch, 1998; Shigley and Breeding, 2015). Such yellow to yellow-green gems are commonly referred to as ‘green transmitters’ (although they should really be called green *emitters*), and their coloration comes from the well-known H3 colour centre (Fritsch, 1998). More recently, HPHT-treated brown type Ia diamonds have demonstrated the same optical effect. Some green amber also owes its colour to luminescence, although it is rarer than blue amber (which is also coloured by luminescence; Liu et al., 2015).

Mn²⁺-doped flame-fusion synthetic spinel often exhibits bright green luminescence, stemming from its dopant, Mn²⁺, in tetrahedral coordination (Kane and Fritsch, 1991). As a man-made material, it has attracted much less attention for its daylight-induced emission than the present opal. Two other compounds are known for their bright green daylight-induced colour component. The first is ‘uranium glass’—also known as ‘Uralite glass’ (unrelated to the Ural Mountains of Russia)—which usually is a silicate glass doped with traces of uranium. This material was sometimes faceted as a gem, or made into other objects (particularly tableware), and was very popular in the early 20th century. In the USA, its opaque variety is known as ‘Vaseline’ glass, a popular collectors’ item. The second material is ‘fluorescein’, an organic-based molecule exhibiting strong green daylight luminescence. Fluorescein is used for many monitoring applications, ranging from cell chemistry to tracing underground water flows to highlighting space capsules after splashdown in the ocean. All of these green materials are especially attention-getting because of their daylight fluorescence.

Many gems besides hyalite may have their colour appearance boosted by luminescence emitted in other parts of the visible range. This has been documented for the Tavernier diamond (Liu et al., 1998) and some rare orange diamonds (Titkov et al., 2015). This is also true of ruby, and probably red spinel (Fritsch and Waychunas, 1993). It is likely that the highly sought-after (but poorly defined) ‘pigeon-blood’ colour of ruby



Figure 2: The opal deposit is located in Zacatecas State in central Mexico.

owes part of its attractiveness to daylight-induced red luminescence caused by chromium.

Location

The hyalite deposit is located in western Zacatecas State, central Mexico (Figure 2). The landowner has requested that more specific information on

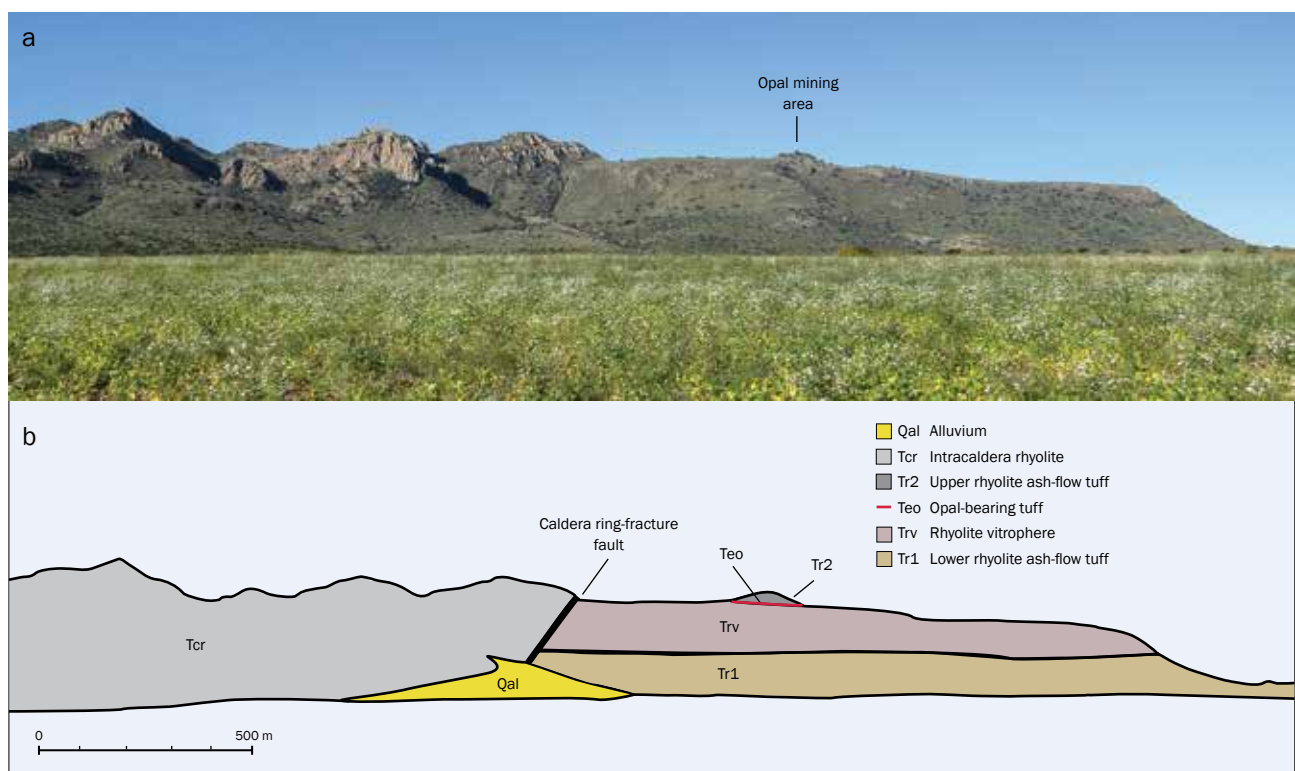
the location be withheld to minimize unauthorized mining. From the nearest municipality, the area is reached by approximately 40 km of paved road followed by 25 km of dirt tracks that wind through bean and squash fields to the base of a 250-m-high mesa (Figure 3). Then, a rough trail leads 1.5 km up a boulder-strewn and cactus-infested slope to the diggings. The miners have established a camp on site, and return to their homes on weekends to process each week’s production.

Geology

Zacatecas State is largely underlain by the Sierra Madre Occidental Volcanic Province (McDowell and Clabaugh, 1979), and the hyalite is hosted by mid-Tertiary (37–28 million year old) rhyolitic rocks that resulted from repeated volcanic eruptions.

To unravel the geological origin of the opal, it is important to understand the formation of its volcanic host rocks, which were deposited by violent eruptions from ‘super-volcanoes’ similar to Yellowstone in the USA. Instead of erupting through a central vent like familiar conical

Figure 3: This panoramic view (a) and interpretive geological section (b) show the location of the opal deposit in Tertiary volcanic rocks related to an adjacent caldera. The opal-bearing knob protrudes from a long, flat mesa consisting of a vitrophyric welded ash-flow tuff. A ring-fracture fault separates intracaldera unit Tcr from outflow units Tr1, Trv and Tr2. Opal is hosted by poorly welded tuff Teo at the base of the knob held up by Tr2. Photo and drawing by P.K.M. Megaw.



volcanoes (cf. Mount Fuji, Mount Rainier or Mount Vesuvius), these erupt around the circumference of the magma chamber (tens to hundreds of kilometres in diameter) through an annular ring-fracture zone (Smith and Bailey, 1968). During eruption, rocks within the ring-fracture zone settle piston-like into the underlying space left by the erupting magma, creating a circular depression called a *caldera* into which some of the hot ejecta accumulate. Thinner *outflow* facies extend outward from the intracaldera zone. Much of the erupting lava chills instantly into frothy siliceous volcanic glass, which is shattered into myriad tiny shards and pumice fragments that mix with fine volcanic ash to comprise *tuff*. As the eruptive pile cools, settles and compacts, escaping heat and volatiles fuse the ejecta into a hard, compact rock known as *welded ash-flow tuff* or *ignimbrite*. The most densely welded tuffs are compacted into *vitrophere*, a crystal-rich volcanic glass containing rock fragments. The thinner and cooler parts of the eruptive pile escape welding, leaving unconsolidated ash mixed with loosely bound crystals (mostly feldspars and quartz) and rock fragments (i.e. *poorly welded crystal-litic tuffs*; Smith and Bailey, 1968). In all cases, the volcanic glass that makes up most of the tuff is unstable and decomposes over time. Silica, uranium, iron and other constituents liberated from the decomposing volcanic glass are initially incorporated into vapours emanating from the cooling volcanic pile, which interact with circulating heated groundwaters that emerge as hot springs (Goodell and Waters, 1981; Breit and Hall, 2011). Transformation of glass shards into clays also releases silica and uranium into descending surface waters, and such solutions may redeposit silica as opal, chalcedony or quartz, depending on a number of factors (e.g. Berger et al., 1994; Markússon and Stefánsson, 2011). Uranium and other liberated elements are also deposited, either as discrete mineral species or within the framework structure of the chalcedony or opal.

Within the mining area, the daylight-fluorescent hyalite occurs around the base of a 40 × 125 m elongate knob that protrudes from the top of a 1.3-km-long mesa composed of outflows

from a 20-km-diameter caldera. The ring-fracture zone lies approximately 450 m from the hyalite occurrence. The mesa consists of a 90-m-thick section of very densely welded rhyolite vitrophere that overlies 160 m of moderately welded ash-flow units (Figure 3). The hyalite occurs in a 10–15 m thick, poorly welded, crystal-rich rhyolite tuff that sits atop the vitrophere and was protected from erosion by an overlying 30 × 100 m remnant of a younger welded tuff unit (Figure 4). The hyalite-bearing tuff probably once covered the entire mesa but it, and any opal it contained, has long-since been eroded away.

The hyalite-bearing layer is composed of 3–50 mm rhyolite rock fragments mixed with 1–4 mm dipyrarnidal β-quartz and limpid sanidine phenocrysts in a weakly welded, porous, siliceous, tuffaceous matrix. Groundwater could have readily percolated through this highly permeable unit, leaching silica and uranium from the devitrifying glass, and precipitating opal and the associated species described below. The hyalite occurs sparsely in voids and in fractures cutting the host tuff unit (Figures 5 and 6). The hyalite locally fills the fractures completely, but more commonly it occurs as isolated blebs and botryoidal coatings up to 3 cm in thickness, in most places covering less than 10% of the surface. The intensity of the opal's fluorescence varies widely within and between fractures and pockets, with less than 10% showing the strongest luminescence. The miners report that the daylight fluorescence is strongest in material found within a metre or so of the surface and drops off rapidly below that, so few fractures have been followed any deeper.

A series of uranium-containing minerals is found on the surface of the veins, and the opal locally formed on top of them. They generally consist of yellow sprays or spherulites of fibrous crystals. The most prominent species were identified by Spano et al. (2015) with X-ray diffraction as meta-autunite ($\text{Ca}(\text{UO}_2)_2(\text{PO}_4)_2 \cdot 6\text{H}_2\text{O}$), haiweeite ($\text{Ca}(\text{UO}_2)_2[\text{Si}_5\text{O}_{12}(\text{OH})_2] \cdot 6\text{H}_2\text{O}$), uranophane ($\text{Ca}(\text{UO}_2)_2(\text{HSiO}_4) \cdot 5\text{H}_2\text{O}$), and meta-uranospinite ($\text{Ca}(\text{UO}_2)_2(\text{AsO}_4)_2 \cdot 8\text{H}_2\text{O}$). The silica that formed the opal probably originated from groundwater-based weathering and dissolution of the glass shards in the tuff, as described above.

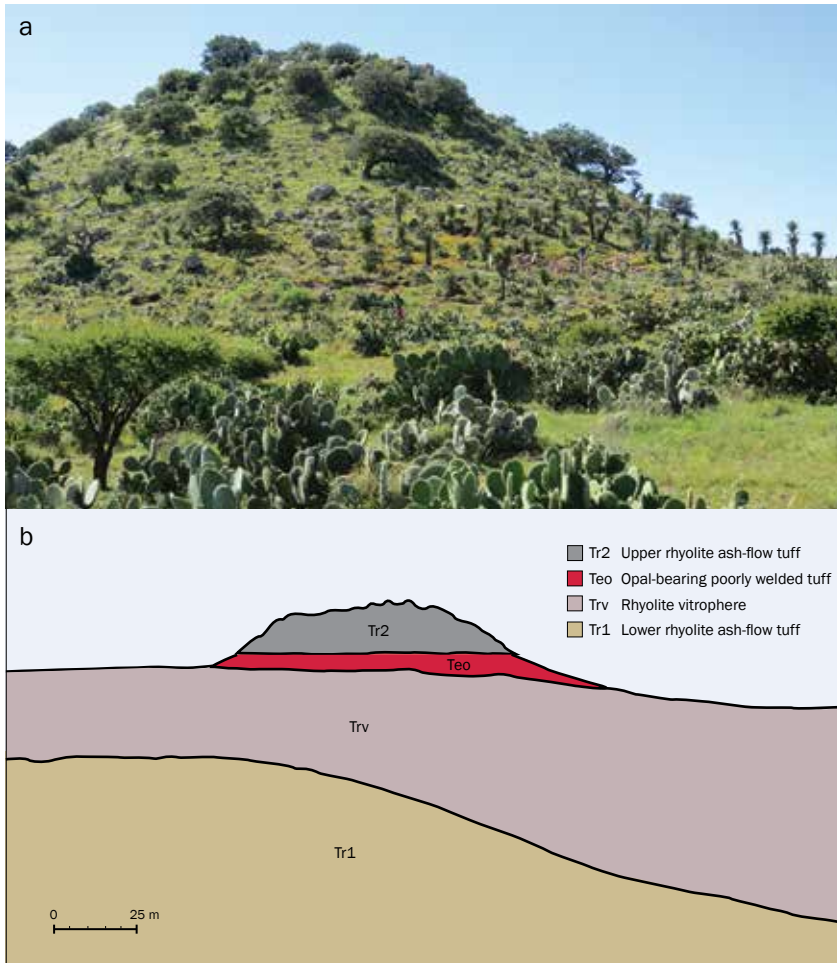


Figure 4: As shown in this photo (a) and interpretive geological section (b) of the mining area, the opal-bearing layer Teo is situated between an overlying welded tuff unit Tr2 and an underlying vitrophere Trv. Note the relatively steep topography and large boulders of Tr2 that protected the Teo layer from erosion. Photo and drawing by P.K.M. Megaw.

Mining and Production

Mining of the hyalite has been done exclusively with pry bars, picks and shovels, and a small gasoline-powered drill. The miners locate and follow iron-oxide stained fractures, and dig until hyalite-bearing voids are encountered. During

the rainy season, water collected in earlier excavations is used to wash out the pockets to assist with recognizing the better-coloured opal. During the dry season, the clayey iron-oxide-stained vein fillings fall away to reveal the opal. The voids range from 2 to 20 cm across and each

Figure 5: This view of a trench wall shows hyalite mineralization filling fractures and corrosion voids. Photo by P.K.M. Megaw; image width 26 cm.



Figure 6: This corrosion pocket is partially coated with hyalite. Several kilograms of good specimens were produced from this pocket. Photo by P.K.M. Megaw; image width 57 cm.





Figure 7. This hyalite specimen (5.6 cm across) contains botryoidal masses of gem-quality material. It is shown under daylight-equivalent strobe lighting (left) and under SW UV radiation (right). P.K.M. Megaw specimen; photos by Mark Mauthner.

typically produces a few kilograms of rough (including matrix). Weekly production ranges from 100 to 200 kg total of opal-bearing rock, of which less than 5% is specimen or cutting quality (e.g. Figures 7 and 8).

Through early 2015, the production totalled approximately 30 kg of top-quality specimens, 10 kg of facet-grade rough and 30 kg of pieces containing areas suitable for cutting good cabochons. Another 150 kg of moderate-quality and 250 kg of low-quality specimen material also were mined. It is difficult to predict future reserves, in part because the depth and lateral extent of

the strongly coloured zone of opal mineralization is unknown. Nevertheless, it appears that there is good potential for another 100–250 kg of top-quality specimen and gem rough.

Cutting and Polishing

Most of the larger gems faceted so far have been cut by one of the authors (MG). The grinding and polishing of this opal have presented no unusual problems compared to transparent opal from other localities. The minor heat sensitivity of opal requires the use of a cold dipping method

Figure 8: These gem-quality botryoids of hyalite display strong green luminescence in shaded daylight. P.K.M. Megaw specimens and photo; image width 10 cm.



for attaching the stone to the dop stick. The low RI of this opal (1.45–1.46; see below) requires a pavilion angle of at least 45°, as the critical angle is 43.6° (based on the lower RI range). The low SG of opal dictates that it takes more volume to attain a given weight as compared to most other gems. For example, a 1 ct standard round brilliant would measure nearly 8 mm in diameter.

The main problems with cutting the material are the various types of inclusions. Fibrous minerals are commonly associated with hollow tubes in the opal, and voids occur near the remnants of the matrix or at the intersection of botryoidal domains. If opened during the cutting process, these voids fill with debris from the wheel, so they must be either left completely enclosed within the finished gem or entirely ground away.

Materials and Methods

All of the rough samples were obtained by one of the authors (PKMM), either directly from the miners or through his Mexican mineral dealer associate. Three polished pieces were prepared by Jacques Le Quéré (JackyGems, Auray, France) for this research: one round brilliant (1.32 ct), one flat rectangular cabochon (1.81 ct) and one piece with the botryoidal surface kept on one side and a rounded cabochon polished on the other side (0.83 ct). Five matrix specimens were examined, including two on which green-fluorescing pale yellow hyalite formed in continuity with milky white hyalite showing no daylight luminescence.

All rough and cut samples were examined with a binocular Leica MZ6 microscope equipped with a Nossigem gemmological lighting system, and the three polished opals were tested with a GIA Gem Instruments refractometer and a Mettler Toledo XS104 electronic scale (for mass and hydrostatic SG measurements). UV luminescence observations of all samples were done using a VL-215.LC Vilber-Lourmat filtered UV lamp that contained two ~30-cm-long UV tubes of 15 W each: one for 254 nm SW and the other for nominally 365 nm LW UV radiation. For qualitative intensity descriptions, the sample was placed at a fixed distance of 7 cm from the lamp. Fluorescence colour and intensity were judged compared to two reference stones: a flame-fusion

synthetic ruby used as a ‘very strong’ and ‘red’ reference for both LW and SW, and a colourless flame-fusion synthetic sapphire representing a ‘strong’ and ‘blue’ reference in SW (inert in LW). For this specific case of a visible-light luminescing gem material, we used a 405 nm (InGaN) 0.5 mW laser pointer to stimulate emission under violet radiation. (These devices are often incorrectly referred to as ‘blue’ lasers, and they may be harmful to the eyes, even operating at such low power.) Two additional faceted stones of large size (12.25 and 12.63 ct), which were cut by author MG to show the diversity of their internal features, were examined by one of us (NR) using a Nikon SMZ1500 trinocular microscope fitted with a Nikon DS-Ri2 camera, and selected inclusions were analysed with a Renishaw InVia Raman spectrometer utilizing a 514 nm argon-ion laser.

The identity of purple blocky crystals found within tubes in the hyalite was established as fluorite using single-crystal X-ray diffraction. Crystals suitable for diffraction were manually isolated, and one was selected for unit-cell determination. A matrix of data was collected using a series of 0.3° frames in ω with a collection time of 10 seconds/frame. Data were collected on an Apex II diffractometer with Mo($K\alpha$) X-radiation and a Bruker charge-coupled device (CCD) detector. Unit-cell dimensions were obtained through refinement of 718 reflections using Fast Fourier transform techniques.

Raman spectra of all samples were obtained with a Bruker MultiRAM Fourier-transform Raman spectrometer. Excitation was provided by a 2 W Nd:YAG laser at 1064 nm, in continuous mode, and the data were collected at the standard resolution of 4 cm⁻¹, accumulating 1,000 scans.

Imaging of the opal microstructure in one rough sample was performed using a JEOL 7600 scanning electron microscope (SEM). The opal was fragmented using a mortar, and the pieces were etched in hydrofluoric acid (10% HF by volume) for 30 seconds (a standard etch procedure to reveal opal structure; e.g. Gaillou et al., 2008b). The freshly broken and etched surfaces were coated with platinum to ensure electrical conductivity.

Luminescence emission and excitation spectra as well as 3D block diagrams were obtained for the three fashioned opals and two

of the rough samples using a Horiba Fluorolog spectrofluorometer in conjunction with Fluor-Essence software. Two types of detectors were used: a standard photomultiplier and a Synapse CCD detector coupled to an iHR320 imaging spectrometer. A resolution of <1 nm was obtained by juxtaposing many scans to cover a given spectral domain in several sections. The samples were positioned to maximize the measured emission. For comparison, we analysed a reference specimen of whitish hyalite crust with green UV luminescence from Grimes Sexton Quarry, Inyo County, California, USA. Emission spectra were obtained using 365 nm excitation with a 1 nm bandpass, a sampling interval of 1 nm and a 0.2 second integration time. Excitation spectra were obtained for the 524 nm emission using the photomultiplier with a 3 nm spectral bandwidth; the excitation was scanned with a 1 nm bandpass and sampling interval, and a 0.3 second integration time. In addition, emission spectra of a 0.23 ct round brilliant were recorded on a GGTL-PL6 Raman/photoluminescence system using 405 nm laser excitation, and a high-resolution echelle spectrograph (average resolution of 0.04 nm) by Catalina Scientific equipped with a Peltier-cooled sCMOS camera. The spectra were recorded with the opal at room temperature and also cooled to 77 K by direct immersion in liquid nitrogen.

UV-visible (UV-Vis) absorption spectra were recorded using a Cary 5G spectrophotometer with a resolution of ~ 1 nm (sampling and spectral bandwidth were each 1 nm). Each point was collected for 0.1–0.5 seconds. The spectrum selected for illustration in this article was obtained from the 1.81 ct flat cabochon sample, and then double-checked on five other rough samples.

Energy-dispersive X-ray fluorescence (EDXRF) analysis of the three polished samples was performed with a Rigaku NEX CG spectrometer (a 'secondary target' or 'Cartesian geometry' instrument), with analytical parameters optimized for four successive energy ranges of secondary X-rays. This provided enhanced sensitivity, intermediate between that of standard EDXRF and ICP-MS techniques. The chemical analyses are reported as if water is not present, since this technique cannot detect water.

Water content was determined with thermogravimetric (TGA) analysis, using a Netzsch



Figure 9: The measurement geometry used to assess the radioactivity of the hyalite is shown here. The three fashioned samples (0.83–1.81 ct) are positioned face-down on the detector. Photo by Michael Bailly.

Jupiter STA 449 F3 instrument on a 60 mg sample that was powdered in an alumina crucible. The sample was heated from room temperature to 1,000°C (1°C/minute) under a synthetic dry air flow (nitrogen-oxygen mixture with $N_2:O_2 = 80:20$) of 50 ml/minute.

The radioactive dose rate of the three polished samples (total weight ~ 0.8 g; Figure 9) was measured for $\sim 1/2$ hour with the NaI detector of a Canberra InSpector 1000 instrument. The measurements were done with the samples placed face-down and directly on the detector, which is a geometry comparable to wearing the three hyalites directly on the skin. The nature of the radioisotopes was revealed by gamma spectroscopy of the 1.81 ct flat rectangular cabochon, using a high-purity germanium detector (Canberra Xtra) with low background. The efficiency of the detector was defined for each point of the sample chamber, and the volume of the gem was modelled to increase efficiency and precision (hence the choice of the flat cabochon, which was easiest to model). Because of the low levels measured, a count time of 250,000 seconds (almost three days) was used. These data were collected at a laboratory specialized in the measurement of low radioactivity levels (Subatech-SMART) at the Nantes School of Mines, Nantes, France.

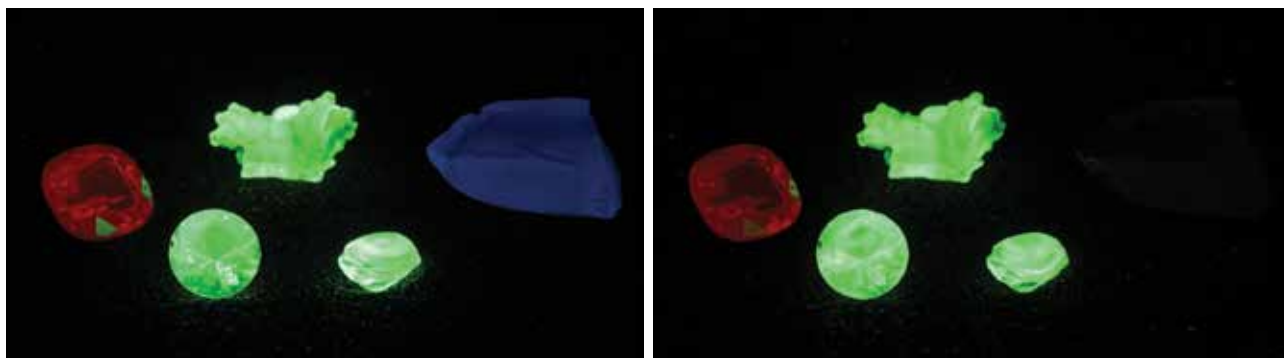


Figure 10: Shown here in SW (left) and LW UV radiation (right), the three hyalite specimens display much more intense luminescence than the fluorescence reference stones: a flame-fusion synthetic ruby with 'very strong' luminescence to both SW and LW, and a colourless flame-fusion synthetic sapphire representing 'strong' emission in SW (inert to LW). Both reference stones appear dimmer than expected since the exposure had to be shortened to avoid overexposing the very bright hyalite. The round-brilliant-cut hyalite weighs 1.32 ct. Photos by B. Chauviré.

Results and Discussion

Visual Observations and Gemmological Properties

The rough specimens showed a botryoidal or concretion-like morphology (e.g. Figures 7 and 8), which is typically associated with hyalite opal (opal-AN) from many localities. Their diaphaneity ranged from transparent to opaque. The colour appearance of the rough and cut material showed a dramatic change from incandescent or fluorescent lighting (colourless to moderate yellow) to shaded sunlight (vivid greenish yellow to yellowish green; e.g. Figure 1 and the cover image). This change arises from visible-light-induced green luminescence. The phenomenon is apparently enhanced by faceting, which provides a longer optical path length for excitation, as well as reflection of the emitted green colour toward the eye as compared to rough specimens. Shaded sunlight is best for viewing the phenomenon, since the brightness of direct sunlight overwhelms the fluorescence.

Exposure of all the samples to the SW UV lamp excited green luminescence that was even more intense than our 'very strong' luminescence reference stone (e.g. Figure 10, left); it was one of the most intense reactions we have documented in a natural gem. All samples, large or small and with or without zoning of diaphaneity, showed an apparently homogeneous luminescence. The fluorescence was only slightly weaker in LW UV, but still much more intense than our 'very strong' reference stone (Figure 10, right). Excitation with a 405 nm laser pointer, emitting in the violet

region of the visible spectrum, also spectacularly induced the green coloration (Figure 11).

RI values ranged from 1.45 to 1.46, and 1.455 was measured from a flat polished surface of one faceted stone. SG values spanned from 2.12 to 2.16. These figures are typical of opal in general. No hydrophane effect was noticed while doing the hydrostatic measurements, suggesting that the samples were not porous. Neither did the stone appear to absorb RI contact liquid.

Viewed with the microscope in transmitted light, the botryoidal nature of the opal was easily observed in the faceted stones. Curved growth zoning resulted from slight differences in the index of refraction between the thin successive layers (Figure 12). Yet, we observed no noticeable colour zoning in diffused lighting; this is consistent with Figure 11 of Crowningshield (1985). The curved growth zoning showed

Figure 11: These fashioned hyalites (1.32 and 0.83 ct) display bright green luminescence due to excitation from a 405 nm laser pointer. For the purpose of photography, the laser is directed near the stones, but not at them, to avoid generating 'hot spots' in the samples. Photo by B. Chauviré.

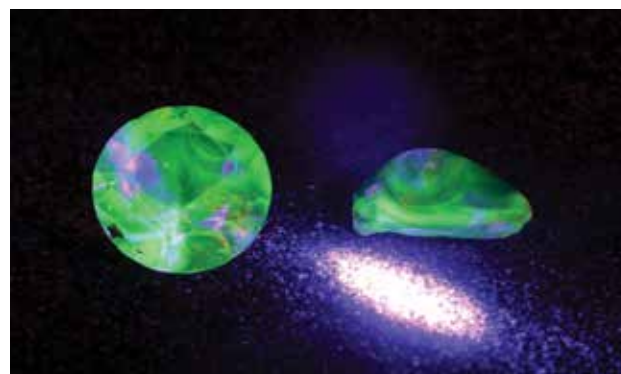


Figure 12: Botryoidal growth zoning is prominent in the faceted hyalite. Photomicrographs by E. Fritsch; image width 3.5 mm (left) and 2.0 mm (right).

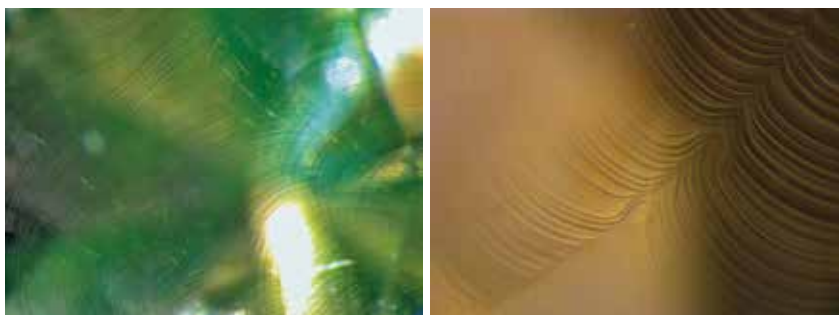


Figure 13: Between crossed polarizers, high-order interference colours are seen following botryoidal growth patterns in the hyalite. Photomicrographs by E. Fritsch; image width 2.1 mm (left) and 2.5 mm (right).

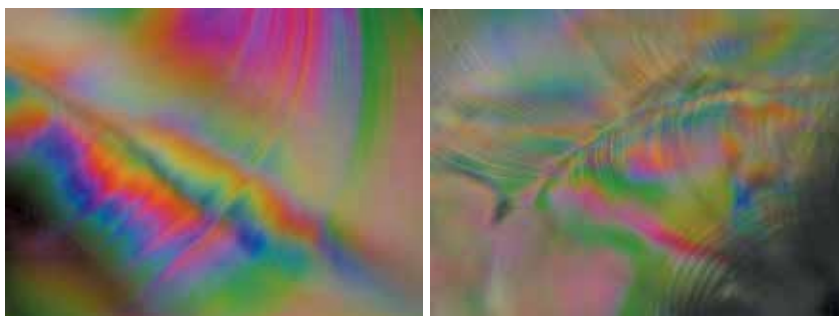


Figure 14: Colourless-to-yellow mineral inclusions in the hyalite were identified as a phosphate mineral by Raman spectroscopy. In the left photo (image width 4.8 mm), some of them are associated with curved fluid inclusions. They also were present as radiating crystal clusters (right, image width 1.5 mm). Photomicrographs by N. Renfro.



corresponding anomalous birefringence when observed between crossed polarizers (Figure 13). Such spectacular high-order interference colours reflecting the depositional layering of the opal are characteristic of hyalite (Graetsch, 1994).

Other internal features in both the rough and cut stones consisted mostly of small rock fragments, fractures (often nearly planar), colourless-to-yellow mineral inclusions (Figure 14), and very small two-phase inclusions containing liquid and a bubble (Figure 15). The fluid inclusions were trapped between curved botryoidal growth zones and as irregular flat planar fluid bodies between depositional layers. The mineral inclusions consisted of prismatic single crystals with a hexagonal cross-section and crystal clusters that were observed scattered throughout the two large faceted stones. Raman analysis confirmed them to be a phosphate. Not seen in our samples, but documented by Spano et al. (2015), were uranyl phosphate minerals contained within transparent silica tubes, which gave an acicular appearance to the normally platy U-phosphates.

Elongate tubular voids were locally present in our samples, and may represent areas in which U-bearing inclusions were leached after opal deposition. Some of these tubes, hosted by opal protuberances on some rough samples (Figure 16, left), contained minute blocky purple crystals of fluorite (Figure 16, right) that were identified by X-ray diffraction. The tubular inclusions were common in one of the large cut stones examined. They had blocky outlines and were filled with an amorphous solid material that could not be identified with Raman microspectroscopy.

Identification as Hyalite Opal-AN

This Mexican opal does not display play-of-colour, suggesting that its microstructure probably does not consist of the regular stacking of spheres as in opal-AG (such as typical opal from Australia). Instead, visual observations suggest that the samples are opal-AN. Commonly called *hyalite*, this is probably the rarest variety of gem opal.

Fourier-transform Raman scattering spectroscopy is a reliable method to characterize opal, as

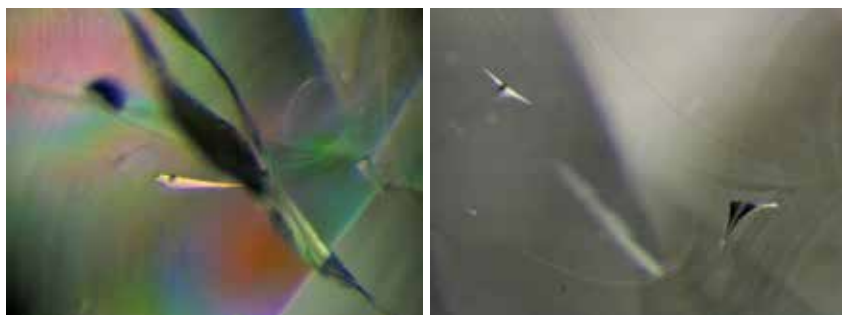


Figure 15: Fluid inclusions in hyalite occur at the intersection of curved botryoidal growth zones. The left image, taken with crossed polarizers, clearly shows a bubble inside the fluid inclusion. On the right, two fluid inclusions adopt the curved surfaces resulting from botryoidal accretion of the host opal. Photomicrographs by E. Fritsch; image width 1.3 mm (left) and 2.3 mm (right).

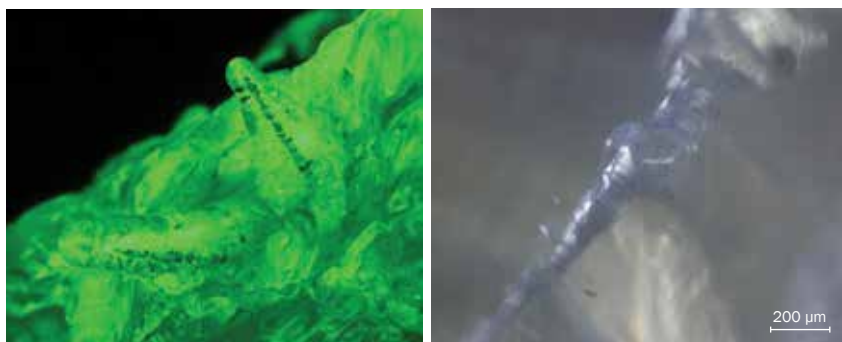


Figure 16: Two of the protuberances on this hyalite specimen contain tubular inclusions (left, image width 12.9 mm) that host minute blocky purple crystals of fluorite (right). Photos by B. Chauviré (left, under LW UV radiation) and B. Rondeau (right).

it avoids many of the challenges caused by opal's strong luminescence (e.g. Smallwood et al., 1997; Ostrooumov et al., 1999; Rondeau et al., 2004). The specimens yielded spectra typical for opal-A (e.g. Figure 17), showing a distinctive broad band with a maximum at $\sim 435\text{ cm}^{-1}$, and an abrupt drop in Raman scattering at $\sim 500\text{ cm}^{-1}$. This is different from typical opal-AG, which shows a more Gaussian-like (symmetrical) band centred at $\sim 420\text{ cm}^{-1}$ (Rondeau et al., 2004). Bands also were observed at ~ 790 , 970 and 1075 cm^{-1} , as noted in the publications cited above. A relatively broad band terminating in a sharp peak at about 1550 cm^{-1} seems unique to this Mexican hyalite; it has never been observed in the Raman spectra of other opal-AN specimens studied by the authors,

and is not documented in the literature. The broad band with an apparent maximum at $3110\text{--}3120\text{ cm}^{-1}$ is related to water, but its intensity was not reproducible with our equipment and thus is not a reliable indicator of water content. Raman scattering therefore established that this hyalite is opal-A, but was not sufficient to establish unambiguously that it is opal-AN.

To establish the exact variety of this opal-A, it was necessary to determine its microstructure through SEM imaging. At all magnifications, the samples showed the characteristics of a glass, with a smooth surface containing no holes or spheres (Figure 18). There were only traces of conchoidal fractures and associated patterns, as in glass. These features identified it as opal-AN (cf. Graetsch, 1994).

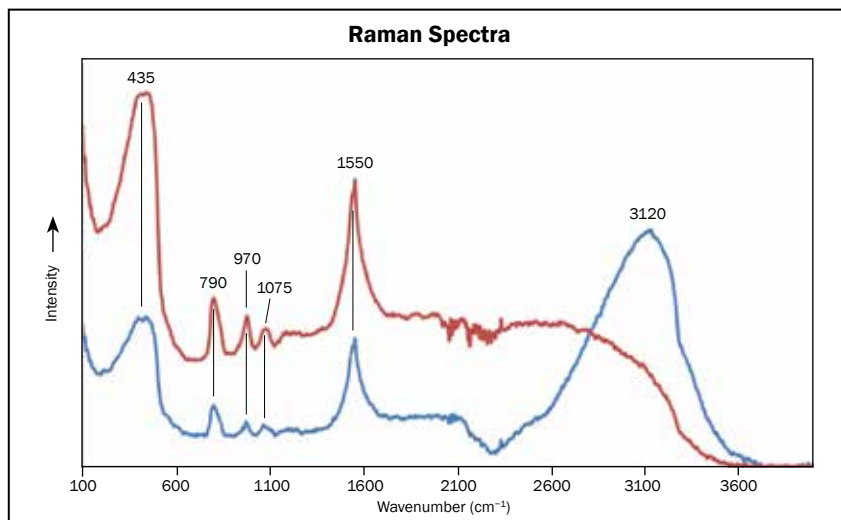


Figure 17: These representative Raman spectra of two different specimens prove that the hyalite is opal-A. They also display a band at $\sim 1550\text{ cm}^{-1}$ that has not been recorded previously in such opals.

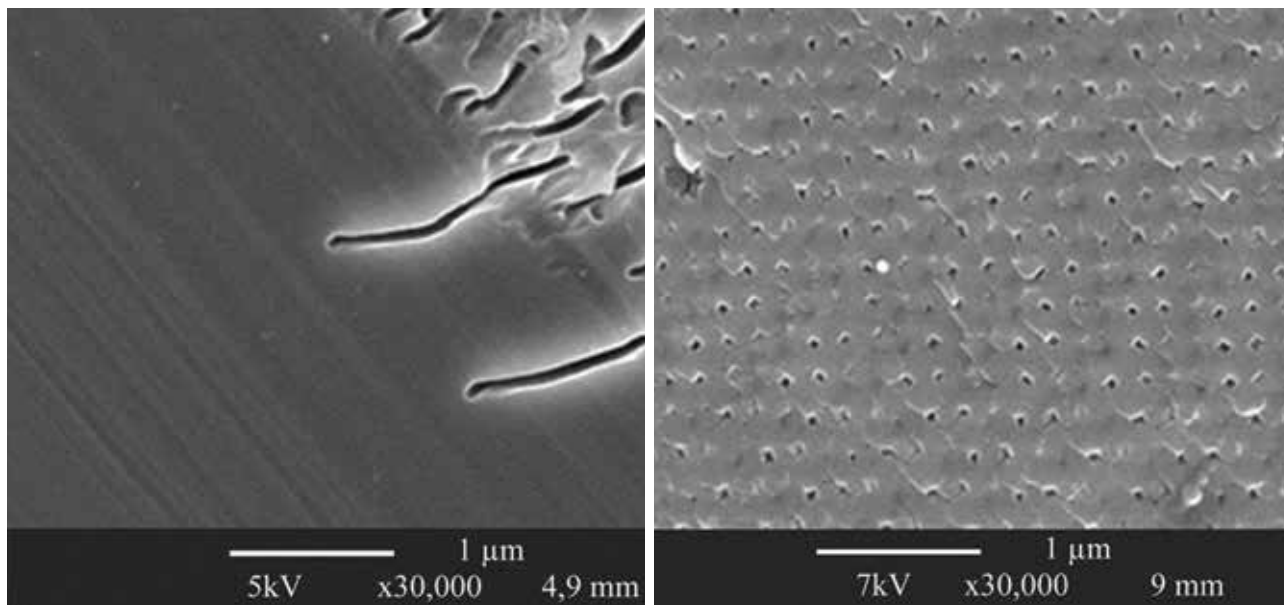


Figure 18: These scanning electron micrographs show the microstructure of the green-fluorescing hyalite from Mexico (left) compared to typical opal-AG (right, a play-of-colour specimen from Australia). The hyalite shows a glass-like structure that proves it is opal-AN, while the play-of-colour sample displays the classic regular stacking of silica spheres (as revealed by a network of holes). The worm-like features in the Mexican sample are related to conchoidal fractures and micro-cracks that were widened by hydrofluoric acid etching. Micrographs by B. Chauviré (left) and Eloise Gaillou (right).

Luminescence and UV-Vis Absorption Spectroscopy

Green UV luminescence of opal is common and well understood. It is usually stronger in SW than in LW UV excitation, and it originates from U^{6+} in the form of the uranyl (UO_2)²⁺ ion (cf. Gaillou et al., 2011). What is striking about this hyalite is that the luminescence is also excited in daylight. To understand this behaviour, we first collected the emission spectrum, which is the spectral composition of the luminescence. The green luminescence of the five samples was identical, and showed typical uranyl emission (e.g. Figure 19), with a wide band extending from about 450 nm (end of the violet range) to almost 700 nm (red region). There were five maxima, at ~504, 524, 546, 572 and 604 nm; the most intense was at 524 nm, in the green region, as expected from the colour of the emission. The emission was the same whether obtained using a standard dispersive spectrometer with 365 nm excitation (Figure 19, left) or using a 405 nm laser (Figure 19, right). At liquid-nitrogen temperature, the emission peaks shifted slightly toward shorter wavelengths.

To understand the cause of a given emission, we collected an excitation spectrum across all excitation wavelengths, measuring the intensity

of the green fluorescence excited or induced by each one. In this case, excitation spectra were obtained for the 524 nm emission (the maximum of the emission), for the same five samples (e.g. Figure 20, bottom curve). The results showed several intense bands in the UV, increasing gradually toward the SW range. This explains why the green luminescence was more intense under SW UV radiation. However, an additional, less intense pattern was present in the visible range, extending from about 375 nm (still in the UV) to about 445 nm, covering almost all of the violet range. This feature showed several maxima at ~400, 409, 419 and 432 nm. This pattern of excitation in the violet part of the visible range explains why the green luminescence is excited by visible light, and why daylight, which contains violet radiation, so effectively excites the luminescence. It also explains why 405 nm laser light produces such intense fluorescence.

The UV-Vis absorption spectra (e.g. Figure 20, top curve) were very similar regardless of body colour (which ranged from pale to moderate yellow). Absorption in the violet range explains the yellow body colour. This pattern is well known to be due to uranyl absorption (cf. Gaillou et al., 2011; Smith et al., 2013; Faulques et al., 2015 and references therein).

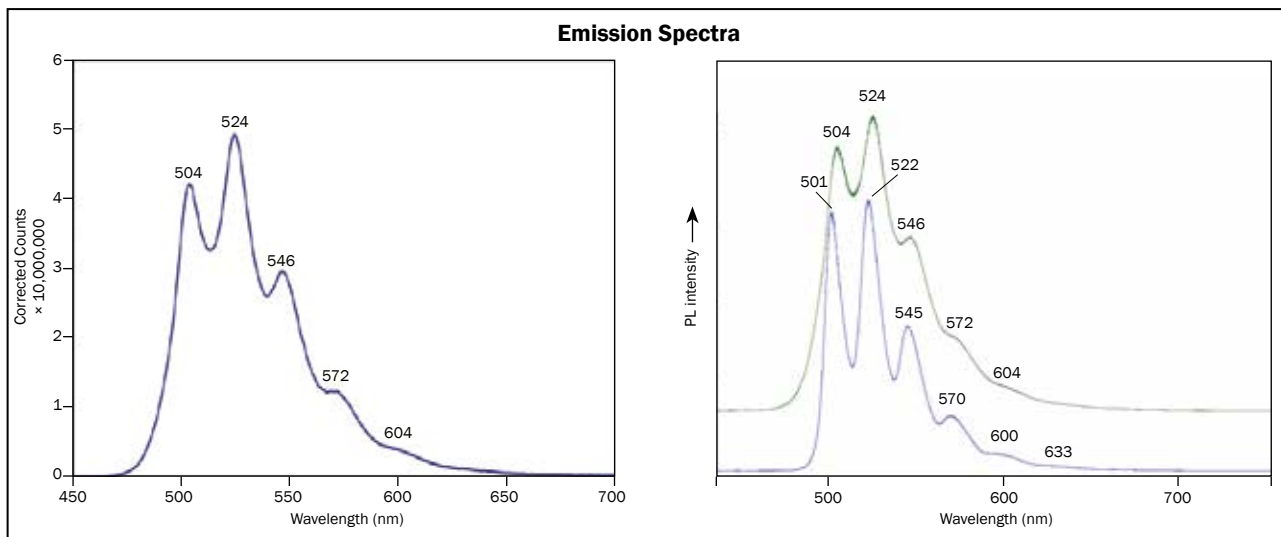


Figure 19: These emission spectra of Mexican hyalite show a characteristic uranyl pattern with five maxima. The left spectrum was taken with standard 365 nm excitation (LW UV) on a 1.32 ct round brilliant. The most intense emission (524 nm) is in the green region of the spectrum, as expected. The spectra on the right are from a 0.23 ct round brilliant excited by a 405 nm (violet) laser photoluminescence system. The top spectrum was collected at room temperature, and is identical to the spectrum on the left. The bottom spectrum, taken at liquid-nitrogen temperature, shows minor shifts. (The stone survived the thermal shock associated with the cryogenic conditions.)

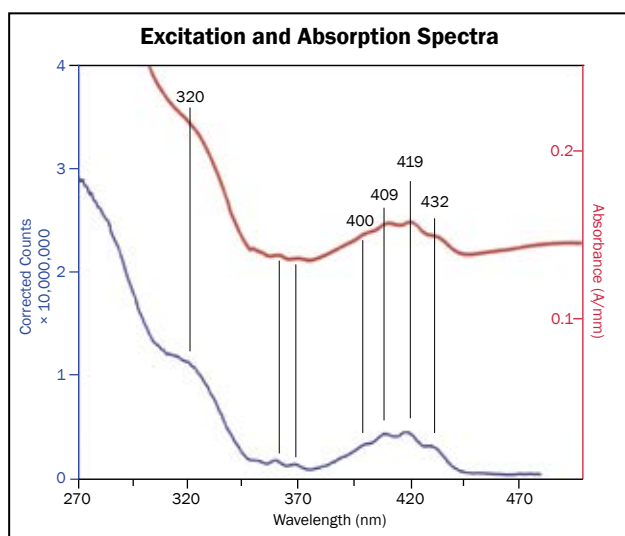


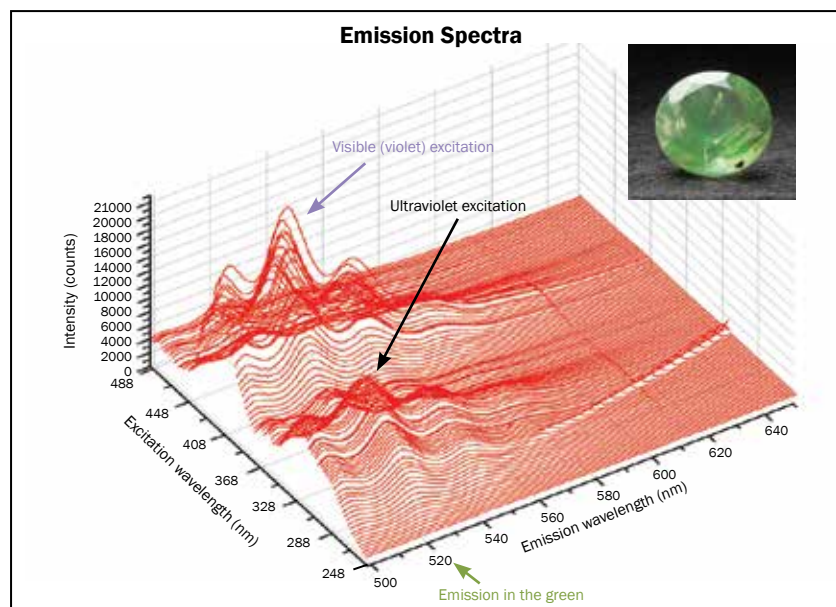
Figure 20: These curves show the excitation versus absorption spectra of the green-fluorescing hyalite from Mexico. The excitation and the absorption patterns are identical, a rare occurrence in natural gems. The path length of the beam used to collect the absorption spectra is ~3 mm.

The almost perfect superposition of the excitation and absorption spectra (again, see Figure 20) is a rare occurrence in natural luminescent materials. It suggests that all the energy absorbed by the uranyl molecule is transformed into green light. This makes the system remarkably efficient (similar to a ruby laser). In addition, this means that there is little to no outside influence on the luminescence/

excitation, which is rare in natural systems. Often, for example, one expects $O^{2-} \leftrightarrow Fe^{3+}$ charge transfer to introduce modifications between absorption and actual excitation in natural gem materials (Fritsch and Waychunas, 1993). The broadness of the emission bands in this hyalite is typical of a disordered material, not of a crystalline impurity. This strongly suggests that the uranyl ion is dispersed in the opal matrix.

Another way to view this hyalite luminescence is to plot a 3D block diagram (Figure 21) showing the emission spectra from 500 to 650 nm (red traces) as a function of excitation wavelength from 248 to 490 nm, in 3 nm intervals. The emission spectra show the same shape (with the five maxima described above, in the same relative proportions) within the excitation range that was investigated, which confirms that only one luminescence centre is involved. Only the intensity of the emission varies with excitation. Within the excitation range there are two regions of maximum emission: one is in the UV and the other is in the visible range (centred within the violet). This is consistent with the excitation spectrum noted above. However, because the 3D scan was not obtained using the same detector, and is uncorrected, the overall shape of the excitation curve is different from that described above, especially where it dips in the

Figure 21: This 3D block diagram of the hyalite luminescence shows emission spectra from 500 to 650 nm that were recorded at excitation wavelengths from 248 to 490 nm (at 3 nm intervals). Four uranyl emission peaks are visible, from ~500 to 600 nm, with the most intense emission in the green region at 524 nm. There are two main excitation regions of the green emission, one in the UV and one in the visible (violet) range. Inset photo of a 1.32 ct opal by B. Chauviré.



UV. Nevertheless, this type of data is useful to visualize the two regions of excitation.

These results were compared to those obtained for our green-luminescing reference hyalite from Inyo County, California. This sample showed the typical behaviour of stronger luminescence in SW than in LW UV radiation, and no emission with daylight illumination. The spectral data were essentially similar in the UV, but there was only a very weak maximum in the visible range. When a 3D block diagram was plotted in a similar fashion to that shown Figure 21, only the UV excitation zone was clearly seen.

Chemical Analysis and Water Content

The EDXRF data should be considered slightly high since the water content of the opal was not taken into account by the instrument. The uranium concentration ranged from approximately 20,600 to 32,400 ppmw UO_2 . This is consistent with the value of 22,604 ppmw UO_2 obtained by Spano et al. (2015) using electron microprobe analysis; they also recorded about 94.5% wt.% SiO_2 and 6,384 ppmw CaO. Calcium was also the only other significant impurity we detected (13,300–35,800 ppmw). Spano et al. (2015) proved that U is incorporated into the opal together with Ca. (All the accompanying uranium minerals also contain Ca.) We detected some Fe (<1,000 ppmw), which is much less than the 3,000 ppm necessary to quench green luminescence (Gaillou et al., 2008a). Possible traces of K were noted in

all of the analyses, and one sample showed an unquestionable trace of arsenic (~1,000 ppmw).

The water content of the opal determined by TGA analysis was 2.71 ± 0.3 wt.%. This is one of the driest opals we have measured. Added to the chemical analysis determined by Spano et al. (2015), the sum of oxides and water does not quite reach 100% (rather ~97%). This discrepancy is not surprising, considering the very different principles of operation of the two instruments used and that these data originate from different samples.

Radiometry

The ambient background level of radioactivity was 0.052–0.065 $\mu\text{Sv/h}$, and the three opals measured together were in the range of 0.055–0.069 $\mu\text{Sv/h}$. Therefore the radioactivity level of these samples was barely above background. Gamma spectroscopy revealed that only U-related radioisotopes were present above detection limits, despite the long counting time of almost three days. Three decay products of the ^{238}U family were measured: ^{234}Th at 19.4 ± 8.7 Bq/g; ^{214}Pb at 25.3 ± 2.8 Bq/g and ^{210}Pb at 26.5 ± 3.8 Bq/g. (One becquerel per gram means one disintegration per second and per gram of a particular radioisotope.) Our measurements of such low radioactivity levels over an extended period of time showed that this hyalite is not dangerous to wear (or to cut and polish into a gemstone).



Figure 22: This 3.44 ct hyalite from Zacatecas, Mexico, is shown in incandescent light (left) and in shaded daylight (right). Its green colour appearance is due to daylight-induced luminescence. Courtesy of the Smithsonian Institution; photos by Ken Larsen.

In the experience of one of the authors (PKMM), a significant volume of the bulk opal material will set off radiation detectors at the USA-Mexico border. However, this instrumentation is geared toward the detection of the slightest amount of radioactivity, and has been criticized for its inability to distinguish gamma rays originating from nuclear sources versus those “from a large variety of benign cargo types that naturally emit radioactivity, including cat litter, granite, porcelain, stoneware, banana etc.” (http://en.wikipedia.org/wiki/Radiation_Portal_Monitor). Other gem materials that likely contain some amount of U-bearing opal—such as some chalcedony, ‘crazy lace’ agate (or ‘laguna lace’ agate) and geodes from Las Choyas, Chihuahua State, Mexico—also are known to set off such detectors.

Origin of Daylight-Induced Luminescence

The main interest in this hyalite is its daylight-induced luminescence (e.g., Figure 22). Why is it observed in this opal and in almost no others? It is apparent from our measurements and the literature (in particular, Gaillou, 2006) that most opals luminescing green to UV radiation show very similar excitation spectra to those of this Mexican hyalite (i.e. uranyl absorption in the violet and blue ranges). And indeed, most opals that fluoresce green to UV radiation also will show green luminescence under a 405 nm laser, which is visible light. However, our eyes do not perceive

any green emission when these gems are observed in normal daylight. Why?

Several phenomena compete for the perception of a colour: light transmitted (the body colour), light scattered (‘haze’ in colorimetric terms) and light reflected (gloss) by an object. The most common result of light scattering is seen in milky gems (e.g. white diamond, jade or opal) or the blue adularescence of moonstone, but luminescence is also a scattering phenomenon. The green colour component of the hyalite described in this article belongs to scattered light encountering the eye. One of the matrix specimens examined by the authors was covered by green-luminescing hyalite that abruptly graded into milky white hyalite that showed no daylight luminescence (Figure 23, left). Under UV radiation (or the 405 nm laser), the green luminescence was equally intense over the entire specimen (Figure 23, right). The emission spectra obtained from all of the opal on the specimen were the same, and surprisingly the excitation spectra also were identical. Therefore the entire specimen also should have displayed the same green luminescence in daylight—if this phenomenon could be fully described by spectroscopy alone. Since the visual perception of the specimen was quite different, the daylight luminescence must be dependent upon the interplay of other factors. First, there must be an absence of any sort of luminescence quencher, such as Fe^{3+} . Second, an absence of other forms of scattering besides luminescence is important: for example

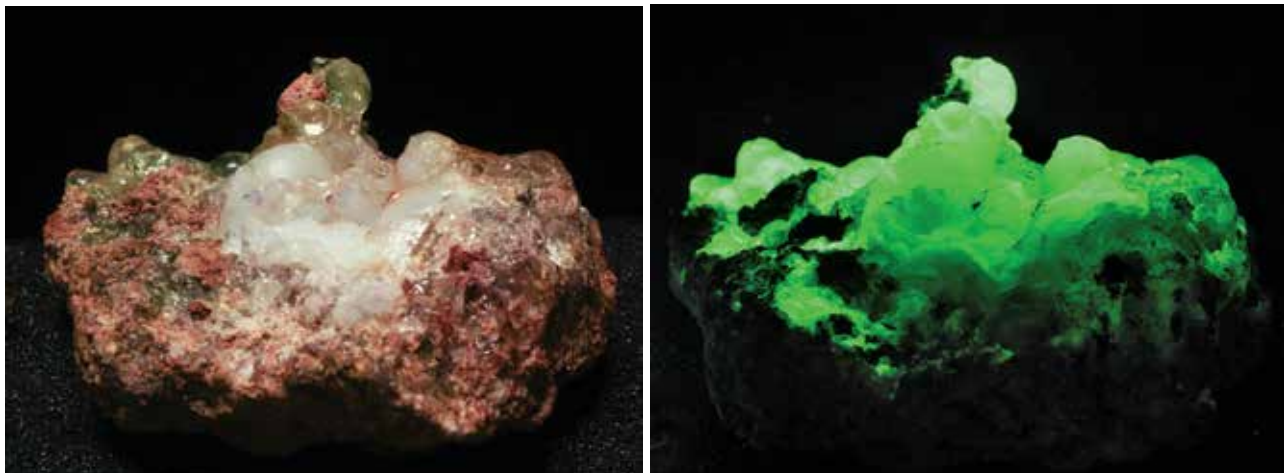


Figure 23: This specimen (~55 mm wide) is covered by hyalite that is milky white, as well as transparent hyalite showing green daylight luminescence (left). When exposed to LW UV radiation, all of the hyalite shows the same intensity of green luminescence (right). Photos by B. Chauviré.

if the sample is milky, it is unlikely that daylight luminescence will be seen. This second condition implies that the gem has to be transparent. Third, the presence of uranyl ions is a prerequisite, probably in a certain range of concentration: if there is not enough, the luminescence will be too weak, and if there is too much, the molecules will absorb one another's emission (a process called *concentration quenching* or *self-quenching*; Fritsch and Waychunas, 1993), reducing the overall luminescence.

The excitation spectrum of the hyalite basically indicates that its luminescence may be excited by visible light, but other conditions, probably not limited to those cited above, are necessary for this rare phenomenon to occur. Obviously, further research is needed to fully understand why certain materials show a luminescence colour in

daylight. A comprehensive study of such materials compared to their counterparts that do not have such an emission colour component would be necessary, and should include an investigation into the details of luminescence perception by the human eye.

Conclusions

Green daylight-luminescing opal from Zacatecas, Mexico (e.g. Figure 24), has been identified as hyalite by a combination of its opal-A Raman signal and glassy texture in the scanning electron microscope. It occurs in a volcanic environment, as is usually the case for hyalite. Its luminescence is due to dispersed uranyl ions, with a maximum emission at 524 nm, and excitation in both the UV and the visible range. Although the opal may

Figure 24: The vivid green colour shown by the hyalite in these matrix specimens (left, 2.5–3.1 cm across) and the 4.2 ct gemstone (right) is due to daylight-induced luminescence. The mineral specimens are courtesy of P.K.M. Megaw (photo by Orasa Weldon), and the cut stone was faceted by author MG (photo by Tino Hammid).



contain up to 0.3% wt.% UO₂, detailed radiation measurements recorded only very low levels of emitted radioactivity, so there is no danger in wearing or cutting this gem. Several factors contribute to the daylight luminescence of this opal—in particular its diaphaneity or ability to scatter light—but more research is needed to fully elucidate the factors governing the perception of daylight luminescence.

Perhaps 20 kg of medium-to-top-quality rough material remains to be faceted, and prospecting for more opal sites is in progress at the time of this writing. Whether more such bright green fluorescent hyalite will be discovered remains to be seen, but the geology of the deposit is reasonably well understood, and only the immediate areas around the known deposit are prospective as elsewhere the host unit has been eroded away.

References

- Berger G., Claparols C., Guy C. and Daux V., 1994. Dissolution rate of a basalt glass in silica-rich solutions: Implications for long-term alteration. *Geochimica et Cosmochimica Acta*, **58**(22), 4875–4886, [http://dx.doi.org/10.1016/0016-7037\(94\)90218-6](http://dx.doi.org/10.1016/0016-7037(94)90218-6).
- Breit G.N. and Hall S.M., 2011. Deposit model for volcanogenic uranium deposits. *United States Geological Survey Open File Report 2011-1255*, 5 pp.
- Crowningshield R.C., 1985. Gem Trade Lab Notes: Yellow green opal. *Gems & Gemology*, **21**(2), 110–111.
- Faulques E., Massuyeau F., Kalashnyk N., Perry D.L., 2015. Application of Raman and photoluminescence spectroscopy for identification of uranium minerals in the environment. *Spectroscopy Europe*, **27**(1), 14–17 and 25, www.spectroscopyeurope.com/images/stories/ArticlePDFs/Perry-27_1.pdf.
- Flörke O.W., Jones J.B. and Segnit E.R., 1973. The genesis of hyalite. *Neues Jahrbuch für Mineralogie, Monatshefte*, **110**(2), 82–89.
- Fritsch E., 1998. The nature of color in diamonds. In G.E. Harlow Ed., *The Nature of Diamonds*, American Museum of Natural History & Cambridge University Press, Cambridge, 23–47.
- Fritsch E. and Rossman G.R., 1988. An update on colors in ge78ms. Part 3: Colors caused by band gaps and physical phenomena. *Gems & Gemology*, **24**(2), 81–102, <http://dx.doi.org/10.5741/gems.24.2.81>.
- Fritsch E. and Waychunas G., 1993. Chapter 15: Gemstones. In M. Robbins, Ed., *Fluorescence: Gems and Minerals under Ultraviolet Light*, Geoscience Press, Phoenix, Arizona, USA, 149–174.
- Fritsch E., Gaillou E., Rondeau B., Barreau A., Albertini D. and Ostroumov M., 2006. The nanostructure of fire opal. *Journal of Non-Crystalline Solids*, **352**, 3957–3960, <http://dx.doi.org/10.1016/j.jnoncrysol.2006.08.005>.
- Fritsch E., Spano-Franco T. and Megaw P., 2014. Gem Notes: Green daylight-fluorescent hyalite opal from Mexico. *Journal of Gemmology*, **34**(4), 294–296.
- Gaillou E., 2006. Relations entre Nanostructure, Propriétés Physiques et Mode de Formation des Opales A et CT. PhD thesis, University of Nantes, France, 310 pp.
- Gaillou E., Delaunay A., Rondeau B., Bouhnik-Le Coz M., Fritsch E., Cornen G. and Monnier C., 2008a. The geochemistry of opals as evidence of their origin. *Ore Geology Reviews*, **34**, 113–126, <http://dx.doi.org/10.1016/j.oregeorev.2007.07.004>.
- Gaillou E., Fritsch E., Aguilar-Reyes B., Rondeau B., Post J., Barreau A. and Ostroumov M., 2008b. Common gem opal: An investigation of micro- to nano-structure. *American Mineralogist*, **93**, 1865–1873, <http://dx.doi.org/10.2138/am.2008.2518>.
- Gaillou E., Fritsch E. and Massuyeau F., 2011. Luminescence of gem opals: A review of intrinsic and extrinsic emission. *Australian Gemmologist*, **24**(8), 200–201.
- Goodell P.C. and Waters A.C., 1981. *Uranium in Volcanic and Volcaniclastic Rocks*. American Association of Petroleum Geologists, Studies in Geology, **13**, 275 pp.
- Graetsch H., 1994. Chapter 6: Structural characteristics of opaline and microcrystalline silica minerals. In P.J. Heaney et al., Eds., *Silica: Physical Behavior, Geochemistry and Materials Applications*, Mineralogical Society of America, Washington DC, USA, 209–232.
- Johnson M.L. and Koivula J.I., 1997. Gem News: Botryoidal white opal from Milford, Utah. *Gems & Gemology*, **33**(1), 63–64.
- Kane R.E. and Fritsch E., 1991. Gem Trade Lab Notes: Spinel, with unusual green fluorescence. *Gems & Gemology*, **27**(2), 112–113.
- Langer K. and Flörke O.W., 1974. Near infrared absorption spectra (4000-9000 cm⁻¹) of opal and the role of water in these SiO₂·nH₂O minerals. *Fortschritte der Mineralogie*, **52**(1), 17–51.
- Liu Y., Shigley J.E., Moses T. and Reinitz I., 1998. The alexandrite effect of the Tavernier diamond caused by fluorescence under daylight. *Color Research and Application*, **23**(5), 323–327, [http://dx.doi.org/10.1002/\(sici\)1520-6378\(199810\)23:5<323::aid-col8>3.0.co;2-y](http://dx.doi.org/10.1002/(sici)1520-6378(199810)23:5<323::aid-col8>3.0.co;2-y).
- Liu Y., Shi G. and Wang S., 2015. Color phenomena of blue amber. *Gems & Gemology*, **50**(2), 134–140, <http://dx.doi.org/10.5741/gems.50.2.134>.

- Markússon S.H. and Stefánsson A., 2011. Geothermal surface alteration of basalts, Krýsuvík Iceland—Alteration mineralogy, water chemistry and the effects of acid supply on the alteration process. *Journal of Volcanology and Geothermal Research*, **206**, 46–59, <http://dx.doi.org/10.1016/j.jvolgeores.2011.05.007>.
- McDowell F.W. and Clabaugh S.E., 1979. *Ignimbrites of the Sierra Madre Occidental and their Relation to the Tectonic Evolution of Western Mexico*. Geological Society of America Special Publication 180, 113–124, <http://dx.doi.org/10.1130/SPE180-p113>.
- Moore T.P., 2014. What's new: Tucson show 2014. *Mineralogical Record*, **45**(3), 345–375.
- Moses T., 1997. Gem Trade Lab Notes: Diamond—Two noteworthy stones from the Americas. *Gems & Gemology*, **33**(1), 54–55.
- Ostrooumov M., Fritsch E., Lasnier B. and Lefrant S., 1999. Spectres Raman des opales: Aspect diagnostique et aide à la classification. *European Journal of Mineralogy*, **11**, 899–908, <http://dx.doi.org/10.1127/ejm/11/5/0899>.
- Rondeau B., Fritsch E., Guiraud M. and Renac C., 2004. Opals from Slovakia (“Hungarian” opals): A re-assessment of the conditions of formation. *European Journal of Mineralogy*, **16**, 789–799, <http://dx.doi.org/10.1127/0935-1221/2004/0016-0789>.
- Rondeau B., Fritsch E., Mazzero F., Gauthier J.-P., Cenko-Tok B., Bekele E. and Gaillou E., 2010. Play-of-color opal from Wegel Tena, Wollo Province, Ethiopia. *Gems & Gemology*, **46**(2), 90–105, <http://dx.doi.org/10.5741/gems.46.2.90>.
- Shigley J.E. and Breeding C.M., 2015. Visible absorption spectra of colored diamonds. *Gems & Gemology*, **51**(1), 41–43, <http://dx.doi.org/10.5741/gems.51.1.41>.
- Smallwood A., Thomas P.S. and Ray A.S., 1997. Characterization of sedimentary opals by Fourier transform Raman spectroscopy. *Spectrochimica Acta A*, **53**, 2341–2345, [http://dx.doi.org/10.1016/s1386-1425\(97\)00174-1](http://dx.doi.org/10.1016/s1386-1425(97)00174-1).
- Smith N.A., Cereface G.S. and Czerwinski K.R., 2013. Fluorescence and absorbance spectroscopy of the uranyl ion in nitric acid for process monitoring applications. *Journal of Radioanalysis and Nuclides Chemistry*, **295**, 1553–1560, <http://dx.doi.org/10.1007/s10967-012-1942-4>.
- Smith R.L. and Bailey R.A., 1968. *Resurgent Calderas*. Geological Society of America Memoir 116, 613–662.
- Spano T.L., Burd A.M., Kovacks J.D. and Burns P.C., 2015. Distribution of uranium and uranyl minerals near and within hyalite opal. Poster presentation at 249th ACS National Meeting & Exposition, Denver, Colorado, USA, 22–26 March.
- Stephant N., Rondeau B., Gauthier J.-P., Cody J. and Fritsch E., 2014. Investigation of hidden periodic structures on SEM images of opal-like materials using FFT and IFFT. *Scanning*, **36**(5), 487–500, <http://dx.doi.org/10.1002/sca.21144>.
- Titkov S.V., Mineeva R.M., Zudina N.N., Sergeev A.M., Ryabchikov I.D., Shiryaev A.A., Speransky A.V. and Zhikhareva V.P., 2015. The luminescent nature of orange coloration in natural diamond: Optical and EPR study. *Physics and Chemistry of Minerals*, **42**, 131–141, <http://dx.doi.org/10.1007/s00269-014-0705-x>.

The Authors

Dr Emmanuel Fritsch

Institut des Matériaux Jean Rouxel (IMN) – CNRS, Team 6502 and University of Nantes, BP 32229, F-44322 Nantes Cedex 3, France. Email: emmanuel.fritsch@cnr-imn.fr

Dr Peter K. M. Megaw

IMDEX Inc., P.O. Box 65538, Tucson, Arizona, 85728 USA

Tyler L. Spano

Department of Civil and Environmental Engineering and Earth Sciences, University of Notre Dame, Indiana, 46556, USA

Boris Chauviré and Dr Benjamin Rondeau

LPGN CNRS, Team 6112 and University of Nantes, BP 92208, F-44322 Nantes Cedex 3, France

Michael Gray

Coast-to-Coast Rare Stones, P.O. Box 647, Mendocino, California, 95460 USA

Dr Thomas Hainschwang

GGTL Laboratories, Gnetsch 42, LI-9496 Balzers, Liechtenstein

Nathan Renfro

Gemological Institute of America, 5345 Armada Drive, Carlsbad, California, 92008 USA

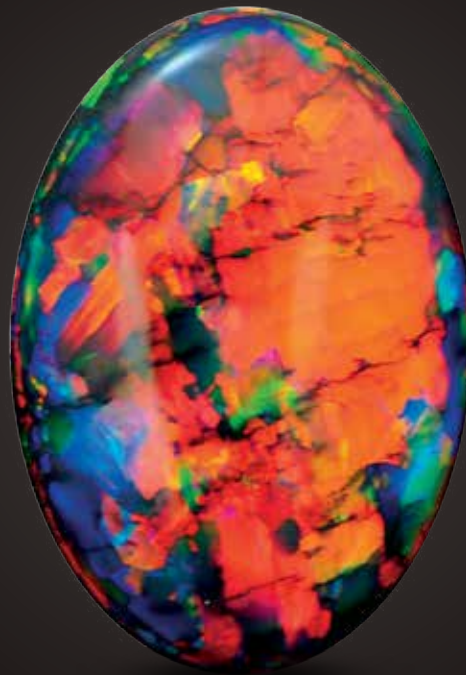
Acknowledgements

The authors thank three anonymous reviewers for their constructive comments. Florian Massuyeau, luminescence engineer at the IMN, Nantes, France, was very helpful with obtaining the spectra and preparing some of the figures.

The Fire Within

“For in them you shall see the living fire of the ruby, the glorious purple of the amethyst, the sea-green of the emerald, all glittering together in an incredible mixture of light.”

- Roman Elder Pliny, 1st Century AD



BLACK OPAL 15.7 CARATS

Suppliers of Australia's finest opals to the world's gem trade.

CODY  OPAL

LEVEL 1 - 119 SWANSTON STREET MELBOURNE AUSTRALIA

T. +61 3 9654 5533 E. INFO@CODYOPAL.COM

WWW.CODYOPAL.COM


INTERNATIONAL
COLORED GEMSTONE
ASSOCIATION
MEMBER

Raman Spectroscopy of Ancient Beads from Devín Castle near Bratislava and of Four Intaglios from other Archaeological Finds in Slovakia

*Magdaléna Kadlečíková, Juraj Breza, Ľubomír Vančo,
Miloš Gregor and Igor Bazovský*

Raman spectroscopy was used to identify violet and red-to-orange beads from a necklace and bracelet dated from the 11th and 12th centuries that were found in an ancient cemetery at Devín Castle near Bratislava, Slovakia. The violet beads (previously described as amethyst) were identified as fluorite and the red-to-orange beads were determined as quartz (carnelian). In addition, four intaglios (one unmounted and three set in ancient rings) from 2nd–3rd century AD archaeological finds in Slovakia also were analysed by Raman spectroscopy. Two of the gems were identified as carnelian (consisting of a mixture of quartz and the SiO_2 polymorph moganite), while the third stone had Raman bands for hematite and subordinate quartz, suggesting it was jasper. The Raman spectrum of the fourth intaglio corresponded to almandine with some vibrational bands for spessartine.

The Journal of Gemmology, 34(6), 2015, pp. 510–517, <http://dx.doi.org/10.15506/JoG.2015.34.6.510>
© 2015 The Gemmological Association of Great Britain

Introduction

The use of Raman spectroscopy to study archaeological materials has a long tradition, mainly because it is a non-destructive technique and does not require removal of samples from their mountings. Various materials have been analysed, including gems, pigments, glass and ceramics (e.g. Hänni et al., 1998; Smith and Clark, 2004; Zoppi et al., 2005; Vandenabeele et al., 2007; Colombari, 2012; Katsaros and Ganetsos, 2012). The aim of the present research is to identify the minerals in selected archaeological items from

Slovak National Museum collections (beads from the Bratislava City Museum and intaglios from the Archaeological Museum in Bratislava) that had been previously described only on the basis of their macro-appearance. Preliminary results of our analyses were published by Gregor et al. (2013).

Materials

Necklace and Bracelet from Devín Castle

Beads were studied from a necklace and a bracelet that were found in graves from the 11th and

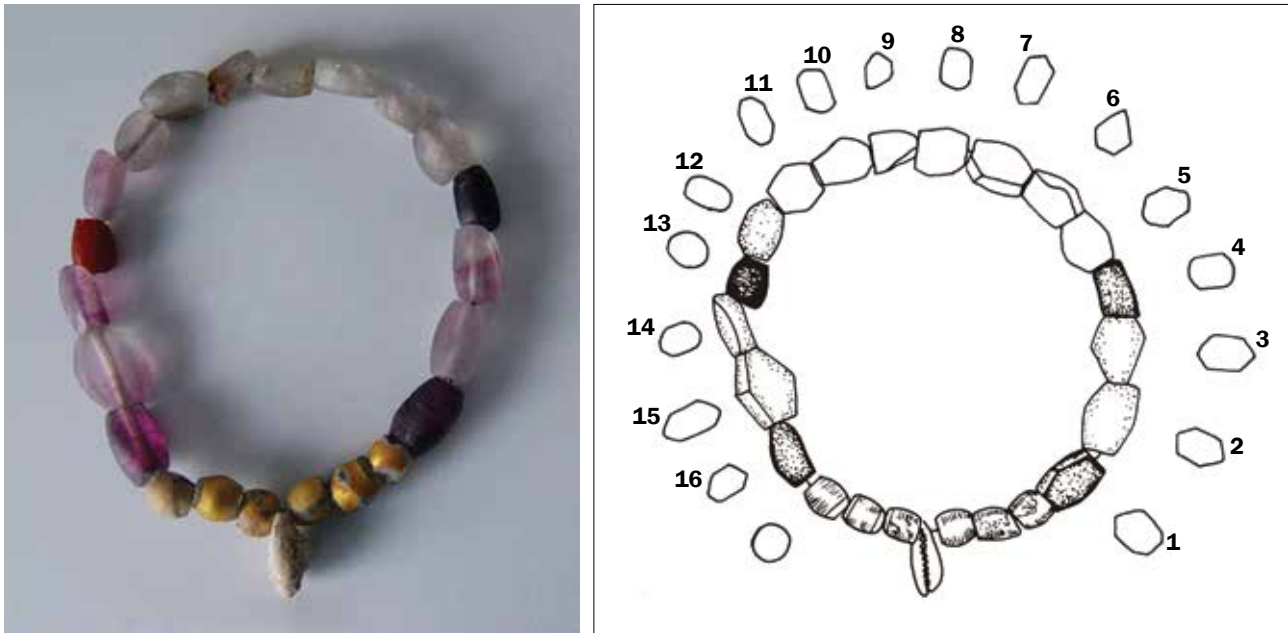


Figure 1: The 23 beads from the necklace found in Devín Castle grave 12/1980 consist of one shell of the cowrie *Cypraea moneta* (bottom), 15 faceted fluorites (sample nos. 1–12 and 14–16), one piece of amber (no. 13) and six ball-shaped beads coated with gold foil (non-numbered). The numbered beads range from 11 to 16 mm long. Photo by D. Divileková.

12th centuries at Devín Castle near Bratislava (Plachá and Divileková, 2012). The necklace, consisting of 23 beads (Figure 1), was found in tomb 12/1980, which contained an incomplete skeleton of a woman. The skull, shoulder blades and lower limbs were preserved in good condition. This grave hosted a rich inventory of artefacts: a silver earring on the left side of the skull, necklace beads between the shoulder blades and a ring at the position expected for the right hand. The bracelet, consisting of six beads (Figure 2), was found in grave 145/1985, in which another woman's skeleton was discovered. The beads were found below the mandible. All the beads are drilled through axially. Selected properties of the beads are summarized in Table I.

Beads from the necklace can be divided into three categories. The first contains only one bead, which is the shell of *Cypraea moneta* (or 'money cowrie', named after the use of this shell as money since ancient times). It was probably positioned as a pendant in the necklace. The second category includes six ball-shaped beads (probably glass) coated with gold foil and typically showing a weathered surface; these beads were studied only macroscopically as they do not correspond to natural gem material. In the third category were 16 roughly faceted oval beads with dull lustre and showing various colours (mostly colourless to dark violet). One of these beads with a dark red colour (no. 13) was previously identified as amber by its macroscopic

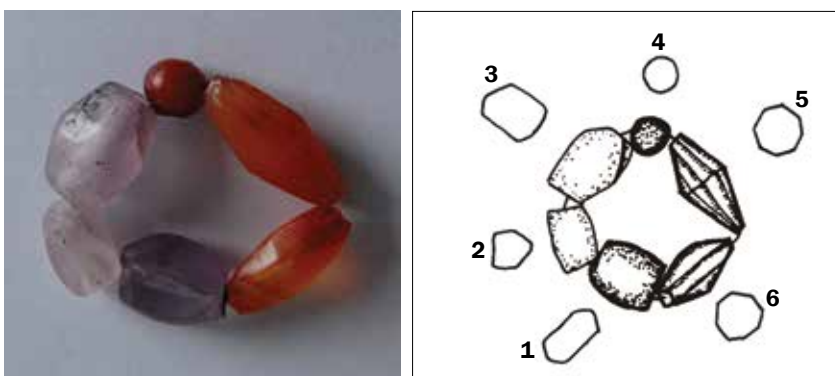


Figure 2: The six beads from the bracelet found in Devín Castle grave 145/1985 were identified as three faceted fluorites (nos. 1–3) and three pieces of carnelian (nos. 4–6). The smallest bead is 7 mm in diameter and the largest is 22 mm long. Photo by D. Divileková.

Table 1: Properties of the beads recovered from Devín Castle, Bratislava, Slovakia.

Item	Bead number	Colour	Transparency	Lustre	Material	Long-wave UV fluorescence	Size (mm)	Drill hole diameter (mm)
Necklace beads from grave 12/1980	1	Dark violet	Opaque	Dull	Fluorite	-	16×11×10	3
	2	Light violet	Translucent	Dull	Fluorite	Blue	16×11×10	3
	3	Light violet	Translucent	Dull	Fluorite	Blue	15×13×8	3
	4	Dark violet	Opaque	Dull	Fluorite	Blue	13×10×8	3
	5	Colourless	Translucent	Dull	Fluorite	Blue	12×12×9	3
	6	Colourless	Translucent	Dull	Fluorite	Blue	13×12×9	3
	7	Colourless with green tint	Translucent	Dull	Fluorite	Blue	13×12×7	3
	8	Colourless with green tint	Translucent	Dull	Fluorite	Blue	12×11×7	3
	9	Colourless	Translucent	Dull	Fluorite	Blue	11×10×6	3
	10	Colourless with green tint	Translucent	Dull	Fluorite	Blue	14×12×8	3
	11	Colourless	Translucent	Dull	Fluorite	Blue	12×11×8	3
	12	Light violet	Translucent	Dull	Fluorite	Blue	14×12×7	3
	13	Dark red	Opaque	Waxy	Amber	-	11×8×7	3
	14	Light violet	Translucent	Dull	Fluorite	Blue	15×10×7	3
	15	Light violet	Translucent	Dull	Fluorite	Blue	16×14×8	3
	16	Dark violet	Opaque	Dull	Fluorite	-	16×12×9	3
Bracelet beads from grave 145/1985	1	Colourless with violet tint	Translucent	Dull	Fluorite	Blue	15×12×9	3
	2	Colourless with violet tint	Translucent	Dull	Fluorite	Blue	14×12×6	3
	3	Light violet	Translucent	Dull	Fluorite	Blue	11×8×7	3
	4	Red	Translucent	Vitreous	Carnelian	-	7×7×7	1.5
	5	Orange	Translucent	Vitreous	Carnelian	-	19×8×8	1.5
	6	Orange	Opaque	Vitreous	Carnelian	-	22×9×9	1

properties (lustre, colour, inferred hardness and specific gravity; see Plachá and Divileková, 2012). This amber bead, as well as the shell bead, were not examined for this report.

The bracelet consisted of three colourless-to-light-violet and three red-to-orange beads. The violet beads were similar in shape to the oval beads in the necklace described above, while the red-to-orange ones consisted of a seed-style bead and two roughly faceted bicone beads.

Other Ancient Gems from Slovakia

These samples consisted of three gems set in rings and one unmounted stone. Figure 3a shows a gold ring (AP 44 419) dating to the second half of the 3rd century AD from Castle Hill in Bratislava, above the Church of St Nicholas. It contains a light red oval intaglio that is engraved with a nude human figure holding a helmet in the right hand and another object (perhaps a mace) in the left hand. The metal part of the ring is undecorated. Figure

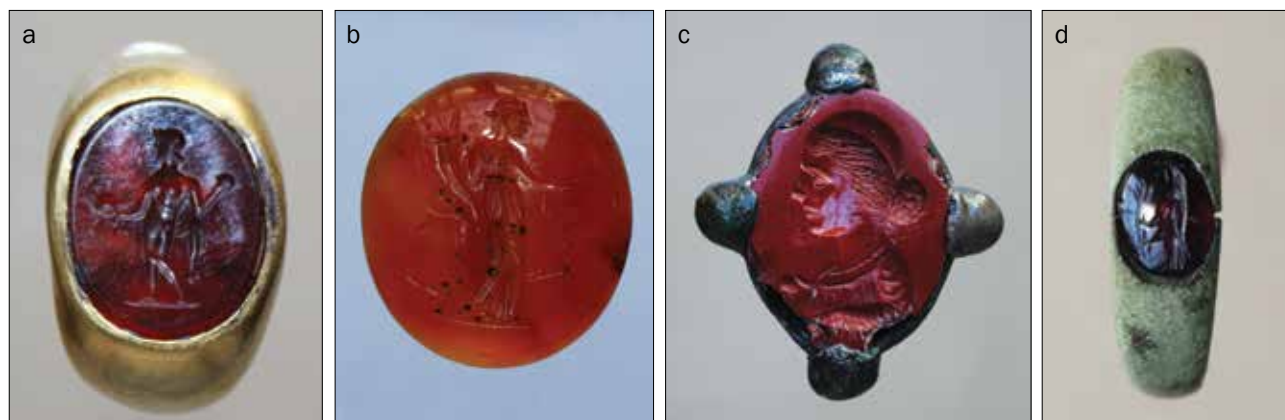


Figure 3: Four ancient gems from various archaeological finds in Slovakia were studied for the report: (a) a gold ring (AP 44 419) containing an intaglio (1.1×1.4 cm) decorated with a human figure, from Castle Hill in Bratislava; (b) an intaglio (AP 44 749; 1.65×1.7 cm) presumably depicting the goddess Fortuna, also from Castle Hill; (c) a ring (AP 17 343) with an intaglio showing a woman's profile (1.8×2.35 cm), from an ancient tomb at Sereď; and (d) a bronze ring (AP 51 487) containing a dark red intaglio (0.56×0.61 cm) with an image of a parrot, from Rusovce near Bratislava. Photos by I. Choma.

3b shows an unmounted orangey red intaglio (AP 44 749) with an image of the goddess Fortuna holding a steer in her left hand and a horn-of-plenty in her right hand. This intaglio is also from Castle Hill (above the Church of St Nicholas), and dates from the middle of the 2nd century AD; it is part of a collection of artefacts from the La Tène culture. Figure 3c shows a ring (AP 17 343) from a tomb at Sereď (located approximately 50 km northeast of Bratislava) that is dated to the 2nd century AD. This ring features a red intaglio that is set in silvery white metal. The opaque stone is decorated by the bust of a woman, viewed from the left profile, holding a round object (probably an apple). Figure 3d shows a bronze ring (AP 51 487) containing a translucent dark red intaglio engraved with a parrot sitting on a sprig. This ring comes from Rusovce (just south of Bratislava) and is dated to the first half of the 2nd century AD.

Methods

The colourless-to-violet and red-to-orange beads from Devín Castle, and all four intaglios from the other archaeological finds in Slovakia, were examined with a binocular visor magnifier and an optical microscope, and their colour, transparency, lustre and UV fluorescence were determined.

The gems selected for analysis by Raman spectroscopy included two violet faceted beads (no. 2 from tomb 12/1980 and no. 3 from grave 145/1985), all three red-to-orange beads (nos. 4–6 from tomb 145/1985) and all four intaglios

from the other archaeological finds in Slovakia. The samples were analysed at room temperature without any preparation. Raman spectra were collected with a Dilor–Jobin Yvon–Spex LabRam spectrometer. The samples were placed on the micrometric manipulator of a confocal microscope (Olympus BX-40) and visualized in a video monitor. The excitation source was an He–Ne laser (632.8 nm, 15 mW). The scattered radiation was focused onto the entrance slit of a grid monochromator (1,800 grooves/mm), and the spectral range was up to 4000 cm^{-1} . The spectrometer was equipped with a multichannel CCD detector with a resolution of 1.3 cm^{-1} ; it was calibrated to the 520.7 cm^{-1} band of monocrystalline silicon. The focused beam was approximately 2 μm in diameter, and the time of data collection ranged from 20 to 200 seconds depending on the intensity of Raman scattering and fluorescence.

The Raman spectra were processed using the LabSpec software package, and the results were compared to Raman spectral databases (e.g. ruff.info) and with the literature (Loudon, 1964; Ganetsos et al., 2013). The signal-to-noise ratio was sufficient for identifying the Raman bands.

Results and Discussion

Beads from Devín Castle

The colourless-to-violet beads from both the necklace and bracelet were 11–16 mm long

and showed roughly faceted oval shapes with rounded edges. They varied from colourless (sometimes with a violet or green tint) to light violet to dark violet. The colourless and light violet beads were translucent, and some of the latter showed colour zoning. The dark violet beads were opaque, and all showed a dull lustre. Most of the beads fluoresced blue to long-wave UV radiation, with two of the dark violet beads being inert. Some of the beads were broken (e.g. no. 9) and they showed perfect cubic cleavage. No inclusions could be observed through the poorly polished surfaces.

Selected Raman spectra of the violet beads are shown in Figure 4. Both spectra correspond to fluorite. The Raman T_{2g} band at 322 cm^{-1} is a triple-degenerated vibration of the F^- anion sub-lattice with respect to stationary Ca^{2+} cations (Loudon, 1964). Previously, violet or dark violet roughly faceted oval beads from early Medieval cemeteries were commonly believed to be amethyst (e.g. Rejholcová, 1974). However, our visual observations of the beads were not consistent with amethyst, and Raman spectroscopy clearly confirmed that they were fluorite.

The red and orange beads from the bracelet were translucent to opaque and showed a vitreous lustre. They were inert to UV radiation. Raman spectroscopy (Figure 5) identified them as quartz (α -quartz, trigonal SiO_2), confirming that they are carnelian (a variety of chalcedony composed of orange-to-red fibrous microcrystalline quartz). Red bead no. 4 also showed Raman bands for moganite, a monoclinic quartz polymorph. The Raman features corresponding to α -quartz are A_1 bands at 207, 355 and 465 cm^{-1} and E bands at 264, 394 and 401 cm^{-1} . The band at 503 cm^{-1} with E symmetry indicates the presence of moganite and corresponds to Si-O-Si vibrations (Kingma and Hemley, 1994).

Other Ancient Gems from Slovakia

All four intaglios were previously described in museum records as carnelian. Intaglio AP 44 419 was translucent and without any observable inclusions. Its Raman spectrum (Figure 6, top) shows a dominant vibrational band centred at 463 cm^{-1} and additional bands at 128, 207, 264, 353 and

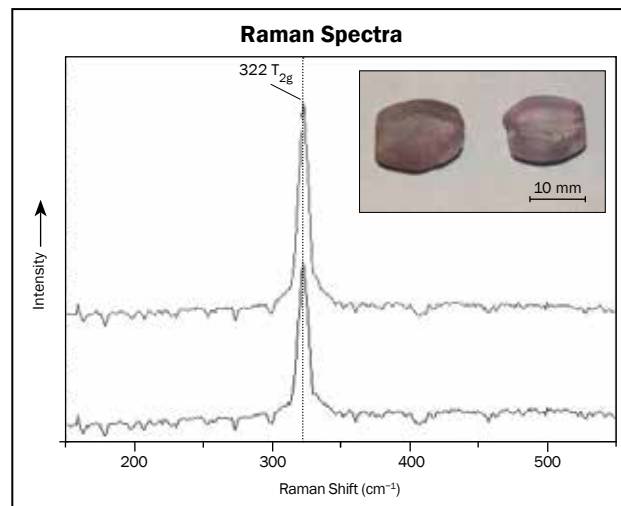
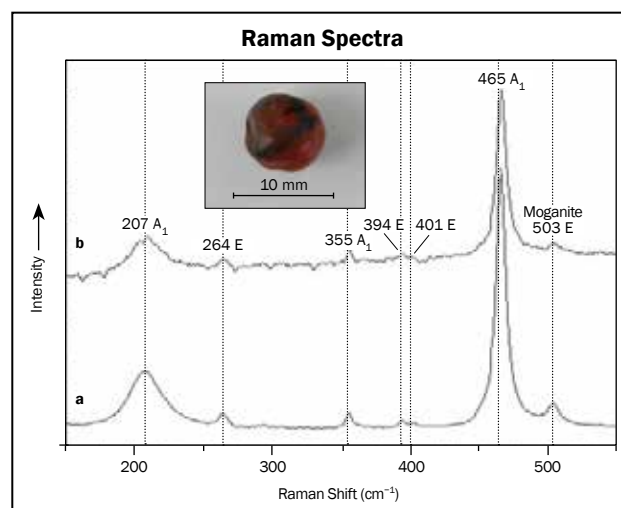


Figure 4: Raman spectra of two violet beads found at Devín Castle correspond to fluorite. These spectra were recorded from two different places on bead no. 3 (shown on the left in the inset) from grave 145/1985. The right bead in the inset is no. 2 from grave 12/1980; it yielded identical Raman spectra. Inset photo by D. Divíleková.

393 cm^{-1} that identify it as α -quartz. In addition, a band at 502 cm^{-1} corresponds to moganite. The presence of quartz could be reliably established not only through the dominant band at 463 cm^{-1} but also by the band at 353 cm^{-1} (Kingma and Hemley, 1994). Our visual observations of this intaglio (i.e. red colour and its inferred hardness)

Figure 5: Raman spectra are shown for red bead no. 4 from the bracelet of grave 145/1985, recorded from an area with an inclusion of an unknown brown mineral (a) and from the typical sample surface (b). The better signal-to-noise ratio of the latter spectrum is probably due to stronger absorption of the incident laser radiation. The major phase is α -quartz (trigonal SiO_2), and the weak band at 503 cm^{-1} corresponds to moganite (monoclinic SiO_2). Inset photo by D. Divíleková.



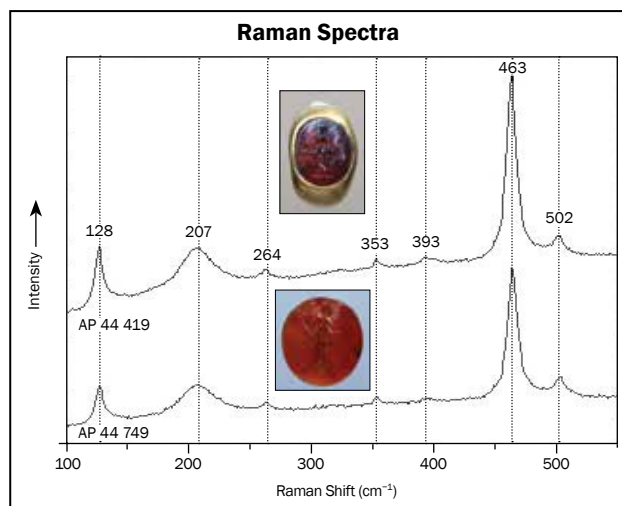


Figure 6: Raman spectra of carnelian intaglios AP 44 419 and AP 44 749 have bands centred at approximately 463 and 502 cm^{-1} that prove the presence of quartz and moganite, respectively. Inset photos by I. Choma.

corresponded to carnelian. Gem AP 44 749 had similar macroscopic characteristics, and its Raman spectrum (Figure 6, bottom) also identified it α -quartz and moganite (i.e. carnelian).

The Raman spectrum of gem AP 17 343 (Figure 7) confirmed the presence of hematite, with vibrational bands centred at 228 (A_{1g}), 248 (E_g), 294 (E_g), 413 (E_g), 501 (A_{1g}), 614 (E_g) and 1322 cm^{-1} (cf. Porto and Krishnan, 1967). The Raman spectrum also contains weak vibrational bands centred at approximately 130 and 466 cm^{-1} that reflect the presence of quartz. The band at 466 cm^{-1} is not expected in hematite using the group theory (de Faria et al., 1997). On the basis of its Raman spectrum and visual macroscopic characteristics (deep red colour, opaqueness, fracture pattern and lustre), we concluded that this gem is jasper.

Gem AP 51 487 in the bronze ring has a distinctly dark red colour and was transparent with a vitreous lustre. Its Raman spectrum (Figure 8) shows bands centred at 171, 217, 347 (subdominant band), 374, 500, 557, 633, 861, 918 (dominant band) and 1028 cm^{-1} , clearly placing it in the garnet structural group. A shift of the band positions can occur as atoms with different masses occupy the cationic sites. Based on data provided by Pinet and Smith (1993), the calcic series uvarovite-grossular-andradite is not a possibility because of differing Raman bands. However, spectra from the aluminian series pyrope-almandine-spessartine fit well with

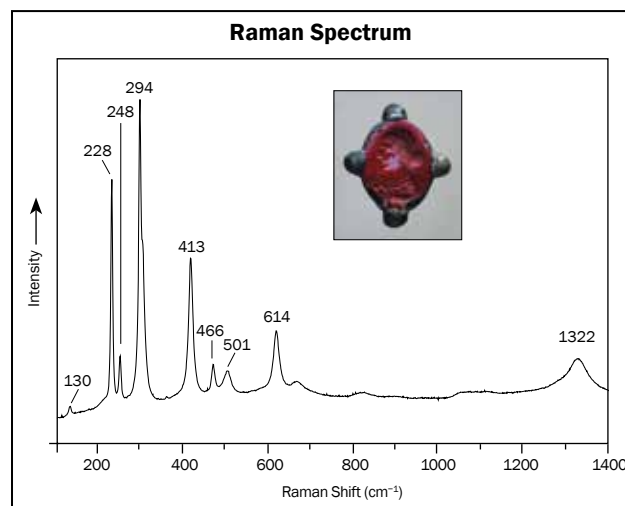


Figure 7: Ring AP 17 343 from the ancient tomb at Sered contains a jasper intaglio that has a Raman spectrum corresponding to hematite and subordinate quartz. Inset photo by I. Choma.

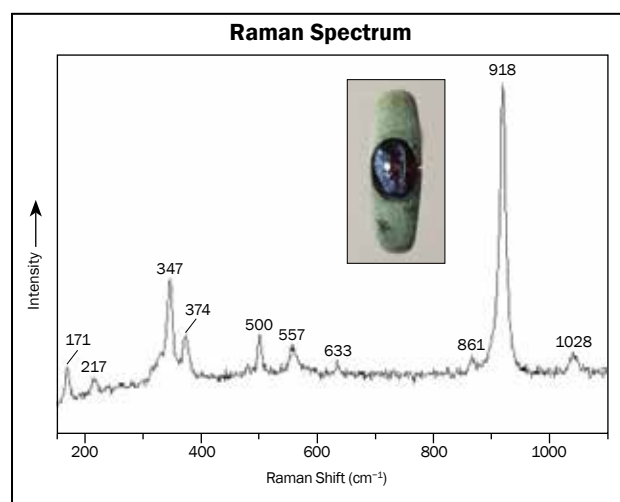


Figure 8: Intaglio AP 51 487 yielded a Raman spectrum with vibrational bands belonging to almandine and subordinate spessartine. Inset photo by I. Choma.

our measured Raman spectrum (cf. Pinet and Smith, 1994). As indicated by the data in Table II, the stone consists of almandine with a spessartine component rather than a pyrope component. Further support for the almandine-dominant composition was obtained by comparing its Raman spectrum with various spectra for almandine (rruff.info/almandine-R040076), spessartine (rruff.info/spessartine-R050063) and pyrope (rruff.info/pyrope-R040159), as well as with the spectra for almandine from Tyrol in Austria and from the historical site of Alabanda in Turkey (Ganetsos et al., 2013).

Table II: Raman bands (cm^{-1}) useful for the identification of garnet intaglio AP 51 487.

Spectral range	Aluminian-series garnets (Pinet and Smith, 1994)			This work	Band symmetry
	Spessartine	Almandine	Pyrope		
1100–750	1030	1038	1062	1028	T_{2g}
	906	915	924	918	T_{2g}
	850	862	867	861	T_{2g}
750–450	632	630	648	633	T_{2g}
	553	557	561	557	A_{1g}
	503	499	511	500	T_{2g}
450–120	375	370	380	374	T_{2g}
	352	345	364	347	A_{1g}
	224	216	208	217	T_{2g}
	175	168	174	171	T_{2g}

Conclusion

Raman spectroscopy was used to analyse selected beads from a necklace and a bracelet dating from 11th- and 12th-century burials at Devín Castle in Slovakia. The violet beads were previously believed to be amethyst, but our investigations confirmed they are fluorite. In addition, red-to-orange beads from the bracelet were identified as carnelian (confirming their previous identification from visual observations). One of the carnelian beads also showed the presence of moganite (monoclinic SiO_2) in its Raman spectrum. The intergrowth of quartz and moganite polymorphs of SiO_2 is typical for agate structures (Heaney and Davis, 1995).

In addition, four ancient gems (intaglios) from elsewhere in Slovakia were analysed. Two of them were identified as carnelian, showing Raman bands for quartz and moganite. Another intaglio had Raman bands corresponding to hematite and subordinate quartz, suggesting it was jasper. The fourth gem corresponded to almandine with some vibrational bands for spessartine.

Carnelian and jasper are relatively common gems that are known from numerous sources, so the provenance of those ancient beads/intaglios is unknown. The provenance of the almandine-dominant intaglio also is not clear. Garnet with this composition is known from various localities in Zillertal in the Austrian Alps (Grundmann, 1988). Also the classical locality of Alabanda in Turkey should not be excluded (e.g. Rapp, 2002; Ganetsos et al., 2013), as it was known in

the Roman age. Clearly, the geographical origin of the ancient almandine-dominant intaglio documented in this article cannot be identified only on the basis of its mineralogical composition.

References

- Colomban P., 2012. The on-site/remote Raman analysis with mobile instruments: A review of drawbacks and success in cultural heritage studies and other associated fields. *Journal of Raman Spectroscopy*, **43**(11), 1529–1535, <http://dx.doi.org/10.1002/jrs.4042>.
- de Faria D.L.A., Venâncio Silva S. and de Oliveira M.T., 1997. Raman microspectroscopy of some iron oxides and oxyhydroxides. *Journal of Raman Spectroscopy*, **28**(11), 873–878, [http://dx.doi.org/10.1002/\(sici\)1097-4555\(199711\)28:11<873::aid-jrs177>3.0.co;2-b](http://dx.doi.org/10.1002/(sici)1097-4555(199711)28:11<873::aid-jrs177>3.0.co;2-b).
- Ganetsos T., Katsaros T., Vandenabeele P., Greiff S. and Hartmann S., 2013. Raman spectroscopy as a tool for garnet analysis and investigation on samples from different sources. *International Journal of Materials and Chemistry*, **3**(1), 5–9.
- Gregor M., Vančo L., Kadlečková M. and Breza J., 2013. Raman spectroscopy of gemstones on the necklaces from ancient graves at the Castle of Devín. In J. Vajda and I. Jamnický, Eds., *Proceedings of the 19th International Conference on Applied Physics of Condensed Matter*, Štrbské Pleso, Slovakia, 19–21 June, 42–45, http://kf.elf.stuba.sk/~apcom/apcom13/proceedings/pdf/042_Gregor_Vanco.pdf.
- Grundmann G., 1988. Metamorphic evolution of the Habach Formation: A review. *Österreichische Geologische Gesellschaft – Mitteilungen*, **81**(3), 133–149.

- Hänni H.A., Schubiger B., Kiefert L. and Häberli S., 1998. Raman investigation on two historical objects from Basel Cathedral: The Reliquary cross and Dorothy monstrance. *Gems & Gemology*, **34**(2), 102–125, <http://dx.doi.org/10.5741/gems.34.2.102>.
- Heaney P.J. and Davis A.M., 1995. Observation and origin of self-organized textures in agates. *Science*, **269**(5230), 1562–1565, <http://dx.doi.org/10.1126/science.269.5230.1562>.
- Katsaros T. and Ganetsos T., 2012. Raman characterization of gemstones from the collection of the Byzantine & Christian Museum. *Archaeology*, **1**(2), 7–14.
- Kingma K.J. and Hemley R.J., 1994. Raman spectroscopic study of microcrystalline silica. *American Mineralogist*, **79**(3–4), 269–273.
- Loudon R., 1964. The Raman effect in crystals. *Advances in Physics*, **13**(52), 423–482, <http://dx.doi.org/10.1080/00018736400101051>.
- Pinet M. and Smith D.C., 1993. Raman microspectrometry of garnets $X_3Y_2Z_3O_{12}$: I. The natural calcic series uvarovite-grossular-andradite. *Schweizerische Mineralogische und Petrographische Mitteilungen*, **73**(1), 21–40.
- Pinet M. and Smith D.C., 1994. Raman microspectrometry of garnets $X_3Y_2Z_3O_{12}$: II. The natural aluminian series pyrope-almandine-spessartine. *Schweizerische Mineralogische und Petrographische Mitteilungen*, **74**(2), 161–179.
- Plachá V. and Divileková D., 2012. Cintorín z 11.–12. storočia na hrade Devín. *Slovenská Archeológia*, **60**, 45–118, English abstract available at www.archeol.sa+5v.sk/docs_slovarch/slovarch_2012_LX-1.pdf.
- Porto S.P.S. and Krishnan R.S., 1967. Raman effect of corundum. *Journal of Chemical Physics*, **47**(3), 1009–1012, <http://dx.doi.org/10.1063/1.1711980>.
- Rapp G., 2002. *Archaeomineralogy*. Springer, Berlin, <http://dx.doi.org/10.1007/978-3-662-05005-7>.
- Rejholcová M., 1974. Cemetery from the 10th–12th centuries at Nové Zámky. *Slovenská Archeológia*, **22**, 433–460 (in Slovak).
- Smith G.D. and Clark R.J.H., 2004. Raman microscopy in archaeological science. *Journal of Archaeological Science*, **31**(8), 1137–1160, <http://dx.doi.org/10.1016/j.jas.2004.02.008>.
- Vandenabeele P., Tate J. and Moens L., 2007. Non-destructive analysis of museum objects by fibre-optic Raman spectroscopy. *Analytical and Bioanalytical Chemistry*, **387**(3), 813–819, <http://dx.doi.org/10.1007/s00216-006-0758-x>.
- Zoppi A., Castellucci E.M. and Lofrumento C., 2005. Phase analysis of third millennium Syrian ceramics by micro-Raman spectroscopy. In H.G.M. Edwards and J.M. Chalmers, Eds., *Raman Spectroscopy in Archaeology and Art History*, RSC Analytical Spectroscopy Series, Royal Society of Chemistry, Cambridge, 217–227.

The Authors

**Magdaléna Kadlečíková, Juraj Breza and
Lubomír Vančo**

Slovak University of Technology
Ilkovičova 3, 812 19 Bratislava, Slovakia
E-mail: juraj.breza@stuba.sk

Miloš Gregor and Igor Bazovský

Slovak National Museum, Vajanského
Nábřežie 2, 810 06 Bratislava, Slovakia

Acknowledgements

The work was supported by grant VEGA 1/0601/13 of the Ministry of Education of the Slovak Republic. We are grateful to specialists at the Bratislava City Museum for their help, and to V. Plachá, D. Divileková, M. Daňová, R. Čambal, V. Turčan, T. Štefanovičová and A. Ruttkay for the use of their information.

Gem-A Members and Gem-A registered students receive 5% discount on books and 10% discount on instruments from Gem-A Instruments

Contact instruments@gem-a.com or visit our website for a catalogue

The First Undisclosed Colourless CVD Synthetic Diamond Discovered in a Parcel of Natural Melee-Sized Diamonds

Thomas Hainschwang and Franck Notari

During the March 2015 Diamond Show in Basel, Switzerland, a parcel of 6,000 melee-sized colourless diamonds was analysed using the GGTL Diamond Fluorescence Imaging (DFI) Laser⁺ fluorescence imaging and spectroscopy system. From the entire parcel, one sample stood out clearly with unusual fluorescence colours and distribution, combined with a photoluminescence spectrum that clearly indicated it was a synthetic diamond grown by chemical vapour deposition (CVD).

The Journal of Gemmology, 34(6), 2015, pp. 518–522, <http://dx.doi.org/10.15506/JoG.2015.34.6.518>
© 2015 The Gemmological Association of Great Britain

Introduction

With the introduction of near-colourless, single-crystal, gem-quality CVD synthetic diamond into the market in recent years, and the enormous progress made in the growth of near-colourless synthetic diamond produced by high-pressure, high-temperature (HPHT) synthesis in the past two years, the gem industry has been very concerned about these synthetics being sold without proper disclosure. One of the main concerns is the mixing of near-colourless melee-sized synthetics into parcels of natural diamond, but so far this has not been confirmed despite many rumours within the trade. The only scientific reports of undeclared melee-sized synthetics detected in parcels of natural diamonds have been HPHT-grown yellow samples (Kitawaki et al., 2008; Hainschwang and Notari, 2012), and recently a single CVD-grown yellow synthetic diamond (Hainschwang, 2014). Until now, near-colourless CVD synthetic diamonds submitted to laboratories were in larger sizes. Since they are straightforward to identify by

a well-equipped lab, they have not caused major concern within the trade.

The efficient testing of melee-sized diamonds is a highly specialized task and requires a lot of expertise and specially adapted analytical methods, particularly for fancy-colour diamonds. GGTL Laboratories is one of the few facilities with the expertise and equipment to test large amounts of colourless and fancy-colour melee diamonds for the watch and jewellery industry. After several years of testing such parcels (with several million pieces analysed), GGTL Laboratories recently found the first undisclosed melee-sized colourless CVD synthetic diamond in a parcel of natural diamonds (Hainschwang and Notari, 2015). This article describes the properties of this specimen.

Materials and Methods

A parcel of 6,000 diamonds, each measuring 1.6 mm in diameter, was analysed by GGTL Laboratories during the Diamond Show in Basel in March 2015. The parcel had been purchased



Figure 1: This 1.6-mm-diameter, F-colour, IF-clarity CVD synthetic diamond was found in a parcel of natural melee (left; photo by T. Hainschwang). Its lamellar appearance between crossed polarizing filters (here, shown immersed in methylene iodide) is typical of CVD synthetic diamond (right; photo by F. Notari).

in Mumbai, India, and consisted of high-quality melee (mainly E-F-G colour and IF to VS clarity).

The distinction of natural and synthetic diamonds and imitations with the GGTL DFI Laser⁺ system is non-automated but very efficient, based on the observation of luminescence colour, distribution and intensity under various excitations, combined with the simultaneous analysis of the photoluminescence (PL) and Raman spectra of the diamonds. The GGTL DFI system uses a suitably filtered 300 W full-spectrum xenon lamp to give six different broadband excitations in the range of 230–420 nm, plus a 250 mW 405 nm laser. Room-temperature PL spectra are collected during luminescence imaging by a single-channel spectrometer (1.5 nm resolution) using a thermoelectrically cooled CCD detector.

The internal features and strain pattern in the synthetic diamond were visualized using a Leica M165C trinocular microscope, equipped with a Leica DFC420 CCD camera with a resolution of 5 megapixels; the strain pattern was observed with the sample immersed in methylene iodide between crossed polarizing filters. Luminescence was observed under 254 nm short-wave (SW) and 365 nm long-wave (LW) UV radiation from a 6 W lamp (model UVP UVSL-26P), and also under broadband UV from the GGTL DFI system using the three different excitations that made the sample luminesce distinctly: 250–350 nm (SW/LW band), 300–410 nm (LW band 1) and 355–375 nm (LW band 2). Luminescence images were acquired with a Leica DFC450 C CCD camera with a resolution of 5 megapixels and the CCD sensor thermoelectrically cooled with a delta of -20°C compared to the surrounding temperature.

The infrared spectra of the sample were recorded with a resolution of 4 cm^{-1} on a PerkinElmer

Spectrum 100S Fourier-transform infrared (FTIR) spectrometer equipped with a thermoelectrically cooled DTGS detector. The beam was transmitted through the diamond using a diffuse reflectance accessory as a beam condenser, over a range of $8500\text{--}400\text{ cm}^{-1}$, with 500 scans.

PL spectra were recorded with the GGTL PL-7 system using 405, 473, 532, 635 and 785 nm laser excitations, and a high-resolution echelle spectrograph by Catalina Scientific equipped with an Andor Neo sCMOS camera (resolution of 5 megapixels) that was thermoelectrically cooled to -30°C . The system was set up to record spectra in the range of 350–1150 nm with an average resolution of 0.04 nm. All of these PL spectra were recorded with the sample cooled to 77 K by direct immersion in liquid nitrogen.

Results and Discussion

Gemmological Properties and Initial Detection

The CVD synthetic diamond (Figure 1, left) was detected by its uncommon 'greenish' orange to pink to purple luminescence under the intense broadband UV excitations of the fluorescence imaging system (Figure 2) combined with relatively strong emission from the Si centre, together with distinct luminescence from the NV^0 and 467.7 nm centres (Figure 3). The sample showed no visible luminescence under the standard LW and SW UV lamp.

This CVD synthetic diamond weighed 0.015 ct and was graded F colour and IF clarity (Figure 1, left). Between crossed polarizing filters, in certain orientations it exhibited distinct grey-to-black lamellar extinction, typical for CVD synthetic diamond (Figure 1, right). However, in some orientations the appearance could be confused



Figure 2: The luminescence exhibited by the 1.6-mm-diameter sample under three different broadband UV excitations is highly unusual for a colourless diamond. The ‘greenish’ orange (under 250–350 nm excitation), pink (355–375 nm excitation) and purple (300–410 nm excitation) luminescence with a slight streakiness are very good indicators of its CVD synthetic origin. Photos by F. Notari (left) and T. Hainschwang (centre and right).

with the so-called tatami strain pattern that is so typical of natural (and HPHT-treated natural) type IIa and low-nitrogen type Ia diamonds.

IR Spectroscopy

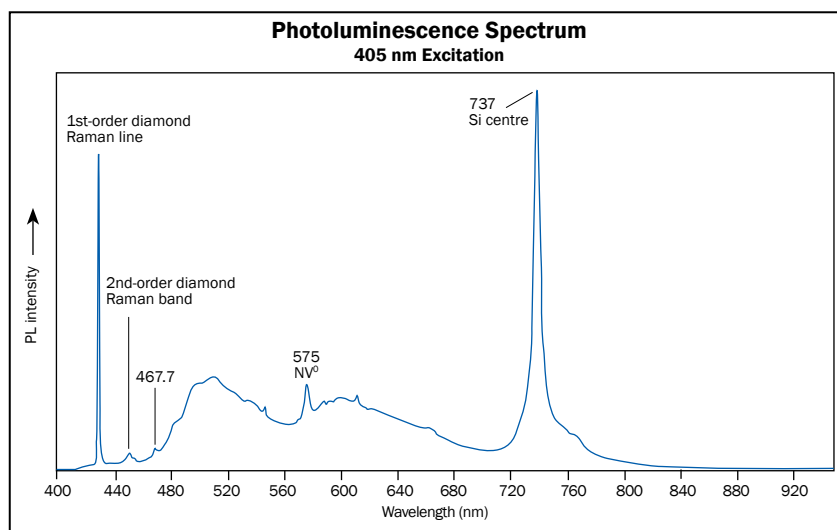
To characterize this small CVD synthetic diamond in detail, it was analysed by several spectroscopic techniques. FTIR spectroscopy showed that it was type IIa with no detectable nitrogen, and the spectrum did not exhibit any additional features indicative of a natural vs. synthetic origin: none of the small absorption lines characteristic of CVD synthetic diamond in the near-infrared range were observed (e.g. 7353, 6425 and 5562 cm^{-1} ; see, e.g., Wang et al., 2007). Since ‘pure’ type IIa diamonds in such small sizes are extremely rare (and even far rarer than larger type IIa diamonds), a melee-sized sample that is truly type IIa is very suspect of synthetic origin.

Although this sample showed the expected SW UV transparency for type IIa diamond, in the experience of the authors, the vast majority of SW UV-transparent melee-sized natural diamonds are low-nitrogen type Ia. SW UV transparency is not—as believed by many—a property that changes abruptly from nitrogen-containing to nitrogen-free diamond. Therefore, stones that are low in aggregated nitrogen (easily identified by IR spectroscopy) are SW UV transparent, just like type IIa diamonds. As a result, such low-nitrogen type Ia diamonds are usually erroneously identified as type IIa by SW UV transparency-based methods.

Low-Temperature PL Spectroscopy

The PL spectra recorded with all five laser excitations at 77 K confirmed what was clearly indicated by the GGTL DFI system: that the sample

Figure 3: The room-temperature PL spectrum of the sample recorded with the GGTL DFI system shows features characteristic of untreated CVD synthetic diamond, with a strong Raman line diagnostic for diamond and bands from the 467.7 nm centre, the NV^0 centre and the Si centre (which identify it as a CVD synthetic).



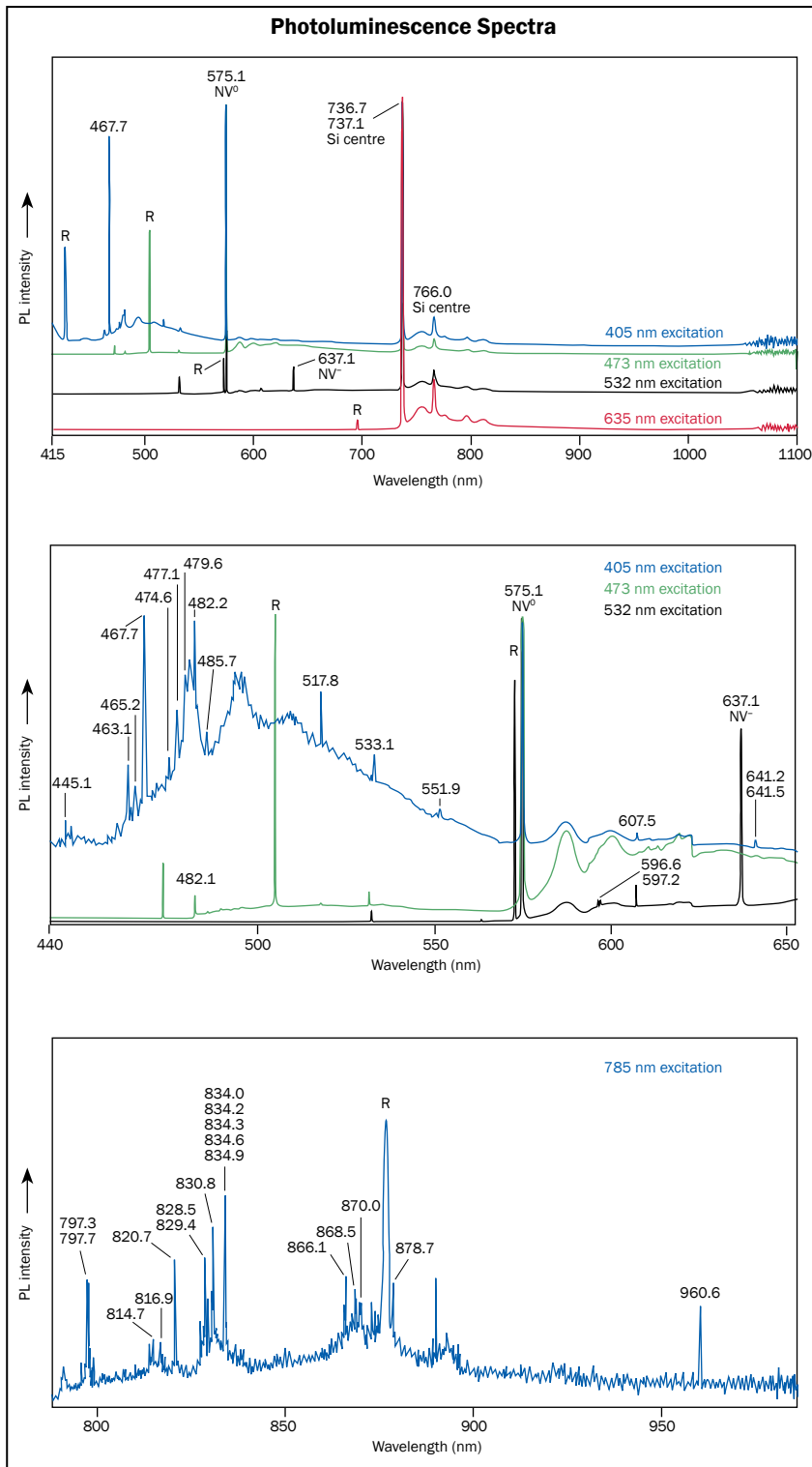


Figure 4: The PL spectra recorded using 405, 473, 532, 635 and 785 nm lasers show many characteristic peaks for CVD synthetic diamond. The well-known doublet at 736.7/737.1 nm is produced by the Si centre, which is the dominant defect recorded with 405, 473, 532 and 635 nm excitations. The 467.7 nm centre is another characteristic feature of CVD synthetic diamond. R = Raman line.

was an as-grown (untreated) CVD synthetic diamond, high in silicon-vacancy defects (Figure 4). The spectra strongly resembled those of violet-grey CVD synthetic diamonds from Orion (PDC) in Hong Kong (Peretti et al., 2013), and also the melee-sized yellow CVD sample recently described by one of the authors (Hainschwang, 2014). Unfortunately the manufacturer of the

latter sample is unknown, although the parcel was supplied from Hong Kong, which may point toward the same company mentioned above. The orange/pink/purple luminescence of the sample clearly originates from the NV⁰ centre with its zero-phonon line at 575.1 nm, while a green component observed under 405 nm laser excitation originates from the 467.7 nm centre

(Figures 3 and 4). Besides the Si centre—which also can be detected in some HPHT-grown synthetic diamonds (D’Haenens-Johansson et al., 2015) and very rarely in natural type IIa stones (Breeding and Wang, 2008)—the 467.7 nm centre is a characteristic defect in untreated CVD synthetic diamond (Martineau et al., 2004).

In addition to the NV-centre emissions, a large number of very sharp and typically rather weak peaks are evident in the PL spectra, all of which appear to be characteristic of CVD synthetic diamond, and which are—in the experience of the authors—unknown in natural diamond.

Conclusions

This 1.6-mm-diameter sample is the first confirmed melee-sized colourless CVD synthetic diamond discovered by a laboratory in a parcel of natural diamonds submitted by a client for testing and described in a scientific publication. Such CVD synthetics can be identified based on their luminescence under intense UV excitation and their PL spectra.

In the millions of melee-sized diamonds screened by the authors, no other near-colourless synthetic diamonds have been found until now, and therefore the CVD sample described here has the same ‘exotic’ status as the yellow CVD synthetic diamond discovered in a melee parcel in the latter part of 2014 (Hainschwang, 2014). Until such cases occur repeatedly and in higher percentages than 0.016% (one sample in 6,000), there is no reason to believe that melee-sized colourless CVD synthetic diamonds are currently a major problem in the market.

References

- Breeding C.M. and Wang W., 2008. Occurrence of the Si–V defect center in natural colorless gem diamonds. *Diamond and Related Materials*, **17**(7), 1335–1344, <http://dx.doi.org/10.1016/j.diamond.2008.01.075>.
- D’Haenens-Johansson U.F.S., Katrusha A., and Wang W., 2015. Colorless HPHT-grown gem diamonds from New Diamond Technology, Russia. Hasselt Diamond Workshop, Hasselt, Belgium, 25–27 February.
- Hainschwang T., 2014. Gem Notes: The first CVD synthetic diamond discovered in a parcel of natural melee-sized diamonds. *Journal of Gemmology*, **34**(4), 300–302.
- Hainschwang T. and Notari F., 2012. Melee-sized synthetic diamonds: A major challenge for the market and for gem testing laboratories. *The GemGuide*, **31**(4), 1–15.
- Hainschwang T. and Notari F., 2015. Lab Alert: First colourless melee-sized (1.6 mm) CVD synthetic detected in a parcel of natural diamonds. *GGTL Laboratories Newsletter*, **5**, March, 2 pp., [www.ggtl-lab.org/media/newsletter/GGTL_Newsletter_ALERT_No_5_March_2015_\(EN\)](http://www.ggtl-lab.org/media/newsletter/GGTL_Newsletter_ALERT_No_5_March_2015_(EN)).
- Kitawaki H., Abduryim A. and Okano M., 2008. Identification of melee-sized synthetic yellow diamonds in jewelry. *Gems & Gemology*, **44**(3), 202–213, <http://dx.doi.org/10.5741/gems.44.3.202>.
- Martineau P.M., Lawson S.C., Taylor A.J., Quinn S.J., Evans D.J. and Crowder M.J., 2004. Identification of synthetic diamond grown using chemical vapor deposition (CVD). *Gems & Gemology*, **40**(1), 2–25, <http://dx.doi.org/10.5741/gems.40.1.2>.
- Peretti A., Bieri W., Alessandri M., Günther D., Frick D.A., Cleveland E., Zaitsev A.M. and Deljanin B., 2013. New generation of synthetic diamonds reaches the market (Part A): CVD-grown blue diamonds. *Contributions to Gemology*, **14**, 1–14.
- Wang W., Hall M.S., Moe K.S., Tower J. and Moses T.M., 2007. Latest-generation CVD-grown synthetic diamonds from Apollo Diamond Inc. *Gems & Gemology*, **43**(4), 294–312, <http://dx.doi.org/10.5741/gems.43.4.294>.

The Authors

Dr Thomas Hainschwang FGA is director and research scientist at GGTL Laboratories, Gnetsch 42, LI-9496 Balzers, Liechtenstein. Email: thomas.hainschwang@ggtl-lab.org

Franck Notari is director and researcher at GGTL Laboratories, 4bis route des Jeunes, CH-1227 Les Acacias, Geneva, Switzerland.

SSEF+

SCHWEIZERISCHES GEMMOLOGISCHES INSTITUT
SWISS GEMMOLOGICAL INSTITUTE
INSTITUT SUISSE DE GEMMOLOGIE



ORIGIN DETERMINATION · TREATMENT DETECTION

DIAMOND GRADING · PEARL TESTING

EDUCATION · RESEARCH



THE SCIENCE OF GEMSTONE TESTING®

The 'Coffee-and-Cream' Effect in Chatoyant Cabochons

Harold Killingback

This article explores the cause of the so-called 'coffee-and-cream' or 'milk-and-honey' effect in chatoyant cabochons. This secondary phenomenon, observed in some cat's-eye gems under oblique lighting, is seen as light and dark halves of the stone located on either side of the bright chatoyant 'eye'. The half nearer to the light source appears dark, while the further side is suffused with a creamy brightness. It is demonstrated that the creaminess is caused by reflections from fibres deeper in the stone than those that cause the 'eye', and that it is impossible for such reflections to reach the observer from the side of the stone that is closer to the light source.

The Journal of Gemmology, 34(6), 2015, pp. 524–530, <http://dx.doi.org/10.15506/JoG.2015.34.6.524>
© 2015 The Gemmological Association of Great Britain

Introduction

Chatoyant gems contain microscopic parallel-oriented fibrous structures or inclusions that scatter light and produce a cat's-eye effect. The 'eye' is oriented perpendicular to the elongation of these features, and may be seen as a series of bright bands reflecting from appropriately oriented inclusion domains (as in tiger's-eye) or as a single bright band in cabochons when viewed under a point light source (as in alexandrite, apatite, etc.). Cat's-eye chrysoberyl and sillimanite (fibrolite) are particularly prized for their sharp 'eyes', especially when such cabochons also show high transparency. In addition to the cat's-eye appearance in such stones, there is also a secondary effect seen with oblique lighting in cabochons of sufficient transparency: the side nearer to the light source is dark while the further side appears bright and creamy. This is referred to variously as the 'coffee-and-cream' or 'milk-and-honey' effect.

The scattering of light by micron-sized fibres has been described by Birkhoff et al. (1977).

The physics of this scattering is complicated, and in the present article such an effect will be simply described as *reflection*. Wüthrich and Weibel (1981) and others have described the manifestation of this phenomenon in chatoyancy and asterism. Yokoi et al. (1986) used an algorithm to model these effects in cabochons. While these studies concentrated on the bright line(s) of the cat's-eye or star, the author is not aware of any explanations in the literature for the coffee-and-cream effect in chatoyant cabochons.

The Coffee-and-Cream Effect

Figure 1 shows four examples of cat's-eye stones, consisting of two chrysoberyls (left) and two sillimanites (right). Figure 2 is a close-up view of one of the sillimanite cabochons, which was lit by a fibre-optic lamp pointing downward from 15° left of vertical. The stone is viewed from directly overhead, and four aspects of the light reflected from it may be noted: 'a' is the bright spot of light to the left of centre; 'b' is the bright vertical arc



Figure 1: These chatoyant cabochons show the coffee-and-cream effect. With the light source located slightly left of vertical, they appear mostly dark on the left side of the 'eye' and show a bright creaminess on the right side. The chrysoberyls on the left weigh 6.76 and 1.05 ct, and the sillimanites on the right are 2.18 and 4.67 ct. Photo by H. Killingback.

to the right of centre (the 'eye'); 'c' is another, but fainter, spot of light further to the right; and 'd' is a general area of creaminess to the right side of effect 'b'. Aspect 'a' is the reflection of the light source from the top surface of the stone; 'c' is the same but from the back surface (not seen in stones that are more opaque or do not have a reflective back); and 'b' is the reflection from shallow parallel fibres oriented parallel to the back of the stone and running horizontally in the photo. This is the cat's-eye effect. But what causes the creaminess shown by 'd'?

Light Paths Through a Chatoyant Cabochon

In this article, the author uses ray-tracing diagrams to demonstrate these four light reflection effects. The diagrams are schematic only, but are based on the sillimanite cat's-eye shown in Figure 2. In particular, the light comes from a direction 15° left of vertical, and an RI value of 1.665 is used for modelling refraction. This number is similar to the RI values for sillimanite (1.658 and 1.675). The RI of the cabochon in Figure 2 (checked by using the remote-vision 'spot' technique) was found to be compatible with the 1.665 value.

Figure 3 shows a cross section, representing the dome of a cabochon, taken on the vertical plane of the minor axis and parallel to the horizontally oriented fibrous inclusions or structure (hereafter termed *fibres*), one of which

is indicated by the short black line. One incident ray in the illuminating beam is shown (red line); it meets the stone at a point where the normal to the surface is oriented θ degrees to the right of the vertical axis. In the drawing, θ is $+5^\circ$. The angle of incidence, i , at this point is therefore $\theta + 15^\circ = 20^\circ$. With the RI of 1.665, the angle of

Figure 2: The 2.18 ct cat's-eye sillimanite is shown with fibre-optic illumination coming from 15° to the left of vertical, and viewed from directly above. The chatoyancy-causing fibres are oriented parallel to the base and to the shorter axis of the cabochon. Photo by H. Killingback. The labels refer to the discussion in the text.



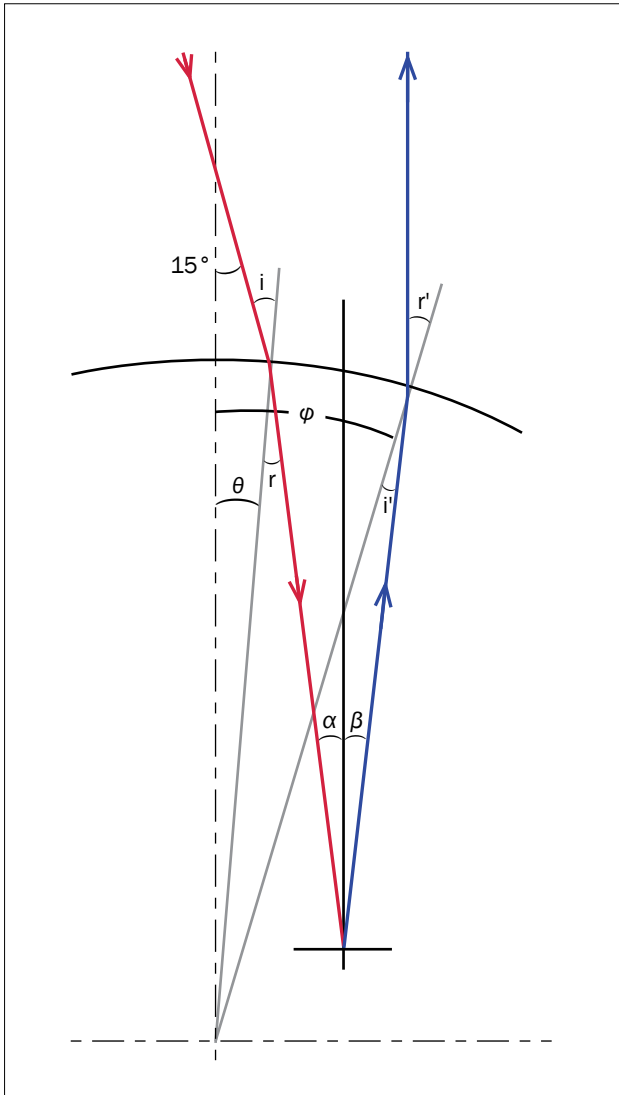


Figure 3: This schematic representation shows a vertical cross section along the minor axis of a cabochon, such as that in Figure 2. An incoming ray (red line) meets the stone at a point where the normal to the surface is θ degrees to the right of the vertical axis (here, $\theta = +5^\circ$). The path of this ray has been calculated to where it meets a horizontal reflecting fibre (short black line). The downward slope of this incoming ray, relative to vertical, is α ; on reflection, it would slope upward at $-\alpha$. Also shown is another ray (blue line) leaving the stone vertically, and so it is visible to the overhead observer. The angle of the normal to the surface at the point of emergence is ϕ . Tracing this ray back into the stone, it slopes upward from the fibre at angle β . The symbols i and r denote angles of incidence and refraction, respectively. If the blue ray is to join the red ray, as drawn, β must be equal to $-\alpha$.

refraction, r , calculated by Snell's Law, is 11.8° . The ray in the stone is oriented at angle $\alpha = -(r - \theta) = -6.8^\circ$ relative to vertical, the negative denoting that it slopes down to the right. It is supposed that this downward ray is then reflected by a

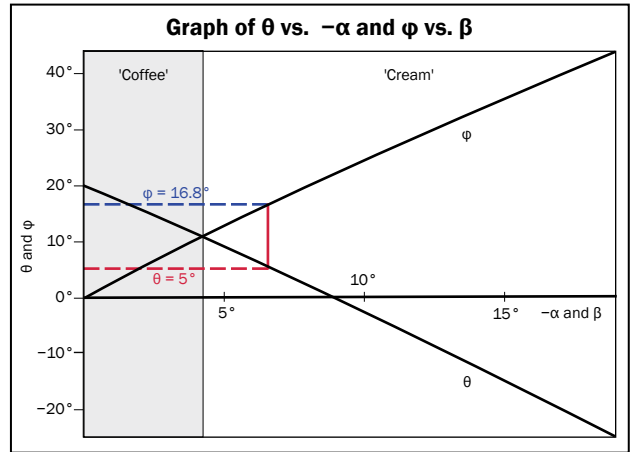


Figure 4: In this graph, θ has been plotted for various values of $-\alpha$, and ϕ is shown for various values of β (see Figure 3 for how these angles are defined). For example, for an incoming ray of $\theta = 5^\circ$, the outgoing ray is $\phi = +16.8^\circ$, as indicated by the vertical red line. The position of the 'eye' occurs where the θ and ϕ angles are the same (i.e. 11°), which is where $-\alpha$ and β are 4.25° .

horizontal surface, whether a fibre or the back of the cabochon. Because α is measured relative to vertical, it is also the angle the ray makes with the normal to the horizontal fibre (i.e. the incident angle here). The ray is then oriented upward at $+6.8^\circ$ since the angle of reflection is equal to the incident angle.

Figure 3 also shows a vertical exit ray (blue line) that would be visible by an observer directly overhead. It is shown leaving the cabochon at a position where the normal to the surface is at ϕ degrees right of vertical. The angle of refraction as the ray leaves the stone is then also ϕ . Tracing the ray backwards down into the stone, the corresponding angle of incidence, i' , can be calculated. The ray is oriented relative to vertical at angle β , where $\beta = \phi - i'$. If this exit ray (blue line) is to be the continuation of the entry ray (red line), β must be equal to $-\alpha$.

While Figure 3 illustrates a particular example, it can be extended for all possible values of θ and ϕ to show how the cream effect occurs. Calculations were made to establish α for various values of θ , and β for values of ϕ . Figure 4 is a graph plotting θ against $-\alpha$ and ϕ against β . As the creaminess occurs for those combinations of θ and ϕ where $-\alpha = \beta$, it is convenient to plot θ and ϕ on a base of $-\alpha$ and β so that the value of ϕ for any value of θ can be read from the vertical ordinate for the same $-\alpha$ and β . For the example shown in Figure 3, where θ



Figure 5: The 2.18 ct cat's-eye sillimanite in Figure 2 is photographed here with both the camera and light source located almost directly above the axis of the cabochon. Note the brightness of the 'eye' and the lack of any coffee-and-cream effect in this orientation. Photo by H. Killingback.

= 5° , the outgoing ray is at $\varphi = +16.8^\circ$ (as indicated by the vertical red line).

In the graph of Figure 4, the θ line crosses the φ line where $-\alpha$ and β are 4.25° . At this position, θ and φ are both 11° . This is the position of the cat's-eye. Here the ray is reflected by fibres slightly below the surface. Having a minimum distance to travel within the stone, this reflection of the light source is the least attenuated, and so is the brightest. Note that the 'eye' is just a special case of the 'cream' effect. The creaminess gets less bright as the distance from the 'eye' increases around the stone, because the depth of the reflecting fibres increases and the ray paths through the cabochon get longer. In opaque stones, only the 'eye' may be seen. The 'eye' is particularly bright if the direction of illumination comes close to the line of sight, for then all the reflections appear at the 'eye' stripe and there is no other creaminess (e.g. Figure 5).

It was stated above that Figure 3 applies to all possible values of θ and φ . What about the situation where φ is less than 11° , which is the 'coffee' area? From Figure 4 it might be deduced that such a

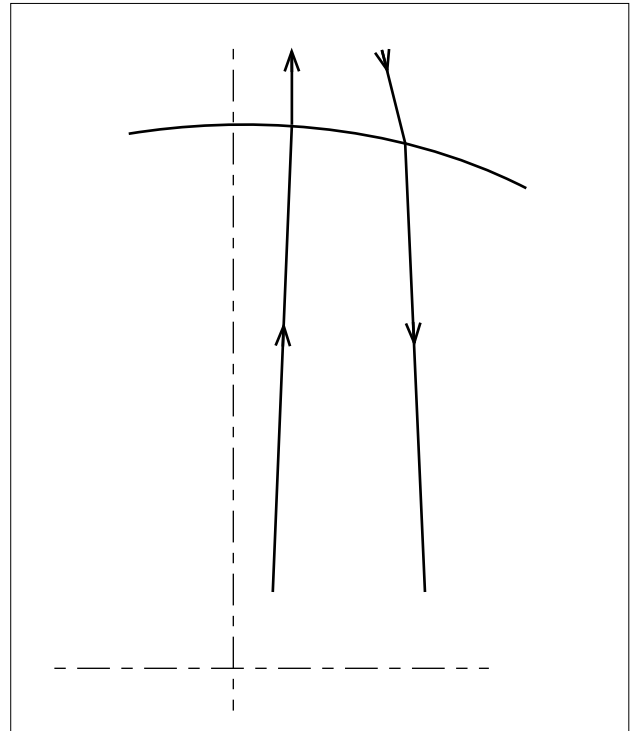
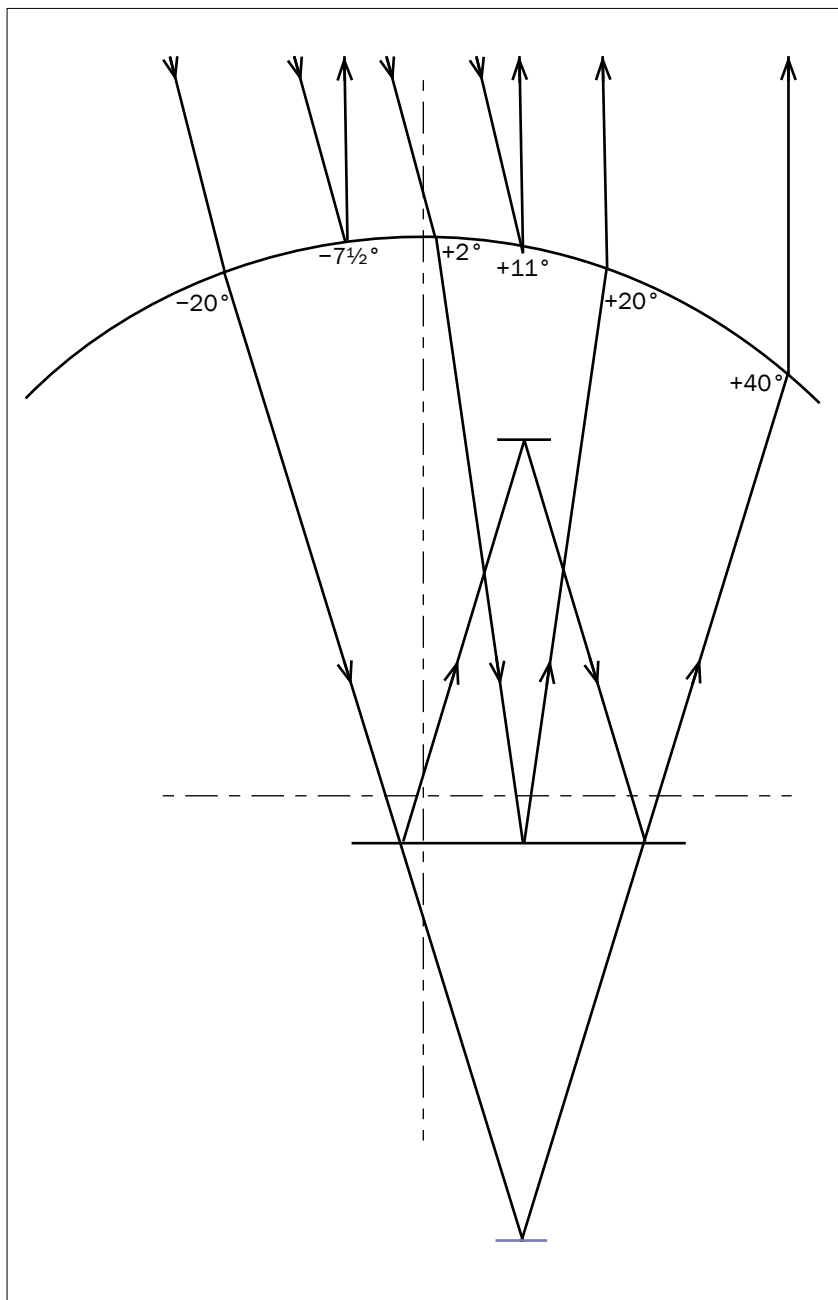


Figure 6: The downward incoming ray cannot join up with the outgoing ray in this configuration, thus showing that the part of the graph in Figure 4 where φ is less than θ represents an area where there can be no reflection reaching the observer. This leads to the conclusion that no creaminess can exist on that side of the 'eye' which is the nearer to the source of illumination.

situation is possible. To test this, consider the situation where $-\alpha = \beta = 2\frac{1}{2}^\circ$. From the graph, θ is then about $+15^\circ$ and φ is about $+5^\circ$. Figure 6 shows the incoming and outgoing sections of the hypothetical ray. They do not converge within the stone, but rather toward a point above the cabochon. Such a condition is allowed by the simple model used because it does not specify that the reflecting surface must be *within* the stone. When this condition is applied, the region where θ is greater than φ has no valid meaning, and φ cannot be less than 11° , the position of the 'eye'. The graph in Figure 4 relates to the specified angles of illumination and observation. For different viewpoints or lighting angles, the position of the 'eye' changes, but in all cases no reflected light can escape from the side nearer to the light source. There can be no cream in the coffee there!

Figure 7 shows different rays in the incident beam that illustrate the effects seen in Figure 2. When an incident ray meets the surface, some

Figure 7: Four additional incident rays are shown in this schematic representation. The ray entering the cabochon at $\theta = -20^\circ$ may contribute to the creaminess in a sufficiently transparent stone, either by reflecting from a fibre (short blue line) if the stone were deep enough, or by multiple reflections involving the back of the stone (long black line) and a fibre (short black line). Part of the incident ray approaching the surface at $\theta = -7\frac{1}{2}^\circ$ is reflected by the surface of the cabochon, and part (not shown) enters the stone. The ray entering at $\theta = +2^\circ$ reflects from the back of the stone. That entering at about $\theta = 11^\circ$ is reflected by fibres near the surface. The shortness of this ray path in the stone results in this being the brightest creaminess, and forms the 'eye'. More ray paths could have been drawn entering anywhere between -20° and $+11^\circ$ to give further examples of the creaminess, but that in Figure 3 is typical.



will be refracted and some reflected but only that portion of relevance to this article is drawn, so as to avoid complexity. It should be emphasized that many ray orientations may contribute to the creaminess (effect 'd' in Figure 2), but some produce greater brightness, either because the ray path is short (effect 'b') or the reflecting surface is more reflective (effect 'c').

The ray entering at $\theta = -20^\circ$ can only contribute to the creaminess if the stone is very transparent, because the ray path within the stone is so long—whether due to a single reflection from a deep fibre (short blue line) or multiple reflections

involving the back surface (long black line) and a fibre (short black line) in a 'W'-shaped path.

Part of the ray approaching the surface at $\theta = -7\frac{1}{2}^\circ$ reflects off the surface of the stone and is seen by the observer directly overhead. The incident angle is $15^\circ - 7\frac{1}{2}^\circ = 7\frac{1}{2}^\circ$, and since the angle of reflection is equal to the incident angle, the reflected ray is vertical and is seen by the viewer's eye (effect 'a' in Figure 2). The rest of this ray enters the stone and contributes to the creaminess in the same way as that entering at -20° , so it is not drawn in Figure 7 to avoid overcrowding the diagram. Its path length in the

stone is, however, shorter so the creaminess it can cause is brighter.

The ray entering at $\theta = +2^\circ$ is reflected by the back surface of the stone. If this is a better reflector than the fibres, it will produce a brighter spot of creaminess (effect 'c' in Figure 2), provided the stone is transparent enough to allow such a long ray path.

The ray forming the 'eye' (effect 'b' in Figure 2) is shown entering at $\theta \approx 11^\circ$. It penetrates just under the surface to the nearest reflecting fibre.

It may be noticed from Figures 3 and 7 that the points of upward reflection (or downward where three reflections are involved) are situated along the line-of-sight and below the 'eye'. As the line-of-sight here is vertical, the reflecting fibres are positioned vertically below the 'eye'.

Figure 8 is a chalk drawing interpolated from the upward ray paths shown in Figures 3 and 7. It was made by first projecting and interpolating onto a horizontal screen these upward rays along the minor axis of the cabochon, together with the rest of the rays producing creaminess in this plane. Reflections from the top and back of the stone are from single surfaces, and result in corresponding spots of brightness. The creaminess was then extended in both directions away from the minor axis (to represent the plan view of the entire cabochon) to account for the multitudes of fibres that are capable of reflecting spots of light to the observer. (Only fibres below the 'eye' and along the line of sight can reflect light to the observer.) These spots combine to produce the general creaminess. Because of the increased path length and attenuation within the stone, rays towards the right-hand edge become fainter. The similarity of the appearance of Figure 8 to the photograph in Figure 2 gives confidence in the model used.

Conclusion

In chatoyant cabochons (e.g. Figure 9), the cat's-eye effect is caused by reflection from fibrous structures or inclusions close to the surface of the stone. With oblique lighting, a creamy brightness may be observed on the side of the 'eye' that is the further from the light source. A simple ray-tracing model has been used to show that the creaminess is due to reflections from fibres deeper in the

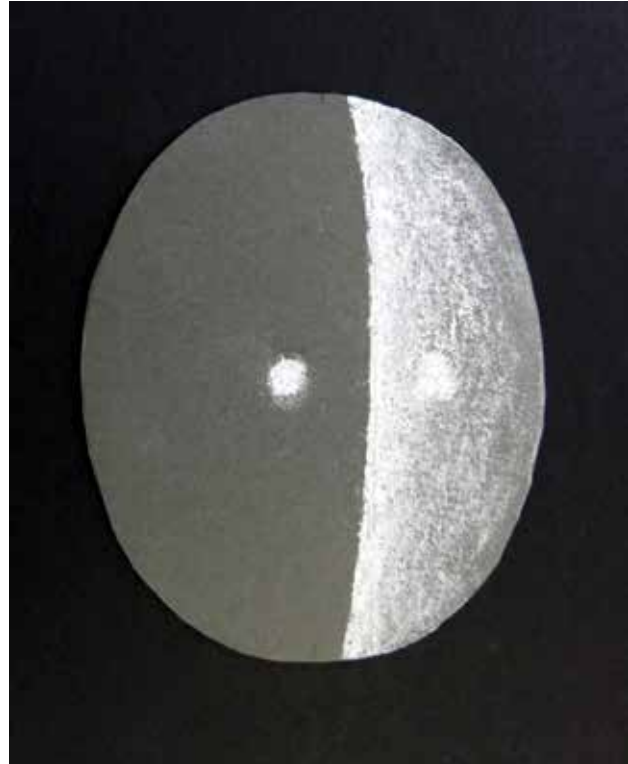
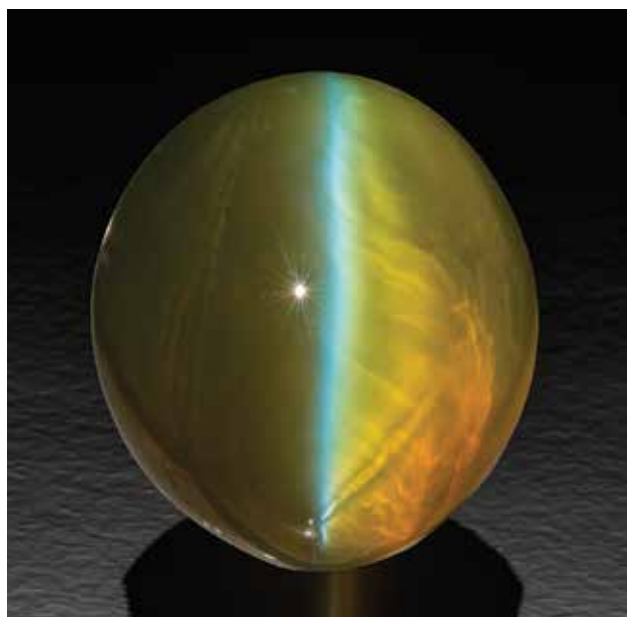


Figure 8: This chalk drawing, based on calculated ray paths, shows a plan view of the cabochon diagrammed in Figures 3 and 7. The width of the cabochon is assumed to be 80% of the diameter of the circular arc that defines its dome. This takes into account the fact that, in most cabochons, the radius of curvature of the top surface decreases sharply toward the edge. The close resemblance of this drawing to the photo in Figure 2 gives confidence in the model used.

Figure 9: This 20.14 ct cat's-eye chrysoberyl provides a fine example of the coffee-and-cream effect. Courtesy of RareSource (Chattanooga, Tennessee, USA) and Palagems.com (Fallbrook, California, USA); photo by Robert Weldon.



stone than those producing the 'eye', and so depends on there being sufficient transparency to allow the longer ray paths to travel through the stone. It has also been demonstrated that no such creaminess can occur on the other side of the 'eye'. The cat can only keep half an eye on the cream!

References

- Birkhoff R.D., Ashley J.C., Hubbell H.H.Jr. and Emerson L.C., 1977. Light scattering from micron-size fibres. *Journal of the Optical Society of America*, **67**(4), 564–569, <http://dx.doi.org/10.1364/josa.67.000564>.
- Wüthrich A. and Weibel M., 1981. Optical theory of asterism. *Physics and Chemistry of Minerals*, **7**(1), 53–54, <http://dx.doi.org/10.1007/bf00308202>.

Yokoi S., Kurashige K. and Toriwaki J., 1986. Rendering gems with asterism or chatoyancy. *The Visual Computer*, **2**(5), 307–312, <http://dx.doi.org/10.1007/bf02020431>.

The Author

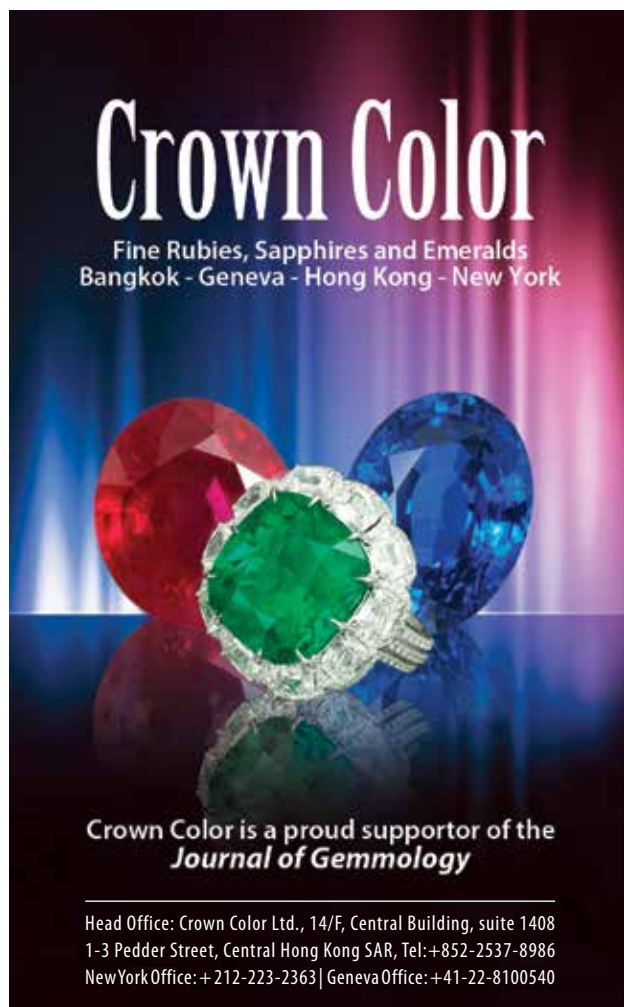
Harold Killingback

Meadowside, 12 Church Lane, Brooke,
Oakham LE15 8RE

Email: haroldkillingback@btinternet.com

Acknowledgements

The author thanks the referees for their constructive suggestions.



Crown Color
Fine Rubies, Sapphires and Emeralds
Bangkok - Geneva - Hong Kong - New York

Crown Color is a proud supporter of the
Journal of Gemmology

Head Office: Crown Color Ltd., 14/F, Central Building, suite 1408
1-3 Pedder Street, Central Hong Kong SAR, Tel: +852-2537-8986
New York Office: +212-223-2363 | Geneva Office: +41-22-8100540




Stone Group Laboratories

Where technology and
experience meet.

- Gem Identification
- Treatment Analysis
- Consultation
- Research

www.StoneGroupLabs.com

SAPPHIRES

Pure Natural Colours



Visit us:

**Hong Kong
Jewellery & Gem Fair**
16.-20. September 2015
Booth: AWE 9E02



Paul Wild OHG

Auf der Lay 2 · D-55743 Kirschweiler (Germany)

Tel.: +49 (0) 6781 / 9343-0

Fax: +49 (0) 6781 / 9343-43

info@paul-wild.de



www.paul-wild.de

Conferences

13th Annual Sinkankas Symposium: Opal

On 18 April 2015, this annual symposium in honour of John Sinkankas took place at the Gemological Institute of America (GIA) campus in Carlsbad, California, and was co-sponsored by the San Diego Mineral & Gem Society. The theme of this year's conference was opal, and the sold-out event was attended by approximately 180 people. As in prior years, the conference was flawlessly organized by **Roger Merk** (Merk's Jade, San Diego, California, USA).

Dr Eloïse Gaillou (Musée de Minéralogie, Mines ParisTech, Paris, France) reviewed the geology, coloration and microstructure of gem opals. Their formation involves the circulation of fluids within a silica-rich host rock, and their various body colours—including pink, blue and yellow-orange-red-brown—are all due to inclusions. **Dr George R. Rossman** (California Institute of Technology, Pasadena, USA) explained how play-of-colour in opal is produced by the constructive interference of light that is reflected from layers of silica spheres with a diameter of 250–380 nm.

Andrew Cody (Cody Opal, Melbourne, Victoria, Australia) discussed the history and characteristics of Australian opals. Large deposits were discovered in 1905 (initially of black opal at White Cliffs), and several additional mining areas came online during and after the 1960s, such as Coober Pedy, Andamooka, Lightning Ridge and Mintabie. Value factors include the type of opal; the brilliance, pattern and hues shown by the play-of-colour; transparency (particularly in white opal); thickness of the play-of-colour area; and shape of the polished stone.

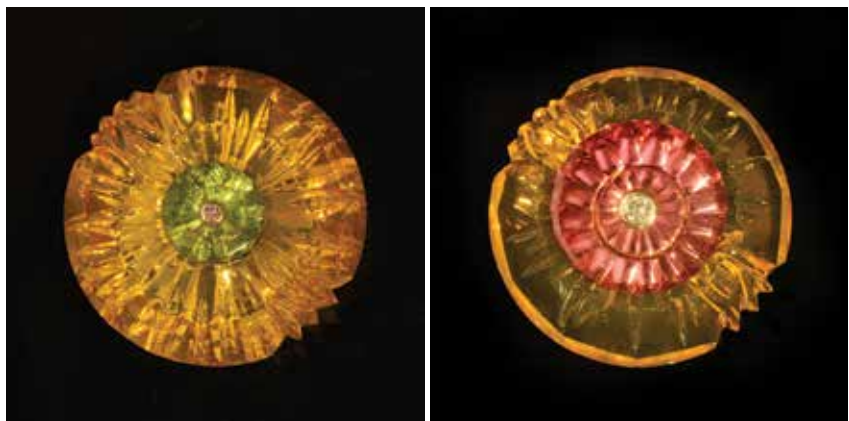
Alan Hart (The Natural History Museum, London) highlighted notable opals in the collection of the

Natural History Museum. Most of the ~2,300 opal specimens originate from Australia, followed by Hungary, Mexico, UK and USA. Some of the more impressive stones include a 17 ct red fire opal from Turkey, a 131 ct black opal from Lightning Ridge and a 3.4 kg piece of rough from Virgin Valley, Nevada, USA, that was acquired from Ward's in the 1920s for US\$20. **Dr Raquel Alonso-Perez** (Harvard University, Cambridge, Massachusetts, USA) described the history and science of opals in the Harvard University collection. Of the 280 specimens from 28 countries, most of them are from the USA (Virgin Valley), Australia and Mexico. Her studies of those from Mexico revealed two main types: fire opal from the Jalisco-Guanajuato area (including Querétaro), and blue and pale brown opals from the Zimapán-Guerrero area.

Renée Newman (International Jewelry Publications, Los Angeles, California, USA) described various types of matrix opal. Such opal is interspersed within the rock in which it formed (rather than occurring in seams, as in typical boulder opal), and may or may not show play-of-colour; the best-known example is boulder matrix opal from Australia, which contains play-of-colour opal hosted by ironstone. **Helen Serras-Herman** (Gem Art Center, Rio Rico, Arizona, USA) reviewed 'common' opals (i.e. those showing no play-of-colour). These underappreciated opals are attractive, colourful (in blue, pink, etc.), take a good polish, may display scenic patterns and are affordable in most cases. They are typically untreated, although some lapidaries may stabilize them with Opticon.

Bill Larson (Palagems.com, Fallbrook, California, USA) provided a collector's perspective on opal. Some of his early acquisitions consisted of fine

Figure 1: This interesting assemblage by gem artist Glenn Lehrer (Lehrer Designs, Larkspur, California, USA), called 'Parallel Universe', consists of a Torus-cut orange Brazilian opal (~30 ct) with peridot (2.4 ct, front side) and pink tourmaline (~10 ct, reverse side). Diamonds are set in the centre, on both sides of the piece. Courtesy of Palagems.com; photos by Mia Dixon.



Mexican fire opal showing excellent play-of-colour, which he obtained directly from the miners or from antique jewellery. These specimens have not shown any evidence of crazing, even after many years in his collection. Larson also showed some innovative cutting/carving styles for opal (e.g. Figure 1).

Meg Berry (Megagem, Fallbrook, California) provided opal lapidary tips. For carving opal, she employs a spindle equipped with tiny burrs and 240 and 600 grit abrasives. This is followed by a much longer polishing process that uses 'Zircon-Brite' (dental paste of ~50,000 grit). For faceting opal, she cold-dops the stone with superglue or epoxy; final polishing is done using 'French cerium' (cerium oxide) on a tin lap.

Robert Weldon (GIA, Carlsbad) described an innovative technique for photographing play-of-colour opal. The stone is placed in a shallow dark-coloured pan filled with water, and the camera (and lights) are positioned overhead. The immersion reduces

surface reflections from the opal, allowing the play-of-colour to show up better. **Nathan Renfro** (GIA, Carlsbad) explored the micro-features of opal through photomicrography, documenting inclusions (e.g. pyrite, amphibole, barite and dendrites) and microstructures (e.g. ignimbrite-related and cellular types). **Jack Hobart** (Los Angeles, California, USA) provided a photographic exploration of Mexican *cantera* opals. These cabochons consist of play-of-colour opal in a rhyolite matrix. The opal shows variations in body colour (orange to colourless or white), structure and transparency, documented in more than 10,000 images he photographed for his database.

A conference proceedings volume is available for US\$35 (plus shipping) from Roger Merk (merkjsade@cox.net); it contains presentation summaries as well as outside contributions (see review on p. 553 of this issue).

Brendan M. Laurs FGA

Accredited Gemologists Association's 2015 Las Vegas Conference

This educational event took place on 28 May, one day before the start of the JCK Las Vegas Show in Nevada, USA. The conference theme was 'Synthetic Diamonds: The Products, the Perceptions, and the Retailers'. The event was attended by approximately 50 people, and chaired by **Stuart Robertson**, AGA president and vice president of GemWorld International Inc. (Glenview, Illinois, USA). **Gary Roskin** (Roskin Gem News Report, Exton, Pennsylvania, USA) was the conference moderator.

Dr Thomas Hainschwang (GGTL Laboratories, Balzers, Liechtenstein) delivered his presentation remotely (via Skype), and reported that recent developments in growth technology by both high pressure, high temperature (HPHT) and chemical vapour deposition (CVD) technologies have resulted in the production of larger and better-quality synthetic diamonds. He learned recently about the production of a 52 ct piece of HPHT-grown synthetic diamond that may be cuttable into 35 carats of faceted gems. Also, attractive gems up to 3+ ct are now cut from material grown by the CVD technique (typically HPHT treated to remove brown colour). Hainschwang indicated that HPHT-grown synthetics have been showing up in parcels of yellow to yellow-orange melee since 2011, but only recently have synthetics been found in parcels of colourless melee (with only one such example published so far; see pp. 518–522

of this issue).

Eric Franklin (D.NEA, Saline, Michigan, USA) estimated that tens of thousands of carats of synthetic diamonds are now being grown annually, but this remains a very small amount compared to the production of mined diamonds. He noted that the main market for synthetic diamonds is for bridal jewellery sold to customers in their 20s–30s who prefer conflict-free and eco-friendly products and/or appreciate the technology involved with growing synthetic diamonds. Compared to their natural counterparts, he stated, synthetics are priced 20–40% less for colourless gems (and even less for coloured synthetic diamonds).

Alex Grizenko (Lucent Diamonds, Denver, Colorado, USA) indicated that the life cycle for many of the largest diamond mines will end in the near future, while global demand for diamond will continue to increase—particularly from countries with emerging economies. This will create problems with demand, and Grizenko advocated the use of advertising to promote synthetics and make them more desirable.

Tamaz Khikhashvili (New Diamond Technology, St Petersburg, Russia) reported that in May 2014 his company made significant developments in HPHT technology that allowed them to grow larger, higher-quality synthetic diamonds, including two that were faceted into gems weighing 5.11 ct (K colour, I₁ clarity) and 4.30 ct (D colour, SI₁ clarity). Most

recently, they produced the world's largest faceted synthetic diamond, a 10.02 ct (E colour, VS₁ clarity) square emerald-cut gem that was fashioned from a 32.26 ct piece of rough.

The formal presentations were followed by a panel discussion that included all of the conference speakers (except Dr Hainschwang), as well as **Tom Chatham**

(Chatham Created Gems) and **Dr James Shigley** (GIA, Carlsbad). The conference concluded with a hands-on session in which participants were allowed to examine the 10.02 ct synthetic diamond mentioned above, and they also tested a new Presidium Synthetic Diamond Screener that debuted at the 2015 JCK Las Vegas show.

Brendan M. Laurs FGA

Mallorca GemQuest 2015

The inaugural Mallorca GemQuest Gemmological Conference was held on 18–19 April in Palma de Mallorca, Spain, at the Hotel THB El Cid. Situated on the 'Playa de Palma' beach in Can Pastilla, the conference organizers promised 'Sea, Sun, Sand & Gemmology', with a programme that featured eight speakers who delivered 11 one-hour presentations, followed by a round-table discussion. For those who could not attend in person, the conference was accessible via free online streaming and a five-day 'video on demand' access pass that was underwritten by sponsors Gem-A, *The Handbook of Gemmology*, the National Council of Jewellery Valuers, the Canadian Gemmological Association, Instituto Gemológico Español, GemDialogue and GemeWizard. In total, the conference reached more than 800 people from 31 countries through online registrations and physical attendance.

Gemmology has evolved dramatically over the years with the emergence of new treatments, enhancements and lab-created gemstones, particularly in the last 50 years. **James Riley** (Gem-A, London) discussed the history and evolution of gemmology and the equipment that is used for gem identification. **Riley** also gave a presentation on his recent visit to Mogok, Myanmar. Secluded from the world for much of the 20th century, the Mogok area is once again accessible to foreigners with the correct permits.

Alan Hodgkinson (Ayrshire, Scotland) explained and demonstrated 'visual optics', a concept he has pioneered, showing how certain gem characteristics can be assessed in a darkened room using only a light source and a pair of tweezers. While this technique cannot establish if a gem is synthetic or treated, it is very useful in helping to narrow down identification possibilities and can be used on both loose and mounted stones. In a separate presentation, **Hodgkinson** explained various techniques that enable users to maximize the efficiency of the refractometer and overcome the many obstacles that may prevent them from obtaining correct results. Unfortunately,

most gemstones are not cut with the determination of RI in mind, and this often causes concern, especially for students who struggle to find the shadow edges, their positions and how they relate to one another.

Today's gem research analyst is required to have a profound knowledge of the gems and pearls tested in the laboratory and also of the instrumentation used to achieve the proper identification of these materials. Gem testing procedures are similar to a crime scene investigation, where every gem presents a new case that must be solved. The solutions for some gems are straightforward, while those for others are complicated and time consuming, and finally there are cases where no solution can be found at all. **Dr Thomas Hainschwang** (GGTL Laboratories, Balzers, Liechtenstein) provided insight into gem identification at the GGTL Laboratories, showing their ambitious instrumental development projects and some interesting examples of day-to-day challenges that are overcome using modern technology. In another presentation, **Dr Hainschwang** discussed the evolution of diamond colour treatments and the techniques used to detect them. He described the use of coatings, radioactive salts, particle accelerators and nuclear reactors (with or without annealing), HPHT treatment, and finally multi-step processing that combines HPHT, irradiation and annealing.

Gemmologist and accomplished gem cutter **Dr Egor Gavrilenko** (Instituto Gemológico Español, Madrid, Spain) was joined by award-winning faceter **Victor Tuzlukov** (Russian Faceters Guild, Moscow) to discuss factors that affect the quality of faceting of coloured gemstones, and also the considerations for producing precision-cut gems including facet design, optimization of angles and proportions based on RI, and the various stages of gem cutting. **Dr Gavrilenko** also delivered a separate presentation that explored the fascinating world of gem inclusions, explaining the various types, how they can assist in gem identification and the techniques used to capture their beauty in photographs.



Figure 2: Deep underground at Lightning Ridge, Australia, miner Fred Mallouck operates a hydraulic excavator in search of black opal. Photo by Tino Hammid.

One of the biggest challenges facing gemmologists, jewellers and appraisers is the grading of coloured gemstones. **This author** looked at the '3 Cs' (clarity, cut and carat weight), discussing the various clarity- and cut-grade classifications, the important carat weight categories and how they impact overall value. Then **Menahem Sevdemish** and **Guy Borenstein** (Gemewizard Ltd., Ramat Gan, Israel) explored the '4th C', colour, using the Gemewizard colour communication system they have pioneered. In particular, they demonstrated how this software can be used for the colour grading of coloured gemstones.

Fresh from his recent trip to Australia, **this author** also gave a presentation on the opal mines of Lightning Ridge (Figure 2), Yowah and Quilpie. The audience learned about not only how opals are formed but also the mining techniques used, the people who mine them, the obstacles they face and the complexities of grading and pricing opals.

The conference concluded with a round-table discussion on valuing and appraising coloured gemstones. Unlike diamonds, coloured gemstones present a myriad of problems because of: the lack of standardization in the industry regarding nomenclature and how they are assessed and described according to colour, clarity and cut; difficulties in finding appropriate comparison stones of similar type and quality for appraisers (especially for opal, jade and top-quality coloured stones); and properly identifying treatments and determining how they affect value. **Adolfo de Basilio, Alberto Scarani, Victor Tuzlukov, Dr Egor Gavrilenko** and **this author** joined moderator **Marian Jaén** in this spirited debate.

A three-DVD set containing all of the presentations given at the conference is available for US\$17.50 (plus \$10.00 flat-rate shipping) at <http://handbookofgemmology.com/shop>. Plans are already in the works for Mallorca GemQuest 2016.

*Geoff Dominy FGA (geoff@handbookofgemmology.com)
Amazonas Publishing, Palma de Mallorca, Spain*

Scottish Gemmological Association Conference

The Scottish Gemmological Association's annual conference was held in Peebles, Scotland, on 1–4 May 2015. Approximately 80 delegates attended from nine countries.

Clare Blatherwick (Bonhams, Edinburgh, Scotland) discussed the use of naturalism in the work of Fabergé, focusing on the firm's experiments in Art Nouveau, as well as animal representations in hardstone carvings and the flower studies that the firm excelled in. She also reviewed naturalistic imagery incorporated into *objets d'art* such as desk seals, caviar dishes, etc.

Dr Emmanuel Fritsch (University of Nantes and Institut des Matériaux Jean Rouxel, Nantes, France) discussed how luminescence can benefit gemmologists. He described how to make meaningful observations with a UV lamp (including knowing the lamp's power and standardizing the distance of observation), and stressed the usefulness of reference stones for both luminescence colour and intensity. In a separate

presentation, in collaboration with **Aurélien Delaunay** (LFG, Paris, France) and **Dr Thomas Hainschwang** (GGTL Laboratories, Balzers, Liechtenstein), **Dr Fritsch** presented how the growth history of faceted diamonds can be elucidated with luminescence imaging equipment, especially the DiamondView. The three fundamental growth modes of diamonds are octahedral (typical of gem diamonds), fibrous and cuboid. All of these can be identified with adequate luminescence imaging. Fibrous growth can be dendritic, giving rise to fibrous pseudocubes (sometimes faceted when relatively free of inclusions). Cuboid growth is often present in gem diamonds, but rarely dominates. 'Mixed-growth' diamonds are more common than previously thought, and consist of a succession of octahedral and cuboid growth, often repeated multiple times (e.g. Figure 3). Simultaneous cuboid and octahedral growth may result in reentrant cubes or asteriated diamonds. **Dr Fritsch** also briefly described a relatively new gem material called 'Mustard Jasper', which is more correctly named

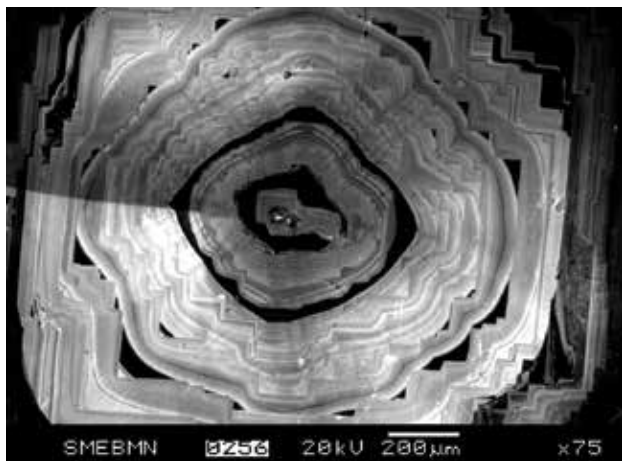


Figure 3: This cathodoluminescence image of an octahedral point of a diamond spectacularly shows the succession of octahedral (straight) and cuboid (curved) growth episodes, repeated over time. Image by Aurélien Delaunay.

‘Bumble Bee Stone’ because of its contrasting bright yellow, black and white colours. This decorative stone is mined from the base of a volcano in Indonesia, and has a hydrothermal origin with layers of realgar (yellow when fine-grained), pyrite (black when fine-grained) and white calcite.

Dr Keith Barron (Potentate Mining LLC, Toronto, Ontario, Canada) covered the geology, character and origin of sapphires from Rock Creek/Gem Mountain, Montana, USA. The wide array of pastel colours displayed by these sapphires has been known for more than a century, but their geological origin remains enigmatic. More than 62 tons have been recovered to date from short ephemeral drainages mostly within a 25 km² area, primarily through hydraulic mining during the period 1900–1930. At first the stones were mined from small-volume alluvials directly in the drainages, but over time activities migrated to the adjacent hillsides (considered perched terraces or ‘benches’ above the active streams). These deposits are actually mud-matrix supported colluvium produced by landslides or ‘mass wasting’. In the drainages the colluvium has been reworked by the streams to produce typical alluvials. The colluvial deposits are widespread and constitute a 2–10 m thick layer of sapphire-bearing material with minimal overburden that can be efficiently mined and processed. Stone populations vary in colour and size across the property. This all suggests multiple proximal undiscovered sources. Potentate Mining LLC has consolidated the district properties and is systematically examining the area geologically and through the use of airborne geophysics, as well as constructing their second gem recovery plant. The company plans to produce 100 kg of rough sapphire in 2015, which will increase after all equipment is acquired and permits secured.

Dominic Mok (Asian Gemmological Institute and Laboratory Ltd., Hong Kong) described the classification of gem-quality jadeite (*fei cui*) into types A, B, C and B+C using FTIR, UV-Vis and Raman spectroscopy. He also outlined how to separate General Electric synthetic jadeite from its natural counterpart by means of FTIR spectroscopy and the Hanneman-Hodgkinson Jade Filter.

Stuart Robertson (Gemworld International Inc., Glenview Illinois, USA) provided an update on the supply, demand and pricing of coloured gemstones. Until ~1960, most of the coloured stones in the world market were sourced from relatively few locations, and the chief determinants of value were rarity and quality. However, during the past few decades the number of gem deposits increased dramatically, producing a broader range of varieties and qualities. Integration of these materials into the market has affected both price and the perception of value. During the past 10 years, no coloured stone has experienced as dramatic a price shift as ruby—particularly of Burmese origin. Today Mozambique is the major producer of gem-quality ruby, and since 2008 its price has doubled and then doubled again. In the sapphire market, fancy colours are perceived as most affordable. Increased interest in many of the lesser-known gem varieties is due at least in part to colour substitution: strong demand for rubellite, spinel and now garnet has benefitted from the high price of ruby. Likewise, Robertson noted a strong relationship between an increase in the price of blue sapphire and the popularity of tanzanite.

Richard Wellander (Historic Scotland, Edinburgh) described The Honours of Scotland (Scotland’s crown jewels), consisting of the King’s crown, made by Edinburgh Goldsmith John Mosman, and the sceptre and sword, which were gifts from the Pope in Rome. The crown contains Scottish ‘river pearls’ and gold from Lanarkshire, as well as various gemstones (Figure 4). Although made especially for the marriage ceremony of James V to Mary of Guise in 1540, the first time the crown was used at a monarch’s inception was at the coronation of their nine-month-old daughter Mary, as Queen of Scotland in 1543.

Several workshops rounded out the conference (e.g. Figure 5). **Dominic Mok** covered jadeite testing, using a variety of samples including types A, B, C and B+C jadeite; chrome-green cat’s-eye nephrite; General Electric synthetic jadeite; and various qualities of jadeite from vivid green to light green (‘pea’/‘bean’ green); lavender, ‘icy’ and ‘glassy’ varieties; and omphacite *fei cui* that appeared deep green in transmitted light and black in reflected light. He also explained how to differentiate between various natural and synthetic diamond types, and showed participants synthetic



Figure 4: The Honours of Scotland include the King's crown, which contains Scottish 'river pearls' and various gemstones. Courtesy of the Royal Scottish Museum.

type Ib diamond crystals with metallic inclusions that were attracted by a magnet, faceted CVD synthetic diamonds and natural diamonds treated by HPHT and irradiation. Other workshops were presented by



Figure 5: Participants examine various types of jadeite in this workshop given by Dominic Mok, which took place in the famous Bannockburn room in the Peebles Hotel.

Dr Çiğdem Lule and **Stuart Robertson** (grading and valuing emeralds), **Claire Mitchell** (practical hands-on gem testing), **David Callaghan** (cameos and intaglios, and extraordinary tales behind some pieces of jewellery), and **this author** (gem identification using visual optics).

On the final day of the conference, **Richard Wellander** guided participants on a tour of The Honours of Scotland at Edinburgh Castle.

*Alan Hodgkinson FGA DGA (alan-hodgkinson@talktalk.net)
Ayrshire, Scotland*

Swiss Gemmological Society Conference

On 19–21 April 2015, the Swiss Gemmological Society held its 73rd annual conference. Approximately 82 members and guests (e.g. Figure 6) met at the Seerose Hotel in Meisterschwanden, on the shore of picturesque Lake Hallwil near Zurich. In addition to lectures about the main topics of gem treatments and early 20th century jewellery designs, presentations covered news and market reports for diamonds, coloured stones and cultured pearls. **Michael Hügi**, head of the society's scientific committee, chaired the conference.

Prof. Dr Henry A. Hänni (SSEF, Basel, Switzerland) started the conference with an overview of gem treatments and their detection. He focused on rather sophisticated treatment methods, such as Be diffusion in corundum and the detection of low-temperature heated corundum based on Raman spectroscopy of zircon inclusions. In an additional short lecture, **Prof. Hänni** covered some new types of doublets that strongly resemble natural gems. **Dr Walter Engel** (GRL Inc., Bern, Switzerland) gave insights

into the fundamental laws of thermodynamics that are important for successfully heat treating corundum. Crystallization, recrystallization and diffusion processes all follow the rules of thermodynamics. Even the construction of the oven and the different heating and cooling methods require a basic knowledge of thermodynamics. **Jean-Pierre Chalain** (SSEF) presented a historical background on the identification of HPHT-treated diamonds. Collaboration between scientists from different laboratories and organizations was instrumental to providing a reliable method (based on photoluminescence spectroscopy) to detect this treatment, which was originally announced as being undetectable by the treaters. **Dr Thomas Hainschwang** (GGTL Laboratories, Balzers, Liechtenstein) reviewed the irradiation of diamond and described features that may be used to distinguish green diamonds of natural and artificially induced colour. Naturally irradiated green diamonds and those that have been treated by modern methods

Figure 6: Some of the participants of the 2015 annual conference of the Swiss Gemmological Society. Photo by M. Hügi.



(such as electron irradiation) reveal no residual radioactivity. However, diamonds that have been embedded in radium salts are commonly radioactive and may present a considerable safety hazard. **Dr Walter Balmer** (Chulalongkorn University, Bangkok, Thailand) described the heat treatment of blue zircon. Heating to ~900°C in reducing conditions can produce a blue colour, particularly for low-metamict material (i.e. 'high' zircon); such coloration is not seen in untreated zircon. Although the cause of this colour behaviour is not completely understood, UV-visible spectra show a strengthening of the U⁴⁺ peak after heating, but a decrease in blue colour at temperatures >1,100°C indicates that U⁴⁺ is not the chromophore. To study the commercial heat treatment of zircon, a traditional charcoal furnace has been constructed in Switzerland and successfully tested. To conclude the topic of gem treatments, **Dr Michael S. Krzemnicki** (SSEF) presented various recommendations (from CIBJO, AGTA and ICA) concerning treatment disclosure and gave examples of laboratory-harmonized terminology (LMHC). Disclosure and correct labelling are an ethical requirement and very important for maintaining consumer confidence. In a second talk, **Dr Krzemnicki** described items studied recently in SSEF's laboratory, such as sapphires from basaltic deposits in Nigeria, low-temperature heated rubies from Mozambique, heated red spinels from Tanzania, a hydrothermal synthetic emerald weighing 67 ct, a star spessartine from Nigeria, and the effect of chemical alteration on conch pearls.

The theme of early 20th-century jewellery designs was kicked off by **Catherine de Vincenti** (CdV Consulting, Lausanne, Switzerland), who described jewellery of the Art Nouveau period. Named after the gallery Maison de l'Art Nouveau in Paris, France, this style was inspired by natural forms and structures. Examples were shown of masterpieces by renowned

artists and designers such as René Lalique, Georges Fouquet, Lucien Gaillard and others. A detailed overview of jewellery of the Art Deco period, which was popular between 1920 and about 1940, was given by **Sophie Vantieghem**, curator at the Museum of Fine Arts (Musée des Beaux-Arts) at La Chaux-de-Fonds, France. She explained the development of such jewellery designs in the context of contemporary architecture and interior trends. She also presented typical examples of Art Deco jewellery by artists such as Le Corbusier, Raymond Templier, and Alexander Calder. **Craig Lynch** (Ouellet & Lynch, Phoenix, Arizona, USA) discussed jewellery recovered from the debris field around the wreck of the famous RMS Titanic, which sank in April 1912. About 80 pieces of jewellery and watches were found, many of them from one well-preserved leather bag. While most of the jewellery and watches were strongly corroded, and the pearls partly dissolved, some of the pieces are in pristine condition. The jewellery shows a broad variety of styles, from Edwardian to Art Nouveau.

Other presentations covered a variety of gemmological topics. **Michael Hügi** (Swiss Gemmological Society) took the audience on a photomicrographic journey exploring the boundaries of inorganic and organic origin for different gem materials. The vanadium found as a chromophore of tsavorite and tanzanite was originally accumulated by microorganisms in marine sediments, and subsequent metamorphism of this organic matter resulted in the V-rich graphite that is commonly observed as inclusions in these gems (e.g. Figure 7). The inclusions in moss agate have long been considered as inorganic formations, but many of these filamentous units apparently had an organic origin based on their geometry and structure. In addition, the structure of opal showing play-of-colour is not restricted only to sedimentary processes: SEM images of colour patterns on the carapace of a tropical beetle

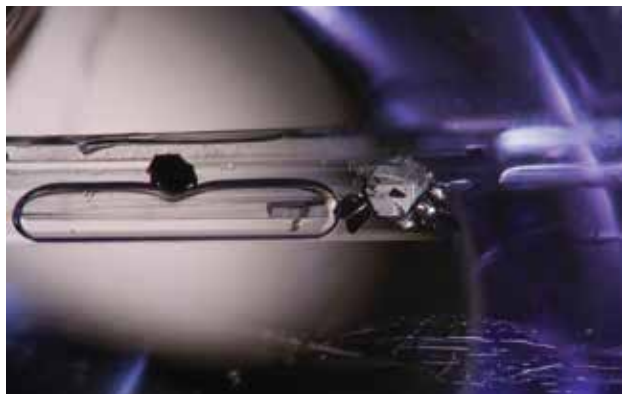


Figure 7: This fluid inclusion in tanzanite hosts a graphite crystal. The V-bearing composition of such inclusions provides evidence for their formation through the metamorphism of organic matter. Photomicrograph by M. Hügi; image width 2.5 mm.

species show exactly the same structure as those opals. **Dr Lore Kiefert** (Gübelin Gem Lab, Lucerne, Switzerland) presented a new find of black opal from the Stayish mine in Ethiopia. The black body colour is due to amorphous organic carbon. Preliminary trace-element analyses show that it is possible to distinguish between two populations of black opal based on their Ba contents: one of volcanic origin, and a second with a sedimentary formation. Some white opals of the Welo (or Wollo) deposit in Ethiopia can be coloured dark brown to black by smoke treatment in order to imitate black opal. This treatment can be detected with the microscope by observing dark spots on the surface and staining of fissures. **Carina Hanser** (University of Freiburg, Germany) presented the results of her Bachelor's thesis on blue cobalt-bearing spinel from Vietnam, carried out under the supervision of Dr M. S. Krzemnicki. Interestingly, part of the analysed blue spinels show a colour change from blue in daylight to bluish purple in incandescent light, which can be explained by the superposition of cobalt and iron absorption bands in the visible part of the absorption spectrum.

Several talks covered marketing and pricing issues. In a short presentation, **Dr Laurent Cartier** (SSEF) gave the current status of various initiatives undertaken recently in ethical sourcing for gems (and gold) by different groups or trade bodies, such as CIBJO (The World Jewellery Confederation), RJC (Responsible Jewellery Council) and UNICRI (United Nations) in collaboration with ICA. He also described how producers of synthetic diamonds address

sustainability issues in marketing their products to consumers. **Gilles Walthert** (Edigem AG, Lucerne, Switzerland), provided a market report on diamond. Since mid-2014, the demand for polished colourless diamonds has slowed, resulting in price reductions for finished goods (e.g. Rapaport diamond price list) and by December 2014 also for rough diamonds. This trend was confirmed during the recent Baselworld show, although some dealers had better prices than expected. By contrast, fancy-colour diamonds have seen increasing prices during the past few years, supported by spectacular results at auction for exceptional stones. **Hans Pfister** (Luigitrade S.A., Geneva, Switzerland) gave an overview on the market situation for ruby, sapphire and emerald. Demand for these gems in areas such as China, Southeast Asia, Russia and the Middle East has decreased significantly in recent years, mainly due to political or economic reasons. Nevertheless, prices for important stones and top qualities have skyrocketed in the same period, mainly due to dwindling supplies from traditional sources, such as Myanmar for ruby and sapphire, and the temporary closure of the Muzo emerald mine in Colombia. **Antoinette Starkey** (Exclusive Personal Jewellery & Gemstones, Geneva, Switzerland) described the evolution of coloured gemstone prices in the last decade. She demonstrated that prices of some less popular gem varieties have increased dramatically during this time. The amount of increase is dependent on the hue and size of the stone. For example, the price of a 10 ct spinel of vibrant red colour has increased six-fold since 2005, while a brownish red spinel of the same size saw only a three-fold price increase during the same period. **René Lauper** (Frieden AG, Thun, Switzerland) indicated that the global cultured pearl market is now recovering after the economic crisis that began in 2008. Traditional markets in the USA and Europe show an increasing demand for commercial qualities of cultured pearls, whereas the market for top qualities is still weak in these regions. By contrast, consumers in Asian countries, and especially in China, are looking more and more for top-quality cultured pearls, resulting in a strong demand and consequently higher prices.

*Michael Hügi FGA (michael.buegi@gemmologie.ch)
Bern, Switzerland*

*Dr Michael S. Krzemnicki FGA
Swiss Gemmological Institute SSEF
Basel, Switzerland*

Gem-A Notices

Bachelor of Science with Honours Degree in Gemmology and Jewellery Studies

The BSc (Hons) degree in Gemmology and Jewellery Studies is now being offered at Birmingham City University and as a final-year option through Gem-A in London. This programme is the culmination of three years' development work between these two organizations, and represents a leap forward in the field of gemmological education.

Already, Gem-A's Gemmology Diploma was one of the world's highest level educational qualifications in this field. Now this Diploma, together with the Gem Diamond Diploma, forms part of the requirements for entry into the final year of this BSc programme. Other requirements are that applicants are registered members of Gem-A and have suitable background to apply the advanced techniques covered within the course. The programme consists of six modules, each covering a different area of advanced testing:

- *Advanced Gemmology 1* provides a grounding in crystallography, including symmetry models and crystal lattice points. It also introduces research and presentation skills that will be required for the following modules.
- *Advanced Gemmology 2* builds on *Advanced Gemmology 1*, and applies the theories learnt to practical applications in real-life scenarios. This involves not only knowing how to operate the equipment (i.e. UV-Vis, FTIR and EDXRF spectrometers), but also which pieces of equipment are used for a particular task, a skill eminently relevant to laboratories today.
- *Advanced Diamonds* brings in the use of advanced testing techniques to analyse diamonds, and the defects that have an effect on the properties of the stone. Advanced use of spectroscopy, and interpretation of the collected data, ensure that the

student is well-versed in many areas of diamond analysis, across a range of testing techniques (FTIR, UV-Vis and Raman spectroscopy).

- The *Valuation and Appraisal Theory* module trains students in real-life skills that can be applied in a variety of scenarios. Being able to effectively complete a valuation to an industry-recognized standard is a relevant skill that complements the students' advanced gemmological testing abilities.
- *Geology of Gemstones*, the fifth module, assesses the rock cycle within a gemmological context, and gives advanced study into the geological processes and rock formations that are involved in the formation of gem-bearing deposits.
- The final module covers the *Research Project*, and it is in this area that the students combine all that they have learnt across the various modules to formulate a hypothesis that they are then allowed to research, through existing literature, and then take it forward with the range of testing techniques available to them, before producing a final research document. This is the summation of all other modules, and allows students to demonstrate not only that they know how to use the equipment, but also how to apply it to the furtherance of gemmological knowledge.

The course is assessed on an ongoing basis, with written and practical examinations, course work and presentations all playing a part in the final grading for each module. Upon successful completion of this course, students are awarded a BSc (Hons) qualification.

For further information and details of how to apply for this course, visit www.gem-a.com/education/bsc-in-gemmology-and-jewellery-studies.aspx or contact Miranda Wells at Miranda.Wells@bcu.ac.uk.



Gem-A
THE GEMMOLOGICAL ASSOCIATION
OF GREAT BRITAIN



BIRMINGHAM CITY
University

GIFTS TO THE ASSOCIATION

The Association is most grateful to the following for their gifts for research and teaching purposes:

Gems in Gems, Seville, Spain, for a cabochon of chrysocolla chalcedony (see page 472).

Melanie Mednuik FGA DGA, Feering, Essex, for faceted quartz and paste, a kyanite cabochon and a

'rainforest' jasper' bead.

Antonio Silva, London, for eight faceted samples of andalusite.

OBITUARY

Catriona Orr McInnes

1938–2015

Catriona McInnes MBE MA FGA was gentle and quiet with a wry sense of humour but also had a stubborn and determined streak when needed.

Catriona grew up in Ayrshire in close contact with her extended family. Her Grandpa Orr was a jeweller, watchmaker and optician, and had a shop in Saltcoats. Catriona's brother Alan was born in 1943 and they enjoyed a close relationship. She also had a very close relationship with her cousins, who lived nearby. Catriona attained the accolade of Dux of the school at Ardrossan Academy, before attending Glasgow University where she graduated with an MA degree in Politics and Economics in 1960. She went on to teacher training school before starting her first job as a secondary school teacher of mathematics in Airdrie.

She joined the Glasgow Geological Society and took a keen interest in geology, eventually going back to University in 1976 to pursue a degree in this subject. That year, on a field trip to Loch Lomondside, she met this author (trip leader); a friendship developed and romance then blossomed. We were married in 1977.

We moved to Edinburgh from Glasgow in 1977, where I had accepted a post with the Institute of Geological Sciences (later to become the British Geological Survey). Holidays were spent self-catering in Mull and Skye, where eventually our children were introduced to mineral collecting and searching for gemstones. (Our collecting trips initially started in the late 1960s at Leadhills, famous for its lead deposits, and over the years we visited many classic localities as described by M. F. Heddle's *The Mineralogy of Scotland*.) We amassed a large collection of Scottish material over some 40 years. The children 'fondly' remember hours of digging in quarries in the horizontal rain, looking for what they called 'rubble'

and learning survival techniques in the process, such as lighting fires in caves to get out of the cold and rain! Even the dog gave up.

At Boroughmuir School in Edinburgh, Catriona was given the job of computer teacher when the post became vacant following a colleague's illness. She expanded that role within the school and became involved in the development of the subject throughout Scotland.

In collaboration with others, she developed the syllabus for Computer Studies, culminating in the creation and setting of a Higher examination. She also developed a teacher training course in computing at Moray House, later even taking the course herself to get the qualification. Her work was recognized with an MBE in 1997—an award she was going to refuse until I persuaded her to take it. She was asked by a journalist after the ceremony, "What did you get your MBE for?" "I've no idea," she replied. Modest to a fault!

From her early interest in geology, Catriona developed a passion and later, an expertise in gemmology, completing her Gemmology Diploma in 1997 and then teaching the subject at University. She also tutored for Gem-A. Retiring in 1998, she poured her energies into gem collecting and developing her own business, Hyaline. She learned to string beads, and had success selling her own designs and providing stringing services to the trade. We traveled internationally in pursuit of gemstones, often accompanied by Catriona's brother Alan, panning for sapphires in Montana and Australia and gem collecting all over the world, even avoiding mountain lions in Colorado!

With the help of friends, Catriona resurrected the Scottish Branch of the Gemmological Association and took over organization of the annual conference in 1999. The Scottish Gemmological Association was subsequently formed in 2008, and Catriona became



Secretary. Working with others, Catriona helped to establish the SGA Annual Conference as the 'friendliest' gemmological conference in the world. Catriona was meticulous in the organization of conference; it took up much of her life. She wrote her own computerized hotel booking and billing system, and she developed long-term friendships with gemmologists all over the world.

Catriona loved the natural world and got enormous pleasure from the animals, birds, rocks and scenery of Scotland. She was very proud to be Scottish and never lived anywhere else. We have always been interested in birdwatching, and this hobby also developed into a passionate pursuit, taking us all over the world, culminating in a two-week trip to the Brazilian rainforest in 2000.

Catriona was diagnosed with a serious lung condition in 2013. Despite that, her positive attitude

shone through and she always approached life looking on the bright side, a smile and sense of fun never far away. She was so well balanced, serene in her nature and above all, very loving to all her family with a sense of humour steeped in observation of life's absurdities.

Catriona will be missed terribly, but her life and our memories of her will be cherished by us all and will remain forever. In addition to myself (her soulmate), Catriona is survived by her children Andrew, Dougal, Eric and Barbara, and her grandchildren Hannah, Ross, Molly, Oscar, Lorcan, Mari and Lucy, with whom she shared much love and laughter. We may have lost our most precious gem, but there is no doubt that Catriona's luminescence and adamantine lustre will continue to light our lives throughout the years ahead.

John McInnes

MEMBERSHIP

At a meeting of the Council held on 13 May 2015, Jason Williams resigned as Chairman. The Council expressed their gratitude for the work he had carried out and his achievements. Jessica Cadzow-Collins was elected to the Chair. The following were elected to membership:

Fellowship and Diamond Membership (FGA DGA)

Chan Kin Chung, *San Po Kon, Hong Kong*

Fellowship (FGA)

Baduza-Sutton, Buyisa, *Birmingham, West Midlands*

Hui Hang-Chung, Marilyn, *Hong Kong*

Lancaster, Sonya, *Sutton, Surrey*

Meissirel, Mathilde, *Canterbury, Kent*

Nijzink-Brandt, Saskia, *Sydney, New South Wales, Australia*

Raguin, Odiane, *Aix-en-Provence, France*

Shaw, Stephanie, *London*

Shen Tao, *Zhubai City, Guangdong, P.R. China*

Wong Fang, *Singapore*

Zhu Younan, *Beijing, P.R. China*

Associate Membership

Alexandris, Ioannis, *Munich, Germany*

Attie, Edgar, *Monte Carlo, Monaco*

Beckley, Stewart, *Sheffield, South Yorkshire*

Burnett, Mark, *Oslo, Norway*

Delamater, Laurel, *London*

Gozlan, Esther, *Paris, France*

Herries, Jane, *Haugh of Urr, Dumfries and Galloway*

Hoare, Michael, *Witney, Oxfordshire*

Johnston, Patricia, *St Albans, Hertfordshire*

May, Joshua, *London*

May, Steven, *London*

McQuaid, Jessica, *Leeds, West Yorkshire*

Phipps, Joanne, *Abingdon, Oxfordshire*

Sargsyan, Anna, *London*

Taylor, Chris, *Albuquerque, New Mexico, USA*

Valerio, Greg, *Chichester, West Sussex*

Waugh, Anne, *London*

Fellowship of the Gemmological Association of Australia (FGAA) to FGAA FGA

Kovacs, Katherine, *Melbourne, Victoria, Australia*

Smith, Nerrylea, *Maiden Gully, Victoria, Australia*

Corporate Membership

Fairtrade Gemstones Ltd., *London*

Fifi Bijoux Ltd., *St Albans, Hertfordshire*

The Garden Workshop, *London*

May Gems Ltd., *London*

The Rock Hound, *London*

At a meeting of the Council held on 24 June 2015, it was announced that Steven Collins had resigned from the Council. The following were elected to membership:

Fellowship and Diamond Membership (FGA DGA)

Beard, Thomas, *Eastbourne, East Sussex*

Tang Tiankai, *Zhe Jiang, P.R. China*

Fellowship (FGA)

Arrive, Elodie, *Annecy, France*

Attanayake, Rochana, *Pilimathalawa, Sri Lanka*

Bassil, Sophie-Marie, *Malakoff, France*

Beaumont, Elizabeth, *Montreal, Canada*

Belahlou, Fatima, *Nimes, France*

Blanchard, Alain, *Paris, France*

Boemo, Julien, *Lorraine, France*

Buldanlioglu, Gulgun, *Istanbul, Turkey*

Caplan, Candice, *Monnetier, France*

- Carriere, Laurence, *Montreal, Canada*
 Chang Cheng-Yi, *Taichung City, Taiwan, R.O. China*
 Chen Hsiu-Man, *New Taipei City, Taiwan, R.O. China*
 Chen Muyu, *Guilin, P.R. China*
 Chen Qiao, *Beijing City, P.R. China*
 Chen Ruoxi, *Changsha City, Hunan, P.R. China*
 Chen Zhi Sang, *Beijing, P.R. China*
 Chiu Ti, *New Taipei City, Taiwan, R.O. China*
 Chong Yim Mui, *Tseung Kwan O, Hong Kong*
 Chow Hiu Yan, *Central, Hong Kong*
 Cornelius, *Victoria, London*
 Craig, Deborah, *Sundbyberg, Sweden*
 Dai Jun, *Kunshan City, Jiangsu Province, P.R. China*
 Dai Xinru, *Wuhan City, Hubei Province, P.R. China*
 De Bourgues, Ayena, *Oron-La-Ville, Switzerland*
 De Zoysa Jayatileke, *Liyana Gracelyn, Colombo, Sri Lanka*
 Deijen, Stephanie, *Amsterdam, The Netherlands*
 Deng Yihong, *Beijing, P.R. China*
 Disner, Emilie, *Geneva, Switzerland*
 Dong Yiyuan, *Beijing, P.R. China*
 Duffy, Alex, *Sutton Coldfield, West Midlands*
 Earl, Jeremy, *Kettering, Northamptonshire*
 Emanuelli, Odile, *Ivry-sur-Seine, France*
 Fan Deng, *Guilin, Guangxi, P.R. China*
 Fang Liquan, *Beijing City, P.R. China*
 Fauquet, Richard, *Courbevoie, France*
 Fong Lap Kit, *Yuen Long, Hong Kong*
 Fung Hoi Ching, *Yuen Long, Hong Kong*
 Gandhi, Hemang, *Mumbai, India*
 Gong Hancheng, *Wuhan City, Hubei, P.R. China*
 Gong Qingxu, *Dalian City, Liaoning, P.R. China*
 Gui Fu, *Guilin, Guangxi, P.R. China*
 Guo Ruizhi, *Beijing, P.R. China*
 Guo Yilin, *Beijing, P.R. China*
 Gyde, John, *Abingdon, Oxfordshire*
 Hall, Claire-Louise, *Newcastle-upon-Tyne, Tyne and Wear*
 Han Jiayang, *Beijing, P.R. China*
 Hao Haiyan, *Zhanjiang, Guangdong, P.R. China*
 He Chin Ju, *Kaohsiung City, Taiwan, R.O. China*
 Hein Naing Oo, *Yangon, Myanmar*
 Hnin Wutyi Soe, *Yangon, Myanmar*
 Hou Yancheng, *Wuhan, Hubei, P.R. China*
 Htaik Hay Man Than, *Yangon, Myanmar*
 Huang Chanyuan, *Beijing, P.R. China*
 Huang I-Ping, *New Taipei City, Taiwan, R.O. China*
 Huang Li-Lien, *New Taipei City, Taiwan, R.O. China*
 Huang Shu, *Beijing, P.R. China*
 Huang Sipei, *Ezhou, Hubei, P.R. China*
 Huang Ying, *Beijing, P.R. China*
 Huang Yue, *Suzhou, Jiangsu, P.R. China*
 Hubley, Kathleen, *Pointe-Claire, Québec, Canada*
 Hung Hoo, *Tsuen Wan, Hong Kong*
 Ito, Claire, *Carlsbad, California, USA*
 Jia Qiong, *Dalian City, Liaoning, P.R. China*
 Jiang Dong, *Beijing, P.R. China*
 Jiang Haiyan, *Shanghai, P.R. China*
 Jiang Xiaowen, *Shanghai, P.R. China*
 Jiang Xueqin, *Shanghai, P.R. China*
 Jin Xinyu, *Beijing, P.R. China*
 Katsurada, Yusuke, *Tokyo, Japan*
 Korcia, Sandrine, *Marseille, France*
 Lai Hsin Han, *Kaohsiung City, Taiwan, R.O. China*
 Lassau, Clothilde, *Cartigny, Switzerland*
 Law, Suang See, *Singapore*
 Leclerc, Thibault, *Gland, Switzerland*
 Li Huan, *Beijing, P.R. China*
 Li Rong, *Beijing, P.R. China*
 Li Shanshan, *Beijing, P.R. China*
 Li Wen, *Beijing, P.R. China*
 Li Yikun, *Guilin, Guangxi, P.R. China*
 Li Zhechen, *Beijing, P.R. China*
 Li Zhen, *Guilin, Guangxi, P.R. China*
 Li Zhenjia, *Beijing, P.R. China*
 Lin Moqing, *Tseung Kwan O, Hong Kong*
 Lin Yu-Jie, *New Taipei City, Taiwan, R.O. China*
 Liu Cheng Fang, *Kaohsiung City, Taiwan, R.O. China*
 Liu, Jia Hong, *Bangkok, Thailand*
 Liu Kaichao, *Beijing, P.R. China*
 Liu Na, *Shanghai, P.R. China*
 Liu Ying, *Shanghai, P.R. China*
 Liu Yingying, *Beijing, P.R. China*
 Liu Yuli, *Shaoyang, Hunan, P.R. China*
 Long Songyun, *Guilin, Guangxi, P.R. China*
 Luan Dongqi, *Beijing, P.R. China*
 Luk Ka Wa, *Wongtai Sin, Hong Kong*
 Luo Jinglang, *Beijing, P.R. China*
 Ma Chunao, *Beijing, P.R. China*
 Ma Jing, *Beijing, P.R. China*
 Mak Ka Wai, *Kowloon, Hong Kong*
 May, Eric, *Verbier, Switzerland*
 Meidong Zhu, *Guilin, Guangxi, P.R. China*
 Meoni, Annabella, *Montreal, Quebec, Canada*
 Ming Zeng, *Guilin, Guangxi, P.R. China*
 Mournalian, Nicole, *Montreal, Quebec, Canada*
 Nacht, Coralie, *Vich, Switzerland*
 Nassi, David, *Norwalk, Connecticut, USA*
 Nay Hlaing Oo, *Yangon, Myanmar*
 Nayak, Asha, *Egham, Surrey*
 Nian Bofeng, *Shanghai, P.R. China*
 Odake, Shoko, *Tokyo, Japan*
 Pan Yanmei, *Beijing, P.R. China*
 Parkin, Charlotte, *Caterham, Surrey*
 Peng, Mingqiang, *Guilin, Guangxi, P.R. China*
 Polly, Teresa, *Knoxville, Tennessee, USA*
 Porter, Grace, *Stone, Staffordshire*
 Prail, Gregory, *Hockley, Essex*
 Price, Amy, *South Darent, Kent*
 Qiao Lei, *Beijing, P.R. China*
 Qin Qiaohong, *Guilin, Guangxi, P.R. China*
 Quan Xiaoyun, *Beijing, P.R. China*
 Redjem, Sihame, *Nanterre, France*
 Renfro, Nathan, *Carlsbad, California, USA*
 Richard, Genevieve, *Brossard, Quebec, Canada*
 Roux, Zongqi, *Le Pontet, France*
 Sarson, Gregory, *Toowong, Queensland, Australia*
 Senior, Lauren J., *Leeds, West Yorkshire*
 Shen Jiamin, *Guilin, Guangxi, P.R. China*
 Shen Jingyao, *Beijing, P.R. China*
 Shen Rongrong, *Beijing, P.R. China*
 Shi Jiaqing, *Beijing, P.R. China*
 Shi Shuang, *Beijing, P.R. China*
 Shi Shupeng, *Foshan City, Guangdong, P.R. China*
 Sit Mei Mei, *Central, Hong Kong*
 Soonthorntantikul, Wasura, *Bangkok, Thailand*

- Steffens, Hounaida, *Nanterre, France*
 Su Yung Chu, *Kaohsiung City, Taiwan, R.O. China*
 Su Yung-Han, *Taipei City, Taiwan, R.O. China*
 Sun Ziwei, *Fuzhou City, Fujian, P.R. China*
 Tan Yongting, *Beijing, P.R. China*
 Thiel, Gunyasiree, *London*
 Tian Xiufang, *Beijing, P.R. China*
 Tint Yin Moe, *Yangon, Myanmar*
 Tung Jen-Hao, *Taichung City, Taiwan, R.O. China*
 Velickaite, Akvile, *London*
 Wang, Dan, *Beijing, P.R. China*
 Wang Guohua, *Weifang City, Shandong, P.R. China*
 Wang Juan, *Shanghai, P.R. China*
 Wang Kailin, *Beijing, P.R. China*
 Wang Kang, *Beijing, P.R. China*
 Wang Shuang, *Guilin, Guangxi, P.R. China*
 Wang Sisi, *Beijing, P.R. China*
 Wang Yiyi, *Beijing, P.R. China*
 Wang Zhilin, *Shenzhen City, Guangdong, P.R. China*
 Weng Ruizhi, *Beijing, P.R. China*
 Weng Yahui, *Zhengzhou City, Henan, P.R. China*
 Wilkinson, Damien, *Danesfort, Co. Kilkenny, R.O. Ireland*
 Williamson, Anna, *Hamilton, New Zealand*
 Wong Yu Ting, *Tai Po, Hong Kong*
 Wright, William, *London*
 Wu Wenjie, *Foshan City, Guangdong, P.R. China*
 Wu Xuxu, *Beijing, P.R. China*
 Xin Wen, *Beijing, P.R. China*
 Xu Huanling, *Wuhan City, Hubei, P.R. China*
 Xu Lingxiao, *Beijing, P.R. China*
 Xu Qinzi, *Beijing, P.R. China*
 Yang Hsiao-Chu, *Taipei City, Taiwan, R.O. China*
 Yang Xiao, *Beijing, P.R. China*
 Yang Xue-Chang, *New Taipei City, Taiwan, R.O. China*
 Yang Yang, *Guilin, Guangxi, P.R. China*
 Yang Yi-En, *Taipei City, Taiwan, R.O. China*
 Yang Yong, *Ningbo, P.R. China*
 Yang Yuling, *Beijing, P.R. China*
 Yazawa, Emiko, *Woodside, New York, USA*
 Yi Nannan, *Beijing, P.R. China*
 Yiyi Su, *Guilin, Guangxi, P.R. China*
 Yong Chenying, *Beijing, P.R. China*
 Yuan Wei, *Guilin, Guangxi, P.R. China*
 Zhai Mengqi, *Beijing, P.R. China*
 Zhang Guifang, *Beijing, P.R. China*
 Zhang Hongqing, *Beijing, P.R. China*
 Zhang Lingjie, *Beijing, P.R. China*
 Zhang Linqi, *Beijing, P.R. China*
 Zhang Mingxi, *Chongqing City, P.R. China*
 Zhang Peng, *Shanghai, P.R. China*
 Zhang Sirong, *Guilin, Guangxi, P.R. China*
 Zhang Ting, *Montreal, Quebec, Canada*
 Zhang Xiao, *Shanghai, P.R. China*
 Zhang Yiwen, *Beijing, P.R. China*
 Zhao Chengcheng, *Wuhan City, Hubei, P.R. China*
 Zhao Yi, *Beijing, P.R. China*
 Zhao Zhiyang, *Shanghai, P.R. China*
 Zhen Wang, *Guilin, Guangxi, P.R. China*
 Zheng Bingyu, *Beijing, P.R. China*
 Zheng Qiong, *Wenling City, Zhejiang, P.R. China*
 Zhu Xiaofei, *Shanghai, P.R. China*
- Diamond Membership (DGA)**
 Ball, Gareth, *Letterkenny, Co. Donegal, R.O. Ireland*
 Boyce, Georgina Elizabeth, *London*
 Bullmore, Elizabeth, *Birmingham, West Midlands,*
 Chan Lap Yee, *Shuang Shui, Hong Kong*
 Chan Wai Chi, *New Territories, Hong Kong*
 Chan Tak Wai, *Shatin, Hong Kong*
 Chan Hiu Ching, *New Territories, Hong Kong*
 Cheang Chi Ioi, *Macau, P.R. China*
 Chen Xiao Qin, *New Territories, Hong Kong*
 Cheng Wai Ching, *Kowloon, Hong Kong*
 Cheng Wai Lei, *Sai Wan, Hong Kong*
 Cheung Wing Yee, *Tsing Yi, Hong Kong*
 Choi Sze Man, *Kwun Tong, Hong Kong*
 Fu Haitao, *Beijing, P.R. China*
 Fu Xinli, *Beijing, P.R. China*
 Fung Hang Shun, *Jessica, New Territories, Hong Kong*
 Gogarty, Madeleine, *Wimbledon, London*
 Ho Pak Ngai, *New Territories, Hong Kong*
 Ketcher, Alyce, *Wellington, Somerset*
 Kuang, Chuyi, *Beijing, P.R. China*
 Kwong Wai Fan, *New Territories, Hong Kong*
 Kwong San Fong, *Cathy, Kowloon, Hong Kong*
 Lai Ka Man, *London*
 Lam Pui Yu, *Ma On Shan, Hong Kong*
 Lam Yin Han, *To Kwa Wan, Hong Kong*
 Lau Kin Yip, *New Territories, Hong Kong*
 Leicester, Keith, *St Helens, Merseyside*
 Li Dongyang, *Beijing, P.R. China*
 Li Hiu Ying, *Chai Wan, Hong Kong*
 Li Man Wah, *Irine, Tseung Kwan O, Hong Kong*
 Lo Hau Yin, *Kowloon, Hong Kong*
 Marshall, Georgia, *Meopham, Kent*
 McLoughlin, Emma, *Rathfarnham, R.O. Ireland*
 Milo, Nathan, *London*
 Molon, Valentina, *Varese, Italy*
 Moorhead, Lisa, *London*
 Nash-Wilson, Jake, *Bristol*
 Ng Kwok Hung, *Mongkok, Hong Kong*
 Niu Tianju, *London*
 Rexworthy, Simon, *Market Drayton, Shropshire,*
 Saban Makarim, *Tai Po, Hong Kong*
 Schindler, Leo Joseph Peter, *Kingston-upon-Thames, Surrey*
 Shek Sze Wan, *Tuen Mun, Hong Kong*
 Tam Ka Hey, *Tuen Mun, Hong Kong*
 Tam Suk Han, *Sara, Ma On Shan, Hong Kong*
 Ting Evon, *Tsuen Wan, Hong Kong*
 Tse Lai Kwan, *Kowloon, Hong Kong*
 Tso Hau Yee, *Michelle, Causeway Bay, Hong Kong*
 Wang Jinghan, *Beijing, P.R. China*
 Wang Yizhu, *Beijing, P.R. China*
 Wong Ching Lan, *Teresa, Tuen Mun, Hong Kong*
 Wong Hon Lam, *Donald, Kowloon, Hong Kong*
 Wong Kay Yee, *Tseung Kwan O, Hong Kong*
 Wong Kwan Wai, *Alison, Kennedy Town, Hong Kong*
 Wong Kwong Mei, *Ice, Kowloon, Hong Kong*
 Wong Sin Yan, *Sai Wan Ho, Hong Kong*
 Wong, William, *Kowloon, Hong Kong*
 Wu Weiran, *Beijing, P.R. China*
 Xie Zhuohong, *Beijing, P.R. China*
 Yang Dong Wen, *Kowloon, Hong Kong*
 Yang Ning Ning, *Kowloon, Hong Kong*

Yiu King Ting, Eric, *Kowloon, Hong Kong*
 Zhang Zhizheng, *Beijing, P.R. China*

Associate Membership

Ball, John, *Hatfield, Hertfordshire*
 Chappell, Kathy, *London*
 Chib, Phillip, *London*
 Clark, Paul, *Penarth, Vale of Glamorgan*
 Cook, Brian, *Tucson, Arizona, USA*
 Milton, Monica, *Crossgates, Fife*
 Rohtert, William, *Phoenix, Arizona, USA*
 Sokolov, Pavel, *St Petersburg, Russia*
 Wood, Courtney, *New York, New York, USA*

Fellowship of the Gemmological Association of Australia (FGAA) to FGAA FGA

Edwards, Sarah, *Perth, Western Australia, Australia*
 Walker, Susan, *Elwood, Victoria, Australia*

Corporate Membership

The Ebor Jetworks, *Whitby, North Yorkshire*

Transfers

From Fellowship (FGA) to Fellowship and Diamond Membership (FGA DGA)

Cheer, Peter, *Somerton, Somerset*
 Chui Chun Hin, *Sbatin, Hong Kong*
 Kolator, Barbara, *London*
 Leung Ying, *Tsing Yi, Hong Kong*
 Shaw, Stephanie, *London*
 Williams, Kathryn, *Dover, Kent*

From Associate Membership to Fellowship (FGA)

Delaye, Aline, *Singapore*
 Lusher, Lila, *Whangarei, Northland, New Zealand*
 Miller, Mona, *Portland, Oregon, USA*
 Reich, Mary, *Albuquerque, New Mexico, USA*

From Associate Membership to Diamond Membership (DGA)

Saleem, Melanie, *Manchester, Lancashire*
 Spencer, Sally, *Didcot, Oxfordshire*
 Vildiridi, Lilian Venetia, *Knightsbridge, London*

Annual General Meeting

The AGM previously arranged to be held on 24 June was postponed. It is now to be held on 29 July 2015 at 6:00 p.m. at The Crypt, 14 Ely Place, London EC1N 6RY. A full report will appear in the next issue of *The Journal*.



DALLAS
 MINERAL COLLECTING
 SYMPOSIUM

AUGUST 21-23, 2015
 WORLD-RENOWNED SPEAKERS
 ENGAGING SOCIAL EVENTS
 SPECTACULAR FINE MINERALS

Lectures By
 Dr. Robert Bowell
 Dr. Bruce Cairncross
 Brice Gobin
 Tom Gressman
 Dr. Federico Pezzotta
 Tomasz Praszkiar



Aquamarine, Spessartine, Smoky Quartz, Feldspar from Pakistan

REGISTER NOW AT DALLASSYMPOSIUM.ORG
 Use code GEMA10OFF for a 10% discount!

Founding Sponsor | Supporting Sponsors



GEMGAZER

New online gem store for enthusiasts, jewellers and gemmology students. A wide range of rare & collectors gemstones, designer cabochons, Amber with inclusions, fossils, meteorites and other gemmological curiosities.



 www.gemgazer.com
 www.twitter.com/gemgazer
 www.facebook.com/gemgazer
 www.uk.pinterest.com/gemgazer17



YOUR GLOBAL PARTNER

Gem Identification Report and Gemstone Memo

GIT, The utmost advanced Gem and Precious Metal Testing Laboratory in Thailand, is recognized by CIBJO (The World Jewellery Confederation) and also a member of LMHC and ICA, we are well equipped with the world's most advanced instruments operated by highly experienced gemologists.

LABORATORY SERVICES

ensuring the authenticity of your valuable gems & jewelry



The Gem and Jewelry Institute of Thailand (Public Organization)
 140 JTF Tower, Silom Rd., Bangkok 10500, Thailand
 TEL : +66 2634 4999 FAX : +66 2634 4970
<http://www.git.or.th> E-mail: jewelry@git.or.th



Learning Opportunities

CONFERENCES AND SEMINARS

NAJA 44th ACE IT Annual Mid-Year Educational Conference

8–11 August 2015
Washington DC, USA
www.najaappraisers.com/html/conferences.html

Northwest Jewelry Conference 2015

14–16 August 2015
Bellevue, Washington, USA
www.northwestjewelryconference.com

Goldschmidt2015

16–21 August 2015
Prague, Czech Republic
www.goldschmidt.info/2015
Session of Interest: Mantle-Derived Intraplate Magmas, their Xenolith and Diamond Cargo: Processes, Timescales, and Geodynamic Implications

Dallas Mineral Collecting Symposium

21–23 August 2015
Dallas, Texas, USA
www.dallassyposium.org/2015-symposium

1st International Jewelry Industry Forum

21–24 August 2015
Kuala Lumpur, Malaysia
email sumarniparamita@gmail.com

13th Society for Geology Applied to Mineral Deposits Biennial Meeting

24–27 August 2015
Nancy, France
<http://sga2015.blog.univ-lorraine.fr>
Session of interest: Gems and Industrial Minerals

8th Congress on Application of Raman Spectroscopy in Art and Archaeology

Wrocław, Poland
1–5 September 2015
<http://raa.chem.uni.wroc.pl/program>

International Jewellery London 2015

6–8 September 2015
Olympia, London, UK
www.jewellerylondon.com/Whats_On/Conferences/#
Note: Includes a programme of seminars

26th International Conference on Diamond and Carbon Materials

6–10 September 2015
Bad Homburg, Germany
www.diamond-conference.elsevier.com

IRV Loughborough Conference

12–14 September 2015
Loughborough, UK
www.jewelleryvaluers.org/Loughborough-Conference

1st International Emerald Symposium

Bogotá, Colombia
13–15 October 2015
www.worldemeraldsymposium.com

Canadian Gemmological Association Gem Conference 2015

16–18 October 2015
Vancouver, British Columbia, Canada
www.canadiangemmological.com/index.php/about/conference/34-conference/105-gem-conf-2015

American Society of Appraisers International Appraisers Conference

18–21 October 2015
Las Vegas, Nevada, USA
www.appraisers.org/Education/conferences/asa-conference

2015 Geological Society of America Annual Meeting

1–4 November 2015
Baltimore, Maryland, USA
www.geosociety.org/meetings/2015
Session of interest: Gemological Research in the 21st Century – Exploration, Geology, and Characterization of Diamonds and Other Gem Minerals

Gem-A Conference, hosting the 18th International Federation of European Education in Gemmology Symposium

21–22 November 2015
Royal Institute of British Architects, London
www.gem-a.com/news--events/events/gem-a-conference-2015.aspx

2015 China Gems & Jewelry Academic Conference

26 November 2015 (before the Beijing International Gem & Jewelry Fair, 27–30 November)
Beijing, China
email ngtcyjb@ngtc.gov.cn

Compiled by Georgina Brown and Brendan Laurs

EXHIBITS

Australia and New Zealand

A Fine Possession: Jewellery and Identity

Until 20 May 2016

Powerhouse Museum, Sydney, Australia
www.powerhousemuseum.com/exhibitions/jewellery/

Europe

Second Hand: Reused Jewellery in Baroque Monstrances

Until 10 August 2015

Dom Quartier, Salzburg, Austria
www.domquartier.at/en/veranstaltung/exhibit-second-hand-reused-jewellery-on-baroque-monstrances-cathedral-museum

#153 – Selected Pieces from the Danish Arts Foundation's Jewellery Collection

Until 16 August 2015

Design Museum Denmark, Copenhagen, Denmark
www.designmuseum.dk/en/udstillinger/153

The Art of Beauty: Jewelry Creations by Gianmaria Buccellati

Until 30 August 2015

Palace of Venaria, Turin, Italy
www.lavenaria.it/web/en/calendar/mostre/details/247-larte-della-bellezza.html

Inside the Victorian Jewellery Box

Until 6 September 2015

The Royal Pump Room Museum, Harrogate, North Yorkshire
www.visittharrogate.co.uk/things-to-do/royal-pump-room-museum-p1203181

Between Nature and Artifice—Jewellery by Daniel Kruger

Until 27 September 2015

Deutsches Goldschmiedehaus Hanau, Hanau, Germany
www.goldschmiedehaus.com/en/daniel-kruger-zwischen-natur-und-kunstlichkeit-schmuck-1974-bis-2014

Hear of Zug – Think of Jewellery. 400 Years of Gold and Silversmithing

Until 27 September 2015

Museum Burg Zug, Zug, Switzerland
www.burgzug.ch/page/en/ausstellungen/sonderausstellung

The Feel of the City—Jewellery from Centres of this World

Until 1 November 2015

Schmuckmuseum, Pforzheim, Germany
www.schmuckmuseum.de/flash/SMP_en.html

Fitting and Befitting—Fibulae and Brooches

20 November 2015–21 February 2016

Shmuckmuseum, Pforzheim, Germany
www.schmuckmuseum.de/flash/SMP_en.html

Bejewelled Treasures: The Al Thani Collection

21 November 2015–28 March 2016

Victoria and Albert Museum, London
www.vam.ac.uk/content/exhibitions/exhibition-bejewelled-treasures-the-al-thani-collection

Colourful World of Quartz Materials Around Us

Until 2016

Moravian Museum, Brno, Czech Republic
www.mzm.cz/en/dietrichstein-palace-exhibitions/colourful-world-of-quartz-materials-around-us

130 Years of Jewellery Creation in Bastia: The Filippi Workshop

Until 19 July 2016

Musée Municipal d'Art et d'Histoire, Bastia, Corsica
www.musee-bastia.com/musee-bastia/musee.php?nav=16&lang=en

Jewellery: From Decorative to Practical

On display (closing date to be determined)

Nordiska Museet, Stockholm, Sweden
www.nordiskamuseet.se/en/utstallningar/jewellery

North America

Fabergé: Jeweler to the Tsars

Until 27 September 2015

Oklahoma City Museum of Art, Oklahoma City, Oklahoma, USA
www.okcmoa.com/see/exhibitions/faberge

Generations of Mastery: Gemstone Carvings by Dreher

Until October 2015

Gemological Institute of America, Carlsbad, California, USA
www.gia.edu/gia-museum-generations-mastery-gemstone-carvings-dreher

Arthur Koby Jewelry: The Creative Eye

Until 5 October 2015

Kent State University Museum, Kent, Ohio, USA
www.kent.edu/file/arthur-koby-jewelry-creative-eye.jpg

The Greeks – Agamemnon to Alexander the Great

Until 12 October 2015

Canadian Museum of History, Gatineau, Quebec, Canada
www.historymuseum.ca/thegreeks/

Beneath the Surface: Life, Death, and Gold in Ancient Panama

Until 1 November 2015
Penn Museum, Philadelphia, Pennsylvania, USA
www.penn.museum/press-releases/1163-beneath-the-surface.html

Jeweled Objects of Desire

Until 1 November 2015
Tellus Science Museum, Cartersville, Georgia, USA
<http://tellusmuseum.org/galleries-more/special-exhibits/jeweled-objects-desire>

Bent, Cast and Forged: The Jewelry of Harry Bertoia

Until 29 November 2015
Cranbrook Art Museum, Bloomfield Hills, Michigan, USA
www.cranbrookart.edu/museum/CAMec3.html

From the Village to Vogue: The Modernist Jewelry of Art Smith

Until 7 December 2015
Dallas Museum of Art, Dallas, Texas, USA
www.dma.org/art/exhibitions/Art-Smith

Fabergé: From a Snowflake to an Iceberg

Until 31 December 2015
Houston Museum of Natural Science, Texas, USA
www.hmns.org/index.php?option=com_content&view=article&id=594&Itemid=621

Maker and Muse: Women and Early 20th Century Art Jewelry

Until 1 January 2016
Driehaus Museum, Chicago, Illinois, USA
www.driehausmuseum.org

Glittering World: Navajo Jewelry of the Yazzie Family

Until 10 January 2016
The National Museum of the American Indian, New York, New York, USA
www.nmai.si.edu/explore/exhibitions/item/838

Turquoise, Water, Sky: The Stone and Its Meaning

Until 2 May 2016
Hillwood Museum and Gardens, Santa Fe, New Mexico, USA
www.indianartsandculture.org/current/?&eventID=1989

Fabergé from the Matilda Geddings Gray Foundation Collection

Until 27 November 2016
Metropolitan Museum of Art, New York, New York, USA
www.metmuseum.org/exhibitions/listings/2011/faberge

Glitterati. Portraits & Jewelry from Colonial Latin America

Until 27 November 2016
Denver Art Museum, Denver, Colorado, USA
www.denverartmuseum.org/exhibitions/glitterati

Gold and the Gods: Jewels of Ancient Nubia

Until 14 May 2017
Museum of Fine Arts, Boston, Massachusetts, USA
www.mfa.org/exhibitions/gold-and-gods

City of Silver and Gold from Tiffany to Cartier

On display (closing date to be determined)
Newark Museum, New Jersey, USA
www.newarkmuseum.org/SilverAndGold.html

Crystals Transformed Through Vision & Skill

On display (closing date to be determined)
Houston Museum of Natural Science, Houston, Texas
www.hmns.org/index.php?option=com_content&view=article&id=481&Itemid=502

Mightier than the Sword: The Allure, Beauty and Enduring Power of Beads

On display (closing date to be determined)
Yale Peabody Museum of Natural History, Yale University, New Haven, Connecticut, USA
<http://peabody.yale.edu/exhibits/mightier-sword-allure-beauty-and-enduring-power-beads>

OTHER EDUCATIONAL OPPORTUNITIES

Gem Central: Maggie Campbell Pedersen Talks Ivory

15 September 2015
Gem-A, London
www.gem-a.com/news--events/events/gem-central--15-september.aspx

2015 Lectures with The Society of Jewellery Historians

Burlington House, London
www.societyofjewelleryhistorians.ac.uk/current-lectures

22 September—'Golden Threads: Filigree in Islamic Jewellery' by Michael Spink

27 October—'Beauty and Belief: Techniques and Traditions of Omani Jewellery' by Aude Mongiatti and Fahmida Suleman

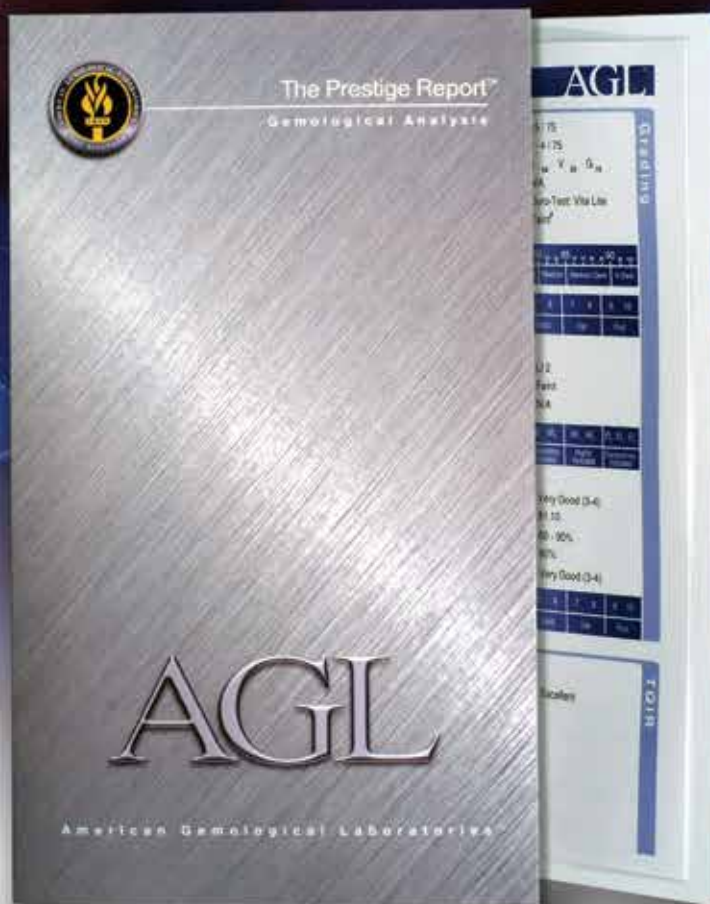
24 November—'Digital Tools and New Technologies in Contemporary Jewellery' by Dauvit Alexander

Gem-A Workshops and Courses

Gem-A, London
www.gem-a.com/education/course-prices-and-dates.aspx

An innovator in gemstone reporting

• Identification of colored gemstones • Country of origin determination • Full quality and color grading analysis



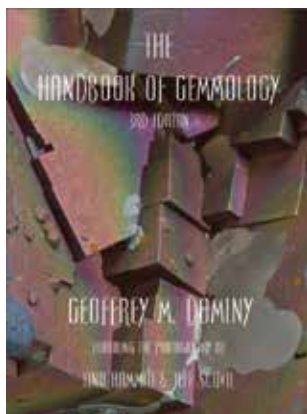
AMERICAN GEMOLOGICAL LABORATORIES



580 5th Ave • Suite 706 • New York, NY 10036, USA
www.aglgemlab.com • +1 (212) 704 - 0727

New Media

The Handbook of Gemmology, 3rd edn.



Geoffrey Dominy, 2015. Amazonas Gem Publications, 1,056 pages, illus., ebook, ISBN 978-0991888221, <http://handbookofgemmology.com>. US\$39.95 for single-format download or \$49.95 for multiple formats.

The 3rd edition of Geoffrey Dominy's *Handbook of Gemmology* continues in the trend set by the previous two editions (2013 and 2014), only in an extended and enhanced form. When it was first issued, the *Handbook* represented a ground-breaking advancement in portability compared to large and heavy gemmology reference books. The initial concept was to bring the textbook platform into the 21st century by means of portable electronic devices such as tablets and smartphones. This was very successful by way of PDFs, e-reader formats, and the use of 'flipping book' technology. This 3rd edition builds on previous successes, and takes the information to more extensive and in-depth levels. At 1,056 pages, this edition of the *Handbook* sets out to be a 'one-stop' comprehensive resource. The 32 chapters and additional sections cover the physical, chemical and optical properties of gem materials, as well as crystallography.

The 'What Is a Gemstone?' chapter covers the basics of beauty and rarity, but it also goes on to consider mineral and rock definitions, explain rock types (igneous, metamorphic and sedimentary), and introduce the concept of groups, species and varieties as applied to gems. 'The Chemical Nature of Gemstones' provides a good introduction to the world of chemistry and atomic concepts including bonding and electron orbitals. 'Physical, Chemical and Optical Properties' lays the foundation for gemmological testing, giving necessary information on hardness, structure and various optical properties exhibited by gems. 'Basic Crystallography' gives explanations of the seven crystal systems and the concepts that define them (e.g. symmetry, axes and habit). This chapter also explains the underpinnings of the physical and optical properties covered in the previous chapter.

The next several chapters cover gemmological instruments and techniques. 'The Absorption of Light and the Spectroscope' gives an explanation of light and its interaction with gem materials, and is illustrated with numerous images and photographs. Both diffraction-grating and prism-type spectroscopes are covered. In the next chapter, on the '3 Rs', Dominy covers the laws and theory behind—and the practical aspects of—reflection, refraction and the refractometer. In addition to the usual methods, several other techniques are considered. Next, 'Polarised Light and the Polariscope' explains the correct use of the polariscope, along with interpretation of the results. 'Pleochroism, the Dichroscope and Colour Filters' then examines the range of colour filters available on the market today, along with the typical dichroscope and Chelsea Colour Filter. A 'Specific Gravity' chapter covers topics ranging from the basic principles of Archimedes to heavy liquids and the Hanneman direct-reading SG balance. Dominy explains how SG is derived, and how it can be used in gem identification. Then a chapter titled 'Luminescence' explains the basics of UV fluorescence as well as its causes (e.g. crystal defects and impurities). The next chapter, titled 'Magnification and Thermal Conductivity', has a much stronger emphasis on photomicrography than on thermal conductivity. Useful instructions are included on how to turn a smartphone into a microscope, with minimal work.

The next series of chapters covers the important aspects of simulants, synthetics and treatments. 'Imitation and Assembled Stones' reviews major imitations and composites, and is a good reference for both students and qualified gemmologists alike. 'Lab-created Gemstones' provides valuable insights into not only the identification of these gems, but also the historical developments that led to the current market situation. Like some previous chapters, it encompasses numerous photographs (i.e. 52 pages). 'Gemstone Enhancements' also is extensively illustrated and describes the currently available treatments, as well as how to detect them (subject to the limitations provided by non-lab gemmological equipment).

The following chapter, 'Gem Mining', explains how valuable stones are recovered from the earth, with special attention given to Sri Lanka (various alluvial gems), Thailand/Cambodia (ruby and sapphire), Canada (diamond), Australia (opal) and Colombia (emerald). Then, 'Gem Cutting' provides general information on lapidary techniques and

diamond cutting. 'Diamond Grading' outlines the key requirements, techniques and limitations for the successful grading of diamond. Next, 'Colour Gemstone Grading' covers a topic that is becoming more important in gemmology, as several organizations are presently involved in the advancement of colour grading. The systems and properties outlined herein provide a valuable basis for considering colour as a gradable quality of a gemstone, and are backed by photographic examples. The next chapter, 'Gem Identification', will be of particular interest to students, or those starting out in gemmology, as a flow chart is provided that allows users to follow a pre-determined set of tests and, from the results, be able to identify the stone or know which test to perform next.

Chapters 20–29 are organized according to gem colour, and provide background information together with tables helpful for identifying stones of each colour. As with most texts, gemmological knowledge and correct testing methodology are prerequisites for this section, but the layout makes it easy to translate results into successful identifications. These chapters are followed by 'Identifying Phenomenal and Unusual Gemstones', which examines the identification of the more unusual stones, some of which exhibit optical phenomena. Although uncommon, the stones covered

are within the range of those that may be seen by a practising gemmologist.

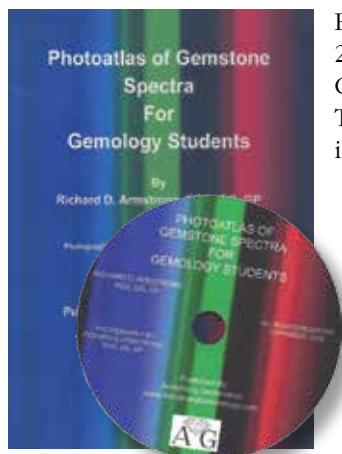
The next chapter, 'Natural, Cultured and Imitation Pearls' is a new addition to the *Handbook*, and covers pearl varieties and identification techniques. Then 'Advanced Gem Testing Techniques' goes beyond the tools available to the average gemmologist, and into the realm of laboratory equipment, covering such techniques as FTIR, EDXRF and Raman spectroscopy, and providing a brief insight into the workings of these instruments.

Before supplying the usual appendix of gem tables and information, the *Handbook* includes a new section titled 'Gemfacts'. For each of the more common gem varieties, a summary of information is provided ranging from coloration through treatments to history. This section alone is of infinite use to students.

In summary, *The Handbook of Gemmology* is lavishly illustrated throughout (with many photographs by Tino Hammid and Jeff Scovil), and provides a wealth of information in an 'at your fingertips' digital format, working on all platforms. This is a valuable resource for any gemmologist, at almost any level, but would be of particular use to modern students familiar with the digital age.

Andrew S. Fellows FGA DGA

Photoatlas of Gemstone Spectra for Gemmology Students



Richard D. Armstrong, 2015. Armstrong Gemmology, Flint, Texas, USA, 78 pages, illus., ebook, ISBN 978-0692298206, www.ArmstrongGemmology.com. US\$9.95 download or \$14.95 on CD (plus p&p).

and effective lighting—and how lighting is critical to getting good results. Chapter 2 provides reference spectra for selected gems that students should obtain for initial practice. Chapter 3 covers spectra by elemental source. Chapter 4 deals with spectra for sphalerite, sugilite and glass (red and green).

Each spectrum is comprehensively discussed with good colour illustrations. Another plus is that Armstrong provides spectra taken with varying light sources, including fluorescent, LED, incandescent, halogen and sunlight, each of which may display its own emission spectrum. This helps the student to avoid any possible confusion between features related to the light source and the gem.

To enhance the spectral illustrations, labels for the wavelength endpoints 400 and 700 nm could be added to spectra for ease of reference when additional wavelengths are present. Also, it would be useful if this publication were available in a format compatible with iPad and other tablet/handheld devices.

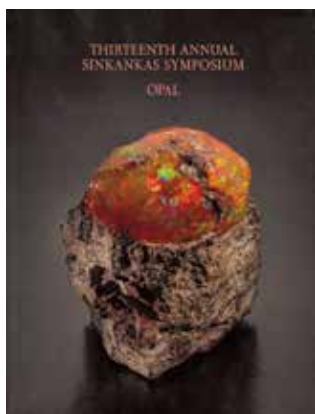
Although not as comprehensive as the spectroscopy coverage in some other gemmology handbooks (both hardcopy and electronic) and websites, this e-book provides a quick and useful reference for those students tackling hand-held spectroscopy for the first time.

Claire Mitchell FGA DGA

This book provides a photographic guide and reference for gemmology students, to help them use the handheld spectroscope and develop a visual memory of spectral patterns for the more common gemstones. Containing colour photos of 40 gems with their spectra, this electronic reference book comes on a CD or is available as a downloadable .zip file. The presentation is in a 'flipping book' format that is very user friendly, with turning pages accompanied by the noise of such, giving a more realistic book-like feel.

Chapter 1 covers general tips and techniques for the successful use of the spectroscope, including correct

Thirteenth Annual Sinkankas Symposium—Opal



Stuart Overlin, Ed., 2015. Pala International, Fallbrook, California, USA, 121 pages, illus., softcover, ISBN 978-0692416884, email merksjade@cox.net. US\$35.00.

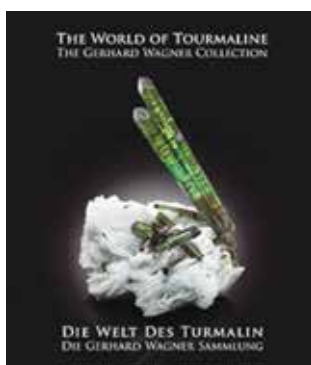
This proceedings volume accompanied the 13th Annual Sinkankas Symposium, which was held on 18 April 2015 at the Gemological Institute of America in Carlsbad, California, and was co-sponsored by the San Diego Mineral & Gem Society. (See pp. 532–533 of this issue for a report on this conference.) The format of this volume is similar to that of previous Sinkankas Symposium volumes, with several contributions by a variety of authors, not all of whom were speakers at the symposium. Also, some of the presentations given at the conference are not covered by articles in the volume. The book begins with the symposium programme listing, followed by biographies of the speakers/authors and then abstracts of most of the presentations.

There are 11 contributions on opal in this volume: geology, colour and microstructure (Dr Előise Gaillou); opals in the Harvard University collection and research on common opal from Mexico (Dr Raquel Alonso-Perez); collecting opals (Bill Larson); matrix opal (Renée Newman); common opal (separate contributions by Renée Newman and Helen Serras-Herman); opal photography (Robert Weldon); microfeatures in opal (Nathan Renfro); lore (Si and Ann Frazier); a listing of literature in the Frazier opal library (Si and Ann Frazier); and a bibliography of opal localities (Dr James E. Shigley). The volume closes with several pages of attractive photos of opals from the collection of Bill Larson.

The volume is attractively laid-out and lavishly illustrated, with many full-page photos that show the diversity and colourful nature of opal. It is printed on high-quality paper and the colour reproduction is exceedingly good. The information presented is educational and informative, although it would have been nice if dimensions or weights were provided for all specimens pictured. Only one minor technical inaccuracy was noted by this reviewer (X-ray fluorescence, not diffraction, was used to determine the chemical composition of the pink opal mentioned on p. 65). This volume is highly recommended for hobbyists, collectors, gemmologists, mineralogists and anyone interested in opal.

Brendan M. Laurs FGA

The World of Tourmaline – The Gerhard Wagner Collection



Mark Mauthner (photographer), Federico Pezzotta, Daniel Trinchillo, Gerhard Wagner, Jim Walker and Mary Fong-Walker, 2015. Ivy Press, Dallas, Texas, USA, 264 pages, illus., hardcover, ISBN 978-1633510487. US\$50.00.

If there ever was a book to capture the eyes and draw someone into the world of minerals this would be it, and what better crystals to do it with than tourmalines. Following a well laid-out introduction in both English and German are 379 stunning colour photographs, all printed on photo-quality paper. Through these

images, this book shares with us the passion and eye of Gerhard Wagner in building this extraordinary collection. Like many collectors he was bitten by the 'rock bug' at a young age, and this book demonstrates that his passion for minerals, especially tourmaline, has remained throughout his life.

The images show a broad variety of tourmaline specimens representing colours and localities from around the world, and ranging from dramatic single crystals to specimens containing various combinations of minerals. Some of the most impressive are of near-colourless quartz with vividly coloured tourmaline, which produces a striking contrast, almost like a work of art.

This is an excellent coffee-table book that will appeal to gem and mineral collectors. In fact, anyone unaware of the beauty and hidden treasures of the mineral world cannot help but be drawn in.

Davina Dryland FGA

OTHER BOOK TITLES*

General Reference***British Silver: State Hermitage Museum Catalogue***

By Marina Lopato, 2015. Yale University Press, London, 400 pages, ISBN 978-0300213201. £100.00 hardcover.

Gemstone Tumbling, Cutting, Drilling & Cabochon Making

By James Magnuson and Val Carver, 2015. Adventure Publications, Cambridge, Minnesota, USA, 128 pages, ISBN 978-1591934608. US\$18.95 softcover.

Mineral Collections in Colorado

Ed. by W. E. Wilson, 2014. Mineralogical Record, Tucson, Arizona, USA, 192 pages. US\$25.00 softcover.

Mineral Collections in Texas

Ed. by W. E. Wilson, 2014. Mineralogical Record, Tucson, Arizona, USA, 304 pages. US\$25.00 softcover.

Jewellery and Objets d'Art***Les Collections de Monsieur, frère de Louis XIV: Orfèvrerie et Objets d'art des Orléans sous l'Ancien Régime***

By Paul Micio, 2015. Somogy Éditions d'Art, Paris, France, 360 pages, ISBN 978-2757207802. £61.80 hardcover.

Egyptian Gold Jewellery—With a Catalogue of the Collection of Gold Objects in the Egyptian Department of the National Museum of Antiquities in Leiden

By Mariëlle Bulsink, 2015. Brepols Publishers, Turnhout, Belgium, 220 pages, ISBN 978-2503553672. £73.28 softcover.

Floral Jewels: From the World's Leading Designers

By Carol Woolton and Joel Arthur Rosenthal, 2014. Prestel, New York, New York, USA, 176 pages, ISBN 978-3791381145. US\$55.00 hardcover.

Grandi Bigiottieri Italiani: Great Italian Costume Jewellers: Ornella Bijoux

By Bianca Cappello, 2015. Universitas Studiorum, Mantova, Italy, 58 pages, ISBN 978-8897683827. €9 softcover.

I Love Those Earrings: A Popular History from Ancient to Modern

By Jane Merrill with Chris Filstrup, 2014. Schiffer Publishing Ltd., Atglen, Pennsylvania, USA, 224 pages, ISBN 978-0764345166. US\$59.99 hardcover.

Jewelry Metals—A Guide to Working with Common Alloys

Ed. by James Binnion, 2015. MJSA Press, Attleboro, Massachusetts, USA, 150 pages, ISBN 978-0979996221. US\$34.95 softcover.

Jewels from History

By Rolf McEwan, 2015. CreateSpace Independent Publishing, 76 pages, ISBN 978-1512102048. US\$9.95 softcover.

Jewels on Queen

By Anne Schofield, 2015. University of New South Wales Press, Kensington, New South Wales, Australia, 128 pages, ISBN 978-1742231433. £31.95 hardcover.

Little Dreams in Glass and Metal: Enameling in America 1920 to the Present

By Bernard N. Jazzar and Harold B. Nelson, 2015. The University of North Carolina Press, Chapel Hill, North Carolina, USA, 280 pages, ISBN 978-1469626369. US\$65.00 hardcover.

Mughal Jewellery: A Sneak Peek of Jewellery Under Mughals

By Nafisa Ali Sayed, 2015. Partridge Publishing, Gurgaon, India, 108 pages, ISBN 978-1482842722. £4.51 softcover or £3.49 Kindle edition.

Petala Aurea: Gold Sheet-work of Byzantine and Lombard Origin from the Rovati Collection

By Marco Sannazaro and Caterina Giostra, 2015. Johan & Levi Editore, Monza, Italy, 240 pages, ISBN 978-8860101563. £22.00 hardcover.

Treasure Box: A Private Collection

By The KK Collection, 2015. Unicorn Press Ltd., London, 450 pages, ISBN 978-1910065181. £500.00 hardcover.

Van Cleef & Arpels: Treasures and Legends

By Vincent Meylan, 2014. Antique Collectors Club, Woodbridge, Suffolk, 344 pages, ISBN 978-1851497706. £55.00 hardcover.

Synthetics and Simulants***Handbook of Crystal Growth, Second Edition: Fundamentals***

Ed. by Tatau Nishinaga, 2014. Elsevier, Amsterdam, The Netherlands, 1,214 pages, ISBN 978-0444563699. £280.00 hardcover or £252.70 Kindle edition.

DVD***AGTA GemFair Tucson Seminar DVD***

2015. American Gem Trade Association, Dallas, Texas, USA. US\$50.00.

* Compiled by Georgina Brown and Brendan Laurs

Literature of Interest

Coloured Stones

La coloration des gemmes par le vanadium trivalent. E. Thoreux, *Revue de Gemmologie*, **191**, 2015, 11–15.

Investigation of hidden periodic structures on SEM images of opal-like materials using FFT and IFFT. N. Stephant, B. Rondeau, J.-P. Gauthier, J. Cody and E. Fritsch, *Scanning*, **36**(5), 2014, 487–500, <http://dx.doi.org/10.1002/sca.21144>.*

Jadeitites and plate tectonics. G.E. Harlow, T. Tsujimori and S.S. Sorensen, *Annual Review of Earth and Planetary Sciences*, **43**, 2015, 105–138, <http://dx.doi.org/10.1146/annurev-earth-060614-105215>.

Mineral mysteries: Star rose quartz. J.S. White, *Rocks & Minerals*, **90**(3), 2015, 282–284, <http://dx.doi.org/10.1080/00357529.2015.1012960>.

Cultural Heritage

Ancient ship treasure confirms Sri Lanka as oldest sapphire source. J. Henricus, *InColor*, **27**, 2015, 34–36.

Un fabuleux saphir de 291 carats redécouvert au MNHN: le “Devonshire-Branicki”. F. Farge, *Revue de Gemmologie*, **191**, 2015, 23–29.

Du Turkestan à la Birmanie: la quête du jade dans les sources chinoises, 2nd partie. L. Long, *Revue de Gemmologie*, **191**, 2015, 16–19.

Diamonds

The origin of large irregular gem-quality type II diamonds and the rarity of blue type IIb varieties. A.E. Moore, *South African Journal of Geology*, **117**(2), 2014, 219–236, <http://dx.doi.org/10.2113/gssaig.117.2.219>.

Visible absorption spectra of colored diamonds. J.E. Shigley and C.M. Breeding, *Gems & Gemology*, **51**(1), 2015, 41–43, <http://dx.doi.org/10.5741/gems.51.1.41>.*

The world of pink diamonds and identifying them. B. Deljanin and A. Peretti, *InColor*, **28**, 2015, 32–41.

Gem Localities

Amethyst from Boudi, Morocco. F. Troilo, A. El Harfi, S. Mouaddib, E. Bittarello and E. Costa, *Gems*

& Gemology, **51**(1), 2015, 32–40, <http://dx.doi.org/10.5741/gems.51.1.32>.*

Blue spinel from the Luc Yen District of Vietnam. B. Chauviré, B. Rondeau, E. Fritsch, P. Ressigeac and J.-L. Devidal, *Gems & Gemology*, **51**(1), 2015, 2–17, <http://dx.doi.org/10.5741/gems.51.1.2>.*

Fluid inclusions in ruby from Asian marble deposits: Genetic implications. G. Giuliani, J. Dubessy, D.A. Banks, T. Lhomme and D. Ohnenstetter, *European Journal of Mineralogy*, **27**(3), 2015, 393–404, <http://dx.doi.org/10.1127/ejm/2015/0027-2442>.

Gem apatite localities. M. Mauthner and T. Ottaway, *Rocks & Minerals*, **90**(3), 2015, 260–269, <http://dx.doi.org/10.1080/00357529.2015.1012957>.

The geology and gem deposits of Sri Lanka. G. Zoysa, *InColor*, **27**, 2015, 38–41.

Mozambique: A ruby discovery for the 21st century. M. Chapin, V. Pardieu and A. Lucas, *Gems & Gemology*, **51**(1), 2015, 44–54, <http://dx.doi.org/10.5741/gems.51.1.44>.*

The Pederneira mine, São José da Safira, Minas Gerais, Brazil. D. Trinchillo, F. Pezzotta and A. Dini, *Mineralogical Record*, **46**(1), 2015, 1–138.

The Rock Creek sapphire mine of Montana - A new era. K.M. Barron and W.F. Boyd, *InColor*, **28**, 2015, 46–57.

Sri Lanka's gemstone cutting journey. J. Henricus, *InColor*, **27**, 2015, 58–61.

Star sapphire from Shandong Province. Y. Liu, J. Wang and Y. Wang, *Acta Petrologica et Mineralogica*, **33**(2), 2014, 85–92 (in Chinese with English abstract).

Instruments and Techniques

Application of surface contact angle and surface tension measurements in the identification of gem materials. X. Bao, T. Lu, R. Wei, Y. Zhang, H. Li, H. Chen and J. Ke, *Rock and Mineral Analysis*, **33**(5), 2014, 681–689 (in Chinese with English abstract).

Packing light: Making the most of portable gem instruments. C.L. Horn and A. Lemaire, *InColor*, **28**, 2015, 42–44.

Miscellaneous

Justifying gem testing reports: The way labs can inform their customers. O. Segura, E. Fritsch and A. Droux, *InColor*, **28**, 2015, 24–26.

Compiled by Brendan Laurs

* Article freely available for download, as of press time

Note: The correct year is 2014.

News Press

Dominican Republic seeks to improve conditions, prospects for informal larimar mining. *Fox News*, 1 April 2015, www.foxnews.com/world/2015/04/01/dominican-republic-seeks-to-improve-conditions-prospects-for-informal-larimar.*

Hoard of 3,000-year-old gold treasure discovered in North Wales. A. Melville-Smith, *Wales Online*, 26 February 2015, www.walesonline.co.uk/news/wales-news/hoard-3000-year-old-gold-treasure-discovered-8724548.*

Rubies, blood-red beauty. V. Gomelsky, *New York Times*, 17 March 2015, www.nytimes.com/2015/03/18/style/international/in-jewelry-rubies-offer-blood-red-beauty.html?_r=0.*

Organic Gems

A multi-analytical approach to amber characterisation. G.I. Truică, N. Ditaranto, M.C. Caggiani, A. Mangone, S.C. Lițescu, E.D. Teodor, L. Sabbatini and G.L. Radu, *Chemical Papers*, **68**(1), 2014, 15–21, <http://dx.doi.org/10.2478/s11696-013-0415-8>.*

Pearls

La première perle porcelainée de culture à noyau identifiée. O. Segura, *Revue de Gemmologie*, **191**, 2015, 21–22.

Study of green coloration technology for pearls. Q. Zhang, Y. Li and L. Feng, *Superhard Material Engineering*, **26**(3), 2014, 44–49 (in Chinese with English abstract).

Social Studies

Contested diamond certification: Reconfiguring global and national interests in Zimbabwe's Marange fields. S.J. Spiegel, *Geoforum*, **59**, 2015, 258–267, <http://dx.doi.org/10.1016/j.geoforum.2014.05.008>.

Mining for peace: Diamonds, bauxite, iron ore and political stability in Guinea. M.D. Bah, *Review of African Political Economy*, **41**(142), 2014, 500–515, <http://dx.doi.org/10.1080/03056244.2014.917370>.

Synthetics and Simulants

Distinction character of synthetic diamond in jewelry (1). H.W. Zhu, T. Li and G.H. Li, *Superhard Material Engineering*, **26**(3), 2015, 26–29 (in Chinese with English abstract).

Note: The correct year is 2014.

Distinction character of synthetic diamond in jewelry (2). H.W. Zhu, T. Li and G.H. Li, *Superhard Material Engineering*, **26**(4), 2015, 14–17 (in Chinese with English abstract).

Identification characteristics of synthetic and colour-altered diamonds. Q. Li and W. Li, *Journal of Gems & Gemmology*, **16**(6), 2014, 21–27 (in Chinese with English abstract).

Treatments

Color enhancement of natural sapphires by high pressure high temperature process. J. Song, Y. Noh and O. Song, *Journal of the Korean Ceramic Society*, **52**(2), 2015, 165–170, <http://dx.doi.org/10.4191/kcers.2015.52.2.165>.*

The filling feature observation and naming suggestions for filled rubies. C. Long, *Acta Petrologica et Mineralogica*, **33**(2), 2014, 147–154 (in Chinese with English abstract).

Multi-process treatments of natural IaAB diamonds. B. Cao, M. Chen and W. Hu, *Journal of Gems & Gemmology*, **16**(6), 2014, 28–33 (in Chinese with English abstract).

Un rubis vraisemblablement huilé. E. Fritsch and Alexandre Droux, *Revue de Gemmologie*, **191**, 2015, 4–6.

Compilations

Gem News International. Tucson 2015: exceptional colored stones and gem artistry, Brazilian Cu-bearing tourmaline and emerald, Oregon sunstone and pearl market updates • Conference reports • Amblygonite-montebrazite carving • Moroccan amethyst • Dumortierite in quartz • Jadeite with high albite content • Moldavite imitation • Iridescent scapolite • Composite quartz beads • CVD synthetic diamond with unstable color • The Foldscope. *Gems & Gemology*, **51**(1), 2015, 68–110, www.gia.edu/gems-gemmology.*

Lab Notes. Cobaltocalcite • FTIR spectroscopy of melee diamonds • Irradiated color-change diamonds • Diamond in diamond • *Tridacna* shell in imitation pearls • Large quahog pearl • HPHT synthetic diamond melee in high-end jewelry • Large HPHT synthetic diamonds • Synthetic moissanite melee in colored diamond bracelet. *Gems & Gemology*, **51**(1), 2015, 58–67, www.gia.edu/gems-gemmology.*

Conference Proceedings

Advances in high pressure research: Breaking scales and horizons. Abstracts volume, Novosibirsk, Russia, 22–26 September 2014, ISBN 978-5769213922.



Gem-A

THE GEMMOLOGICAL ASSOCIATION
OF GREAT BRITAIN



BIRMINGHAM CITY
University



Turn your Diplomas into a degree

If you hold a **Gemmology** and **Diamond Diploma** and are a **current Gem-A Member**, you can now work towards a **BSc (Hons) in Gemmology and Jewellery Studies**.

Offered by Birmingham School of Jewellery and taught at Gem-A's headquarters near Hatton Garden, this one-year top up course covers advanced gemmology practice and theory (including advanced lab equipment), geology theory, advanced diamond grading and jewellery valuation.

To apply for this course, sign up via UCAS (course code 73J9), or for more information contact education@gem-a.com.

Understanding Gems

Join us.



*A*NDRIAMANITRA. *The word up until recent times was used in speaking of... anything valuable or wonderful. It is said that the name was so given because while the body might not be seen, there was a fragrancy attending the name.*

— Richardson, Malagasy–English Dictionary



Palala International
Palagems.com / Palaminerals.com
800-854-1598 / 760-728-9121

Morganite, Madagascar • 70.58 ct • 30 x 23 x 16 mm
Photo: Mia Dixon